4-2017

Dynamic Understeer Control Using Active Rear Toe

Mark Oliver Dixon Kaufman

DYNAMIC UNDERSTEER CONTROL USING ACTIVE REAR TOE

by

Mark Oliver Dixon Kaufman

A Thesis Submitted to the College of Engineering Department of Mechanical Engineering in Partial Fulfillment of the Requirements for the Degree of

Master of Science in Mechanical Engineering

Embry-Riddle Aeronautical University

Daytona Beach, Florida

April 2017

Dynamic Understeer Control Using Active Rear Toe

by

Mark Oliver Dixon Kaufman

This thesis was prepared under the direction of the candidate's Thesis Committee Chair, Dr. Marc Compere, Professor, Daytona Beach Campus, and Thesis Committee Members Dr. Eric Coyle, Professor, Daytona Beach Campus, and Dr. Darris White, Professor, Daytona Beach Campus, and has been approved by the Thesis Committee. It was submitted to the Department of Mechanical Engineering in partial fulfillment of the requirements for the degree of Master of Science in Mechanical Engineering.

Thesis Review Committee:

Marc Compere, Ph.D.
Committee Chair

Eric Coyle, Ph.D.
Committee Member

Darris White, Ph.D.
Committee Member

Charles F. Reinholtz, Ph.D. Department Chair, Mechanical Engineering

Maj Mirmirani, Ph.D. Dean, College of Engineering

Jean-Michel Dhainaut, Ph.D. Graduate Program Chair, Mechanical Engineering

Christopher Grant, Ph.D.
Associate Vice President of Academics

4/7/17

Date

Acknowledgements

First of all, I would like to thank my advisors, Dr. Compere and Dr. Rodriguez for their support, critical comments, ideas, and guidance through my thesis and my masters career.

I would also like to extend a thank you to all my friends and colleges at work and Formula SAE that answered the random questions that came up along the way and gave the push to get through the harder parts.

Lastly, I would like to thank my parents for their constant encouragement and unwavering support through this process and the rest of my college career. It has been quite a journey and I don't think it would have been possible without your understanding and patience with me.

Abstract

Researcher: Mark Oliver Dixon Kaufman

Title: Dynamic Understeer Control Using Active Rear Toe

Institution: Embry-Riddle Aeronautical University

Degree: Master of Science in Mechanical Engineering

Year: 2017

This thesis was conducted to show the ability of Active Rear Toe to control the understeer characteristics of a vehicle. Active rear toe is the ability to control the angle of the rear wheels around the vertical axis, allowing the car's turning radius to change. By changing this radius, the lateral acceleration can be controlled, therefore the understeer of the vehicle can be controlled. The controls scheme is a sliding mode control, specifically a hyperbolic tangent boundary layer and a type 1 zeno controller. The system shows effectiveness to control the understeer of the vehicle up until limit grip on the tire. Once this level is achieved, lateral acceleration can only be removed, not added. It is recommended that ART should supplement controls through the brakes of the car, allowing for the car to be controlled over a larger range of performance.

Table of Contents

Table of Tables

List of Figures

Chapter 1

Introduction

Suspension design and development has changed significantly since the 1920's and 30's when handling and ride quality were first being studied. In 1932, Maurice Olley made a vehicle called the K^2 Rig. The K^2 was a large limousine that had an adjustable center of gravity, CG (Milliken W. F., 2000). After five years of study using the K^2 and early rolling drum testing, Olley published one of the first major reports on suspension and handling. He stated that for the most part, people preferred vehicles that cornered flat and not at the extremes of understeer and oversteer. This is the first time the term understeer was used, but there was mention of oversteer as early as 1908 (Milliken & Milliken, 1995). In simple terms, understeer is the tendency for a vehicle to push through a corner, requiring more steering input to remain on the desired course. Oversteer is the tendency for the back of the car to slide more (drift) and will require less steering input to remain on the desired path.

Problems with Controlling Understeer

It was determined that on a conventional suspension, the understeer gradient is determined by the normal force and the lateral tire stiffness, for the linear region on a tire. Both of these factors have different design constraints. For example, normal force on the tires are effected by the CG position, stiffness of the various components, and for transient conditions the damper tune as well. The understeer for a car without active chassis controls is shown in Figure 1.1.

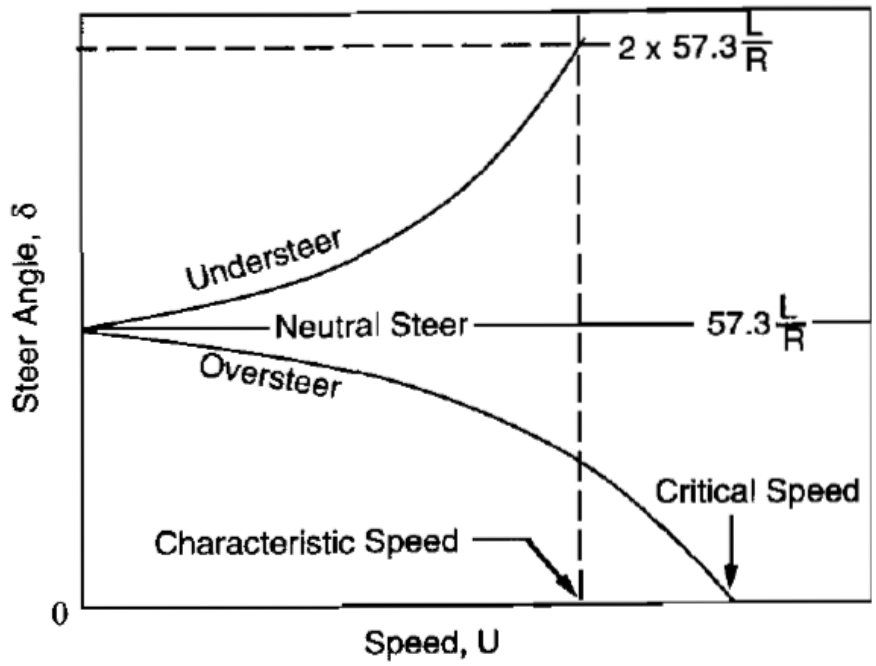

Figure 1.1: Understeer plot for a non-active traditional suspension (Gillespie, 1992).

Often times in a production car, the CG is determined by package space while the springs and damper both effect ride quality and are sometimes constrained by geometry as well. This means that often understeer is not the main design parameter and therefore an afterthought (Gillespie, 1992).

Four-wheel steering came into fruition in the 1980's with many of the Japanese automotive original equipment manufacturers (OEM). Throughout the 80's and 90's, there were a score of cars equipped with a four wheel steering system; however, the trend died out with the changing of the millennium; the only remaining four wheel steering vehicles were long wheelbase vehicles such as the Chevrolet Silverado. The reason for rear steer staying with these longer vehicles is it allows for the car to be more maneuverable at low speed, decreasing the turning radius (Severson, 2015). Fortunately,

as technology has become more advanced, rear steer has started to return to the industry as part of the advanced driver assistance systems (ADAS).

Purpose Statement

The purpose of this study is to show that active rear toe is a viable option for controlling the understeer gradient of a passenger car and can function as part of the ADAS system.

Thesis Organization

Chapter 1

The first chapter introduces understeer and the problems controlling it and provides the thesis statement.

Chapter 2

Chapter 2 is a literature review of causes and effects of understeer for a traditional vehicle. Followed by history and modern application of active rear toe and four-wheel steering, and the available controls systems and theory that could be applied to controlling the understeer of a car. Finally, the different types of models available for simulating active rear toe.

Chapter 3

This chapter also presents detailed analysis of the active rear toe (ART) controller as well as the control strategy used in the simulation. This section presents a 9 DOF vehicle model overview suitable for control system development.

Chapter 4

Within this section, the results and validation are discussed. The model is validated based of a typical production car doing a constant steer turn. The physical tests are then compared to the simulated results. From there, the ART is enabled on the 9DOF model and the results of the ability to control the understeer are shown.

Chapter 5

The conclusion summarizes the effectiveness of understeer control using active rear toe. The report will also explore areas for improvement of the model and further study into additional control strategy and implementation strategies.

Definitions of Terms

PID Controller	A form of classical control using a proportional, integral, and derivative term.
α (alpha)	Slip angle, the angle between the direction the tire is pointed and the direction of travel for the tire.
Slip Ratio	The ratio between the speed a wheel with torque applied and the speed of a free spinning wheel.

List of Acronyms

ART	Active Rear Toe
ADAS	Advanced Driver Assistance System

SMC	Sliding Mode Control(er)
S.R.	Slip Ratio
SAE	Society of Automotive Engineers

Chapter 2

Review of the Relevant Literature

In the following chapter, the thesis will explore research and studies relevant to understeer control and active rear toe. It will begin with a delve into understeer's causes and effects. Then uses and applications of ART and how the proposed thesis fits with the current trends. The next section discusses the different types of control methods available and why sliding mode control was chosen for this controls strategy. The final section is about the different types of vehicle models available.

Causes and Effects of Understeer of a Four Wheel Car

There are two main dynamic broad driving conditions of a car, low speed and high speed. For low speed turning, the steering motion is determined predominantly by the geometry of the car because tire slip is not present. Because the steering is set by geometry, the following equation is applied and is valid for small steer angles.

$$\boldsymbol{\delta_{ack} = \frac{L}{r}} \quad (1)$$

Where:

δ_{ack} = Front Wheel Angle with Respect to the Body

L = Wheelbase

r = Turning Radius

Figure 2.1 illustrates the Ackermann steer angle for a bicycle model (Milliken & Milliken, 1995).

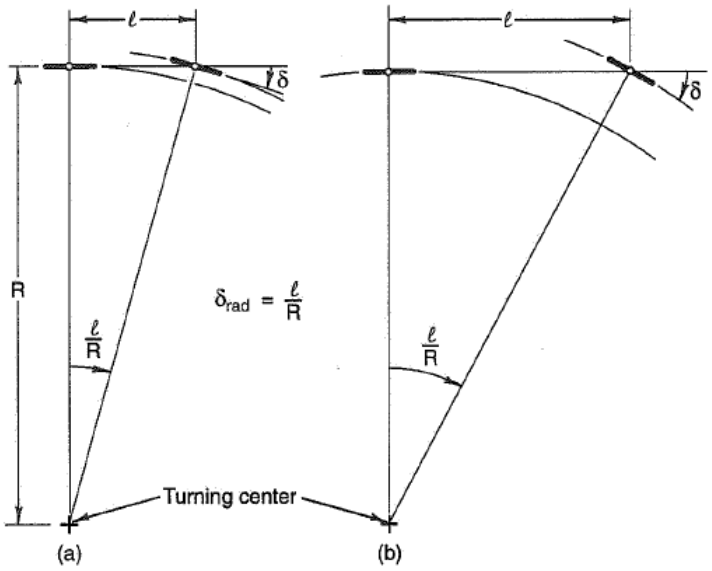

Figure 2.1: Low speed steering motion, note larger δ for longer wheelbase.

On a production car, the other term used in conjunction with steering is Ackermann. A true Ackermann steering is one where the inside and outside wheels use different steering angles so that the car turns around the same turning centroid. This is shown in Figure 2.2.

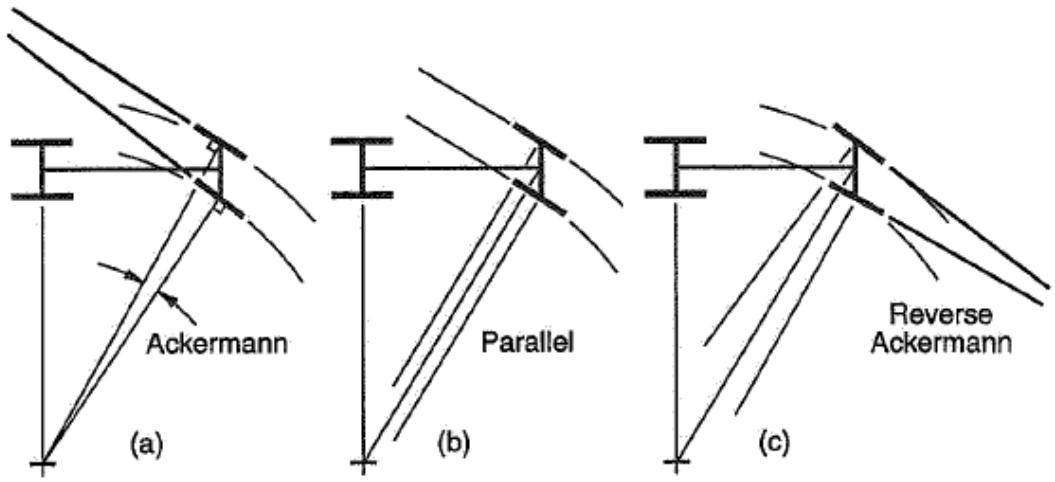

Figure 2.2: Illustrating varieties of the Ackermann steering(a) Ackermann Steering (b) Parallel Steering (c) Reverse Ackermann

As the figure shows, there are different types of Ackermann steering. These different types come into play in more high speed dynamics when the slip angles are non-zero, weight transfers more than the low speed turns and the nonlinearity of tires effects the lateral loads. Therefore, the Ackermann percentage changes to maximize the lateral force generated and the stability of the system (Milliken & Milliken, 1995).

There are a couple of ways to approximate the dynamics of a tire. One of them is the brush model. It consists of a row of elastic bristles that meets the road plane and can deflect in a direction parallel to the road surface. This simulates the tread deforming on the tire and their compliance is representative of the elasticity of the tire. As the tire's slip angle increases, the bristles deform more as shown in Figure 2.3.

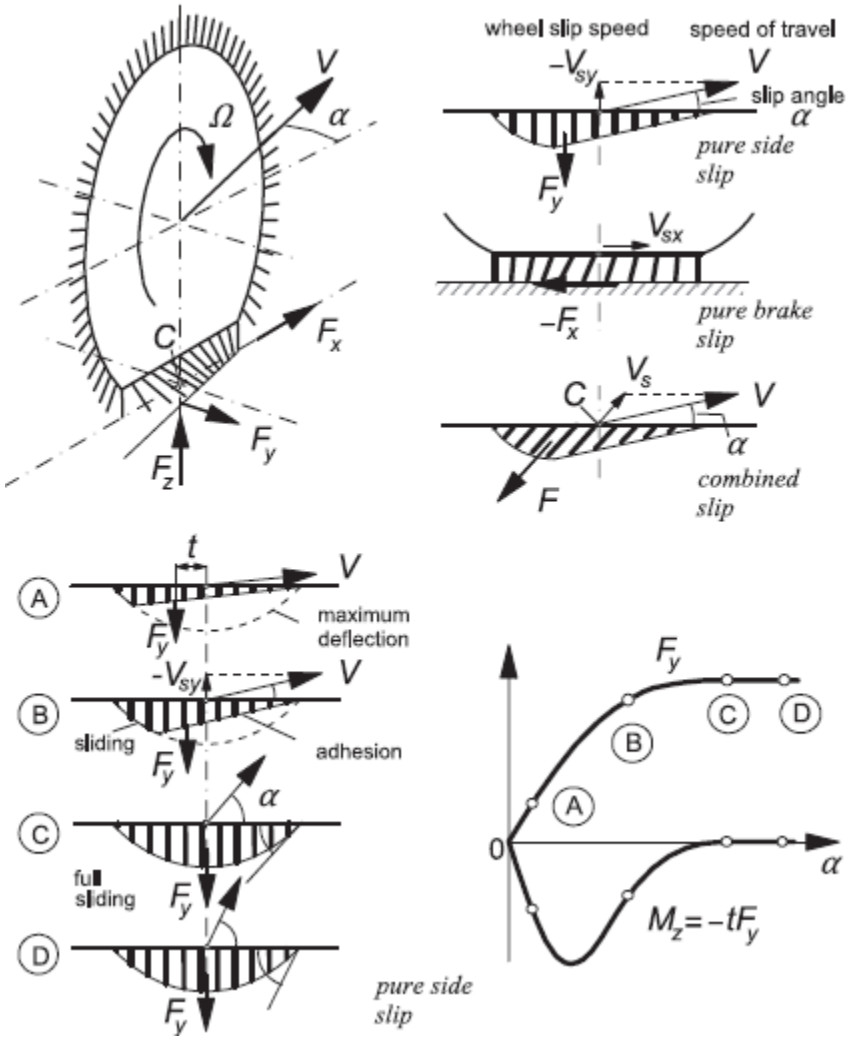

Figure 2.3: The visualization of the brush model of a tire (Pacejka, 2012).

There are three main contact patch effects that this captures, lateral force, longitudinal force, and the pneumatic trail. The trail is the distance from the center of the tire to the lateral force vector, this creates the self-aligning torque (Mz). As the lateral force increases, the pneumatic trail decreases. As the graph in Figure 2.3 shows, the tire eventually becomes saturated and no longer produces more force with increasing slip, points C and D (Pacejka, 2012).

During high speed turning maneuvers, the slip angle of the tire begins to affect the linear relation of steer angle, wheelbase, and turning radius. The equations that determine the front and rear slip angles are below.

$$\boldsymbol{\alpha_f = \frac{W_f}{C_{\alpha f}} \frac{V_x^2}{g * r}} \quad (2)$$

$$\boldsymbol{\alpha_r = \frac{W_r}{C_{\alpha r}} \frac{V_x^2}{g * r}} \quad (3)$$

Where:

α_f = Front tire slip angle

W_f = Weight on front axle

$C_{\alpha f}$ = Lateral front tire stiffness

V_x = Vehicle speed

g = Gravitational acceleration

r = Radius of turn

α_r = Front tire slip angle

W_f = Weight on front axle

$C_{\alpha r}$ = Lateral rear tire stiffness

At high speed, the equation for steering angle becomes as follows due to the increased slip angles. The lateral tire stiffness is in used to determine the lateral force. It can only be used in the linear region of the tire (Wong, 2001).

$$\boldsymbol{\delta = \frac{L}{r} + \alpha_f - \alpha_r} \quad \textbf{(4)}$$

$$\boldsymbol{\delta = \frac{L}{r} + \left(\frac{W_f}{C_{\alpha f}} - \frac{W_r}{C_{\alpha r}}\right)\frac{{V_x}^2}{g*r}} \quad \textbf{(5)}$$

$$\boldsymbol{\delta = \frac{L}{r} + K_{us}\frac{{V_x}^2}{g*r}} \quad \textbf{(6)}$$

Where:

$$\boldsymbol{K_{us} = \left(\frac{W_f}{C_{\alpha f}} - \frac{W_r}{C_{\alpha r}}\right)} \quad \textbf{(7)}$$

K_{us} defines the understeer gradient of the car. This number helps to quantify the car's steering and it determines the understeer, neutral steer, or oversteer (Wong, 2001). The three conditions are shown in Figure 2.4.

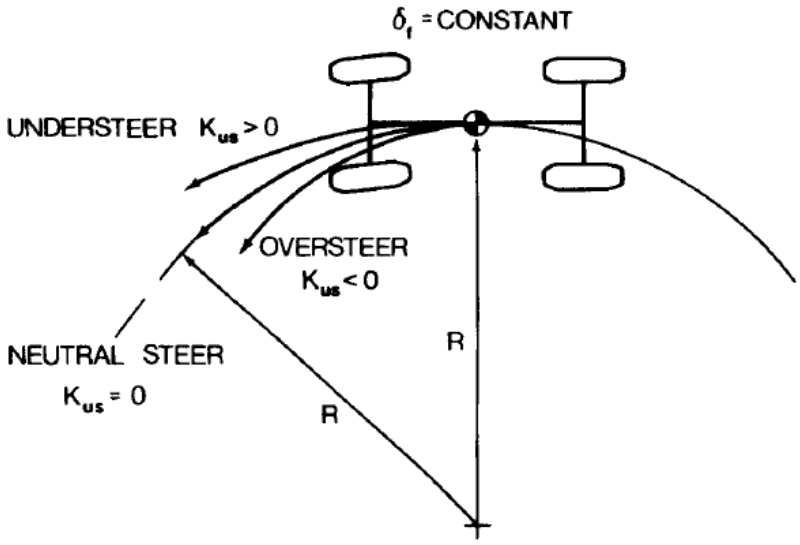

Figure 2.4: The effect of understeer, neutral steer, and oversteer on turning radius.

If $K_{US} = 0$, the car is considered a neutral steer configuration. This is a marginally stable condition where both the front and rear tires loose have equivalent slip angle. A car has understeer when $K_{US} > 0$ and occurs when the front slip angle is greater than the rear. For the driver, this feels like the car is pushing through the corner and more steering then neutral steer is needed to achieve the same turning radius. Oversteer occurs when the rear slip angle is higher than the front slip angle, $K_{US} < 0$. When the car is in an oversteering condition, less steering angle is needed then a neutral car. This is also an unstable condition where a controller must actively actuate the steering and/or throttle to maintain stability (Gillespie, 1992).

Another important parameter to consider is the vehicle slip angle. This is like the slip angle of the tire, but for the entire vehicle. Equation 8 shows the calculation of the value.

$$\boldsymbol{\beta = \tan^{-1}\left(\frac{v_y}{v_x}\right)} \quad (8)$$

Like alpha, beta is the angle between the direction the car is pointed and the direction the car is going. This is important for judging the amount of rotation a car is undergoing. For a production car, higher slip angles are undesirable. If a car is slipping more, the car is more likely to spin and it adversely affects the comfortability of the passengers in the car (Rajamani, 2012).

Active Rear Toe, History and Application

Four-wheel steering was first released in a production car in the late 1980's. Since then, a number of advances in technology have allowed for more complex systems. The Porsche Weissach division developed a four wheel steering system that relied on the compression of the suspension bushings. Before this advancement, their cars had a tendency to toe out under throttle, promoting an oversteer condition. Instead, Porsche designed the suspension to toe in if the throttle closes, promoting stability in the rear of the car. This later became common across many different cars from different brands. The first proper four wheel steering system came in the 1986 Honda Prelude. This system operated with purely mechanical components. A shaft ran from the front steering rack to the rear of the car and worked to steer the rear wheels based of front steering angle. It used a set of offset shafts and gears so that in small angles of steering, it would turn in phase (same direction as the front wheels) up to 1.5 degrees. However, at steering wheel angles above 246 degrees, it turned out of phase (opposite direction of the front wheels) by up to 5.3 degrees. This system, shown in Figure 2.5, reduced the turning radius by 10 feet and promoted on center stability.

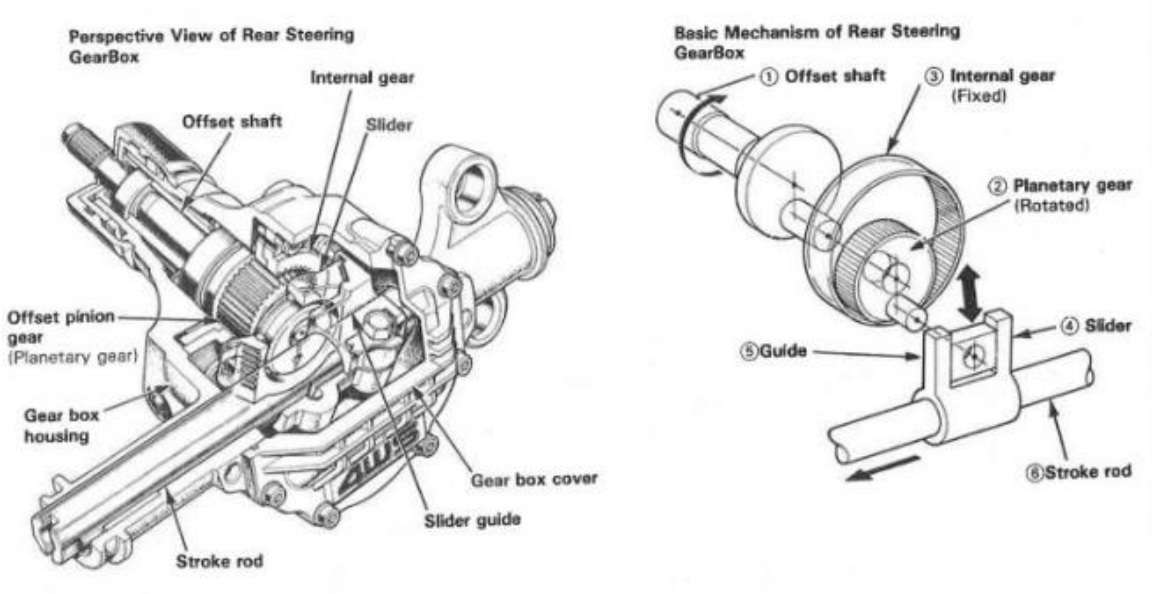

Figure 2.5: The mechanical rear wheel steering system from the 1988 Honda Prelude.

The next improvement in rear steer actuation came on the Nissan R31 Skyline. This car was the first car with a computer controlled, hydraulic actuated controls system. It worked by compressing the subframe bushings, allowing for ±.5 degrees of rear steer actuation. The first electric actuation came with the 1991 Honda Prelude. This system replaced the shaft from the front steering rack with an electric motor reducing weight and complexity. Active rear toe became far less common with the changing of the millennium. It was used on very long wheelbase cars and trucks to reduce the turning radius, like the Chevrolet Silverado. It was hard for the OEM's to substantiate the costs of adding the system to other vehicles (Severson, 2015).

Rear steering has begun to return to production cars. Some of the newer cars from brands like Audi, Porsche, Infiniti, and Honda produced computer controlled,

electronically actuated rear toe systems. With these new, modern systems, there are two main types. There are systems that use a gain based actuation using steer angle and vehicle speed to choose the amount of rear steer. In-phase or out of phase direction is thresholded with speed. This would promote maneuverability at low speeds while allowing for greater stability at high speeds. The other type actively tries to control a specific dynamic of the car. An example of this that is currently in production is direct yaw moment control (DYC). With DYC, the system actively controls the yaw moment of the car, improving handling and safety in vehicle motion with larger slip angles and higher lateral accelerations. These controller strategies have could be achieved through a greater understanding the dynamics of a tire and the overall vehicle dynamics, as well as an application of modern sensing and computing technology (Abe, 1999).

Independent Rear Toe Actuation

Another advancement came in the form of independent toe control using independent actuators. In industry, the term rear steer has grown to mean a central actuator and active rear toe for independent control. This allows for an adjustable Ackermann and can help make up for actuator deficiencies in both speed and power. For instance, if the controller needs to yaw the car, then it can toe out the rear wheels, promoting instability and allowing for the yaw to be achieved. An example of this independent control is the ZF AKC (active kinematics control). This replaces the toe link on a multilink suspension with an electronic actuator, shown in Figure 2.6.

Figure 2.6: The ZF AKC Actuator and the standard link it replaced.

The AKC system is designed to aid in yaw damping at high speed and shorten the turning radius, aiding in maneuverability at low speeds. Another advantage to this approach is it also allows for the car to not have a kinematically defined bump-toe profile which has many advantages. For example, instead of spending the time and money to develop a complex multi-link suspension, one could use a cheaper and simpler style and then use the actuator to determine the bump toe characteristics. Using independent actuation also helps to improve the tire wear and the efficiency of the car since it allows for the wheels to be set straight, if stability is not a concern. It also allows for greater directional stability and performance. Now, the system is able to compensate for split μ conditions on the road surface and banked turns where one tire sees more load. One of

the downsides to this style is it increases the unsprung mass of the car and is sometimes difficult to package (Wiesenthal, Collenberg, & Krimmel, 2008).

Different Controls Methods Available

In the world of controls, there are two main studies, classical and modern controls. The only classical control scheme that was considered for controlling the rear toe is the PID (proportional integral derivative) controller. The controller has three main parts denoted by the terms. The proportional is a linear gain based off the error, the derivative term is based off the derivative error and damps oscillation. The integral term builds over time and rejects building error, removing any steady state offset, like an offset. However, the PID has some issues in this application. To start with, the controls are linear and symmetric, therefore if less actuation is needed to remove understeer then to add understeer the controller is not as effective. One of these nonlinearities is the force generated by the tire as slip angle increases, which is what the actuator is controlling. PID also has issues adapting to unknown nonlinearities. For a car, that works out to only being able to properly control the car when it is not at the limits of performance. Furthermore, it will have trouble adapting to rapidly changing conditions such as a different road surface friction since the gains are normally fixed (Araki).

In the study of modern controls, there were two styles considered for controlling the understeer using ART, robust and adaptive control. Both of the controls strategies have their advantages and disadvantages.

Adaptive controls started being studied in the 1950’s for use in the autopilot systems of aircraft. They work by automatically adjusting the controller parameters to

deal with changing dynamics in the system. Adaptive controls are popular in robotics, aeronautics, and power systems fields. For example, the controller must adapt to changing fuel mass in an aircraft, or a robotic arm lifting parts of different masses. Adaptive controllers do still have their issues. They tend to have a harder time rejecting fast changing disturbances and also suffer from parameter drift. If there are uncertainties that appear periodically, the controller can incorrectly compensate for them resulting in a parameter that will drift and will eventually become divergent. This is shown in Figure 2.7.

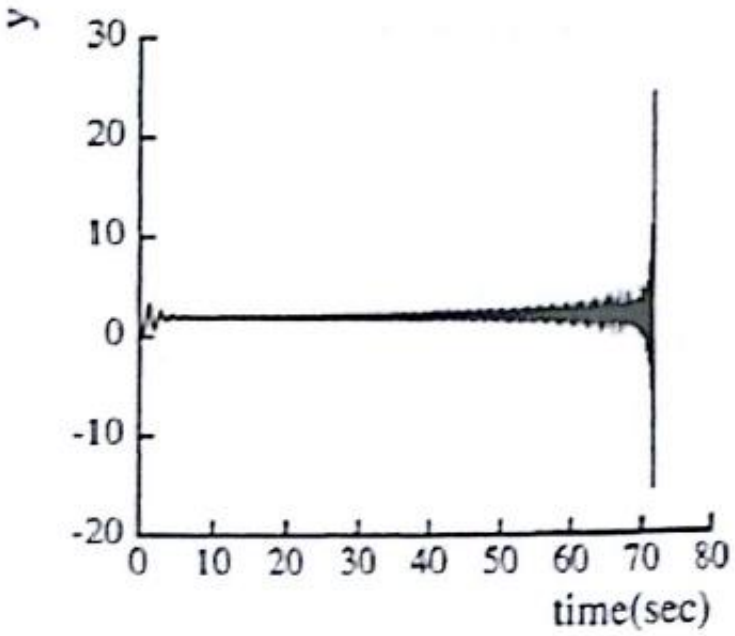

Figure 2.7: The effect of parameter drift in causing instability (Slotine & Wieping, 1991).

The main cause of this type of error comes from measurement noise and does not normally effect tracking accuracy until the instability occurs. This can be remedied by

applying a dead zone around the noise, but if the signal to noise ratio is too low then valuable information can be lost (Slotine & Wieping, 1991).

Robust controls are much better at dealing with uncertainties and noise than adaptive controllers. There are two kinds of uncertainty, structured and unstructured. Structured or parametric uncertainty come from unknowns or inaccuracies in the model. An example of this is the tolerance on the spring rate for the corner springs of a car or the specific tire choice of the customer. The other type of uncertainty is unstructured uncertainty. Both of these adversely affect the ability to control the model. Robust controllers are designed to help deal with these uncertainties. According to Slotine,

> In principle, adaptive control is superior to robust control in dealing with uncertainties in constant or slowly-varying parameters. The basic reason lies in the learning behavior of adaptive control systems: an adaptive controller improves its performance as adaptation goes on, while a robust controller simply attempts to keep constant performance (Slotine & Wieping, 1991).

Because variations in road conditions, normal loads, model unknowns, and nonlinearities in the tire can cause a large effect on the performance of the controller, robust control is superior. This is because the controller attempts to maintain performance, no matter the conditions. For the problem of controlling the understeer of a car, a form of robust control called sliding mode control (SMC) is applied. SMC is one of the more computationally simple forms of robust control. It is designed to provide an approach to the problem of maintaining stability and constant performance in the face of

model imperfections. Sliding mode does this by trying to maintain its position along a sliding surface, denoted by $S(t)$, by switching between positive and negative states. Figure 2.8 shows the graphical application of this theory.

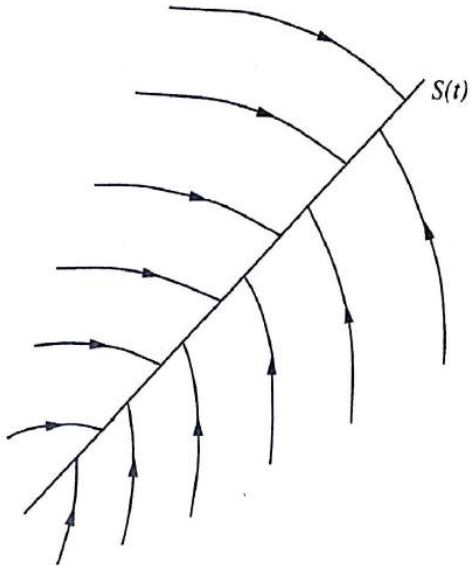

Figure 2.8: Switching between positive and negative control to reach the switching surface.

The sliding surface is the desired function and its error is driven to 0. This is accomplished by switching between two states. Ideally, these states are exactly opposite of each other. For trying to control active rear toe, the two states are turn the rear wheels left or right.

For the purposes of controlling understeer, the error in A_y is used to determine $S(t)$, and the actuator is steering the rear wheels left or right to achieve the desired A_y. Ideally, once the controller reaches the sliding surface, it remains on the surface as shown in Figure 2.9. This is known as exponential convergence.

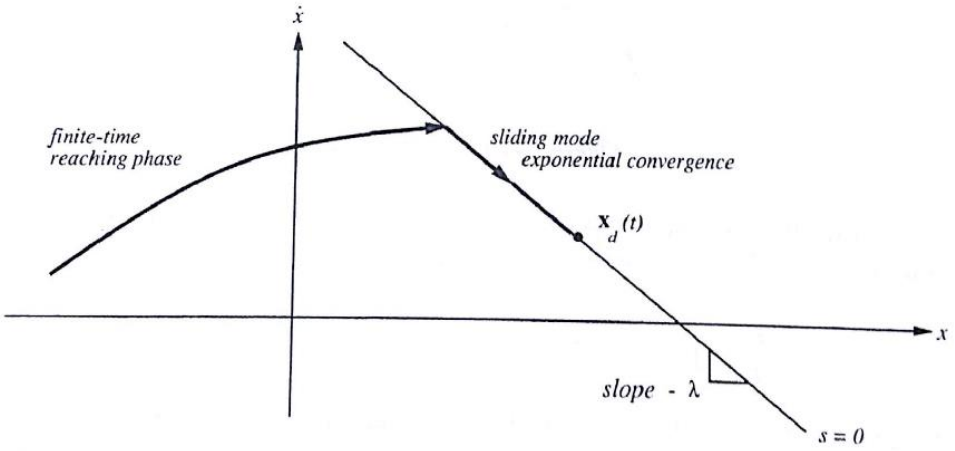

Figure 2.9: Exponential convergence of a sliding mode controller.

However, this is not normally the case. Often times, an imperfect actuator or system noise will result in a phenomena known as chattering. Once the sliding surface is reached, the switching of states is often delayed, therefore the value oscillates around the sliding surface instead of riding on the surface. This can be seen in Figure 2.10.

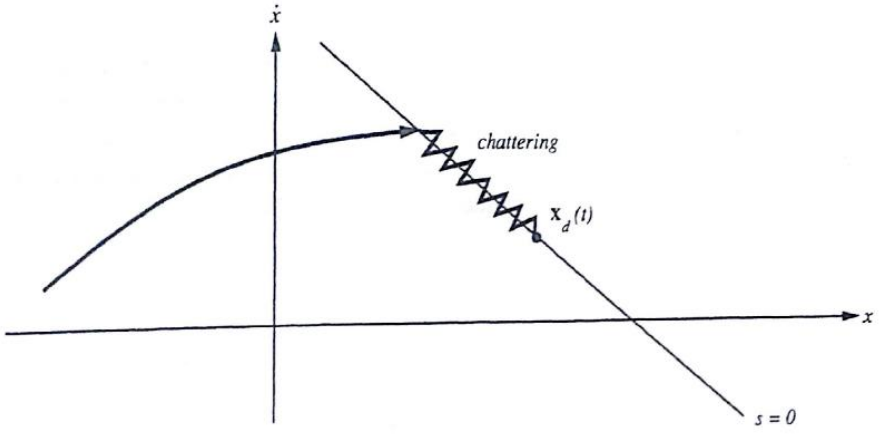

Figure 2.10: The graphical representation of chattering around the sliding surface.

Fortunately, there are ways of negating or solving the chattering problem (Slotine & Wieping, 1991).

One of these solutions to the chattering issue is called the boundary layer solution. It was developed by Slotine and Sastry in 1983 and allows for a region that the switching does not occur. This is written mathematically in the equation below.

$$|\boldsymbol{S(t)}| > \boldsymbol{\varepsilon},\ \boldsymbol{sat(S)} = \boldsymbol{sign(S)} \quad \textbf{(9)}$$

Where:

$S(t)$ = Switching surface

ε = Boundary around the switching surface

Everything inside this region is continuous. Another way to consider this is with a linear piecewise function.

$$\boldsymbol{u(t)} = \begin{cases} \boldsymbol{Msign\big(S(t)\big)\ for\ |S(t)| > \varepsilon} \\ \boldsymbol{\frac{M}{\varepsilon} S(t)\ for\ |S(t)| \leq\ \varepsilon} \end{cases} \quad (10)$$

Where:

M = Proportional gain

$\frac{M}{\varepsilon}$ = Linearly proportional feedback gain

S(t) =Switching surface

ε = Boundary around the switching surface

In simulation, a hyperbolic tangent is used to accomplish the boundary layer strategy. This allows for the *sign(S)* to function outside a threshold with a continuous interior section (Utkin, Guldner, & Shi, 2009). There is greater detail about how this is setup in Chapter 3.

Different Types of Vehicle Models

There are many different variations to a vehicle model. From very basic point-mass, friction circle models to n-DOF (degree of freedom) models that account for the individual parts of a suspension. For the purpose of this thesis, the models studied are limited to a bicycle model, a 9 DOF model, and a 13 DOF model.

A bicycle model is a very common type of vehicle model. They are normally 3 DOF, representing *Ay*, *Ax*, and $\dot{\psi}$ (lateral acceleration, longitudinal acceleration, and yaw rotational acceleration, respectively). Also, these models normally use a linear tire model without a suspension and ignores lateral load transfer. Since model accuracy comes with added complexity, a bicycle model is computationally simple. Because of this, they are able to run faster than a more complex model and therefore are used in many controls systems, such as yaw stability, side slip, and trajectory control. This style model works very well for most driving situations when the car is not at the limits of the tire and in a quasi-steady state condition. This is because one of the main deficiencies in this type of model is their linear nature, which limits the ability to model tires. Luckily, it is possible

to make linear models for the tires, with added computational complexity. One way is using fuzzy logic feedback to tune the front and rear C_α to better cope with the linear, decreasing, and saturated sections of a tire. Another way is using a variable piecewise function to describe the nature of a tire. This is shown in Figure 2.11.

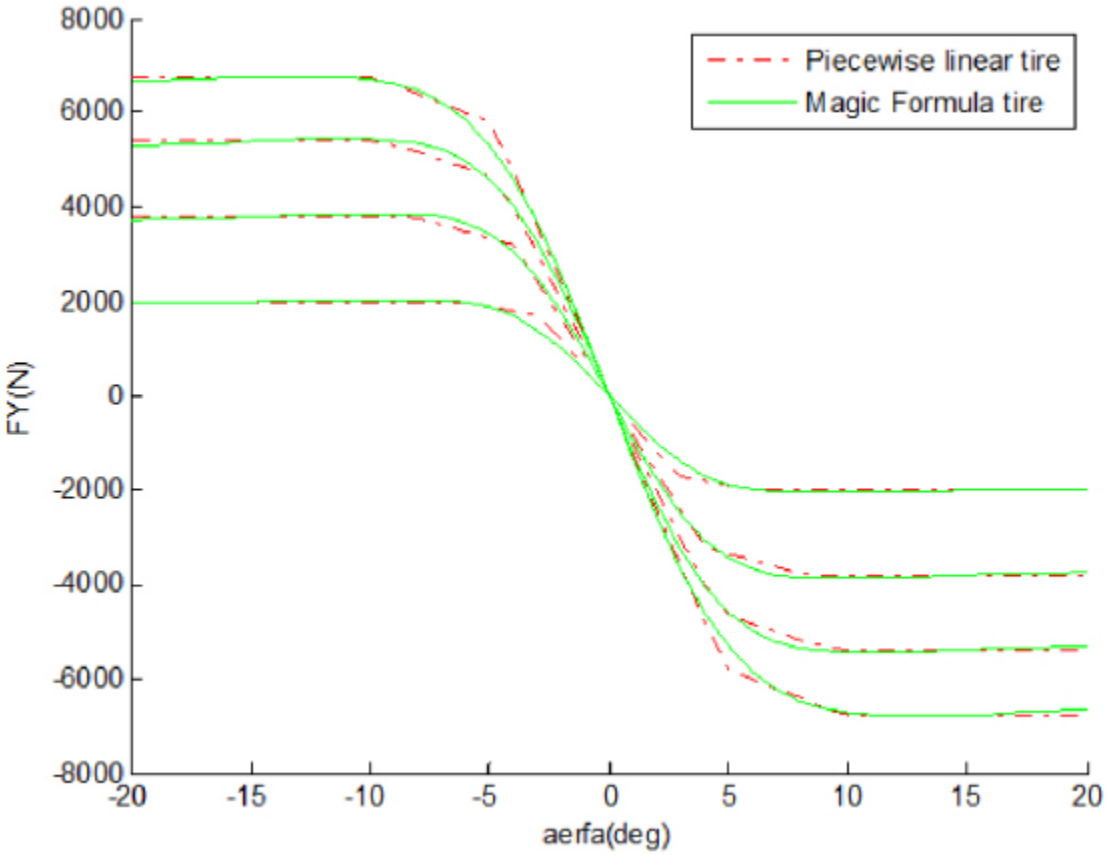

Figure 2.11: Linear piecewise approximation of a Pacejka Magic tire model.

This style is able to split the nonlinear tire force curve into linear segments and can also adapt to changing normal loads to update the lateral and longitudinal force output of the tire (Ren, Shim, Ryu, & Chen, 2014).

The next level model is a 7 DOF model. For the most part, these are rigid body models so they do not account for *Az* of the vehicle frame or wheel assemblies. For the 7 DOF model, there are still inaccuracies due to the lack of a suspension and its rigid body; however, it allows for a rotational subsystem and more accurate tire models. Since the 7 DOF model has four rotating assemblies, torque can be added and removed from each wheel independently as well as the ability to change the slip of the wheels by turning them around their z axis. This allows for more complex powertrain models and longitudinal controls strategies. Although a bicycle model can support rear steer, since it only turns one wheel, it limits the functionality of the system to being one with pure Ackermann steering all the time. It is the addition of the wheel assembly's 4 DOFs (spinning of the tire) that allow it to become a very useful model. It can also handle the nonlinearities of a tire. The most common way to do this is with the magic equations, first postulated by Pacejka in 1993 and expanded on into the 2000's. These sets of equations are a way to approximate the nonlinearity of a tire. They were also shown in Figure 2.11. The inputs for these equations are tire normal force, slip angle, and slip ratio. Their output is the longitudinal, lateral force, and aligning torque generated by the tire (Rajamani, 2012).

The model can always be complex, there can always be more degree of freedoms added and more systems modeled. 13 DOF models, for example, can handle suspension movement and nonlinearity from the dampers. Figure 2.12 shows a high DOF model.

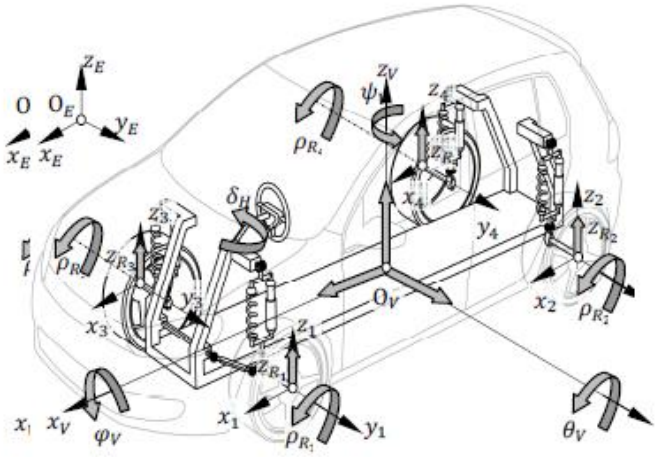

Figure 2.12: All the major degrees of freedom associated with a 13 DOF model.

These models can be used to accurately model the dynamics of a vehicle and are often used as a design the vehicle before time and resources are committed to real world testing and validation. However, due to their computational intensity, these are rarely used in control systems with the exception of controller training. (Louis & Schramm, 2012)

Chapter 3

Model Development

This chapter will discuss the vehicle model used in the 7 DOF simulation. There are two main sections of the simulated vehicle. The first section is the vehicle model, this includes all the components to simulate the 7 degrees of freedom, the Pacejka tire model, and the driver model. The 7 degrees of freedom are acceleration in X and Y, rotation in Z, and rotation of each of the four wheels. The second section of the model is the rear toe controller. It calculates all the necessary parameters for the rear wheel steering and then applies the controller to dynamically control the understeer of the car.

Vehicle Model

The vehicle model follows the SAE (Society of Automotive Engineers) convention for its coordinate system. It was formed in 1994 and documented in SAEJ670. In this convention, the Y positive is direction is out the right side of the car, shown in Figure 3..

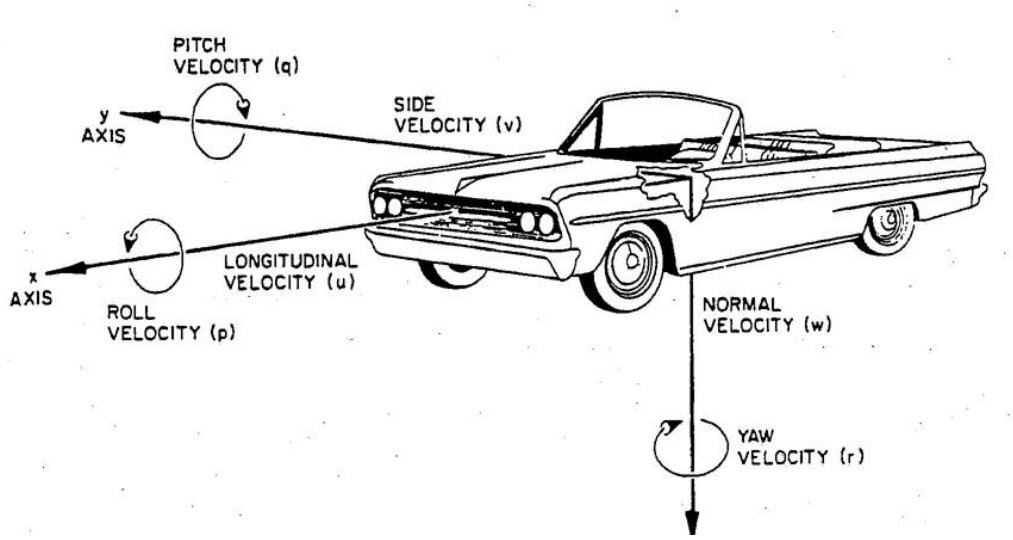

Figure 3.1: The SAE coordinates as stated in SAE J1773.

This system is similar to the conventional right hand rule; however, it is rotated 180^o around the X axis (SAE International, 2008). The simulation also uses vector notation to denote all four wheel assemblies. In the vector, they are ordered as follows: Front Left, Front Right, Rear Left, and Rear Right. This allows for simpler computation when the same calculations need to be performed on the wheel assemblies. The vehicle model is composed by 6 main subsystems, normal force estimation, aerodynamic force calculations, longitudinal controller, wheels and tires, sum of forces and moments, and a coordinate transform.

Normal Force Estimation Subsystem

The 9 DOF model is a rigid body model, however it still accounts for the effects of weight transfer due to the acceleration in the X and Y direction. The normal force is governed by four equations.

$$\boldsymbol{N_{fl} = \left[\left(\frac{b}{L}\right) - \left(\frac{H}{L}\right)\left(\frac{Ax}{g}\right)\right] * \left[\left(\frac{d}{T}\right) + \left(\frac{H}{T}\right)\left(\frac{Ay}{g}\right)\right] * mg} \quad \textbf{(11)}$$

$$\boldsymbol{N_{fr} = \left[\left(\frac{b}{L}\right) - \left(\frac{H}{L}\right)\left(\frac{Ax}{g}\right)\right] * \left[\left(\frac{d}{T}\right) - \left(\frac{H}{T}\right)\left(\frac{Ay}{g}\right)\right] * mg} \quad \textbf{(12)}$$

$$\boldsymbol{N_{rl} = \left[\left(\frac{b}{L}\right) + \left(\frac{H}{L}\right)\left(\frac{Ax}{g}\right)\right] * \left[\left(\frac{d}{T}\right) + \left(\frac{H}{T}\right)\left(\frac{Ay}{g}\right)\right] * mg} \quad \textbf{(13)}$$

$$\boldsymbol{N_{rr} = \left[\left(\frac{b}{L}\right) + \left(\frac{H}{L}\right)\left(\frac{Ax}{g}\right)\right] * \left[\left(\frac{d}{T}\right) - \left(\frac{H}{T}\right)\left(\frac{Ay}{g}\right)\right] * mg} \quad \textbf{(14)}$$

Where:

N_{fl} = Normal force on front left tire (N)

N_{fr} = Normal force on front right tire (N)

N_{rl} = Normal force on rear left tire (N)

N_{rr} = Normal force on rear right tire (N)

a = Distance from CG to front axle (m)

b = Distance from CG to rear axle (m)

c = Distance from CG to left wheels (m)

d = Distance from CG to right wheels (m)

H = Height of the CG from ground (m)

L = Wheelbase of vehicle (m)

T = Track width of vehicle (m)

A_y = acceleration in Y direction (m/s^2)

A_x = acceleration in X direction (m/s^2)

This section accounts for the weight transfer. Due to the rigid body, the weight transfers instantly so it does not capture the transient effects of turning and is only valid

assuming all spring rates are the same. This is because there is no damping in the system. There are also no springs so oscillation does not occur.

Aerodynamic Forces Subsystem

This system augments the normal force calculations on the tires and produces a force in the negative x direction to account for drag force. At lower speeds, the aerodynamic forces are very small and contribute little to the dynamics of the car; however, at higher speeds their effects start to become more apparent. The equations are shown below.

$$\boldsymbol{Fl = .5 * A * \rho * Cl * Vx^2} \quad \textbf{(15)}$$

$$\boldsymbol{Fd = .5 * A * \rho * Cd * Vx^2} \quad \textbf{(16)}$$

Where:

F_l = Force in Z direction (lift) (N)

F_d = Force in X direction (drag) (N)

A = Frontal area (m^2)

ρ = Density of air $\left(\frac{kg}{m^3}\right)$

V_x = Vehicle speed (m/s)

C_d = Drag Coefficient

C_l = Lift Coefficient

This subsystem accounts for the height and longitudinal position of the CG position. Because of the height, a moment is generated and changes the application of force to the wheels because the drag of the car also effects the normal loading on the tires.

Longitudinal Controller

This controller has two parts. The first part is a sliding mode controller used to keep the car at the initial speed set by the setup code. This is necessary for doing constant speed turning maneuvers because the slip angle of the tire will cause the vehicle to slow down. Since the lateral acceleration is determined by V_x^2, this change in speed causes a fluctuation in the lateral acceleration, effecting the understeer of the car. The other section is used for model validation. It imports vehicle speed using a lookup table where the test speed comes from the testing data and the time is the input to the table. This is sent into the sliding mode controller used in the initial sliding mode.

Wheels and Tires Group

The wheels and tires group is responsible for all of the computations governing the dynamics of the tires. There are four subsections under the wheels and tires group, the tire velocity calculator, slip angles and slip ratios, the Pacejka tire model, and the rotational subsystem. In this group, vector notation is used to show the calculation for all four tires. Each of the tires have their own unique coordinate system as shown in Figure 3.2.

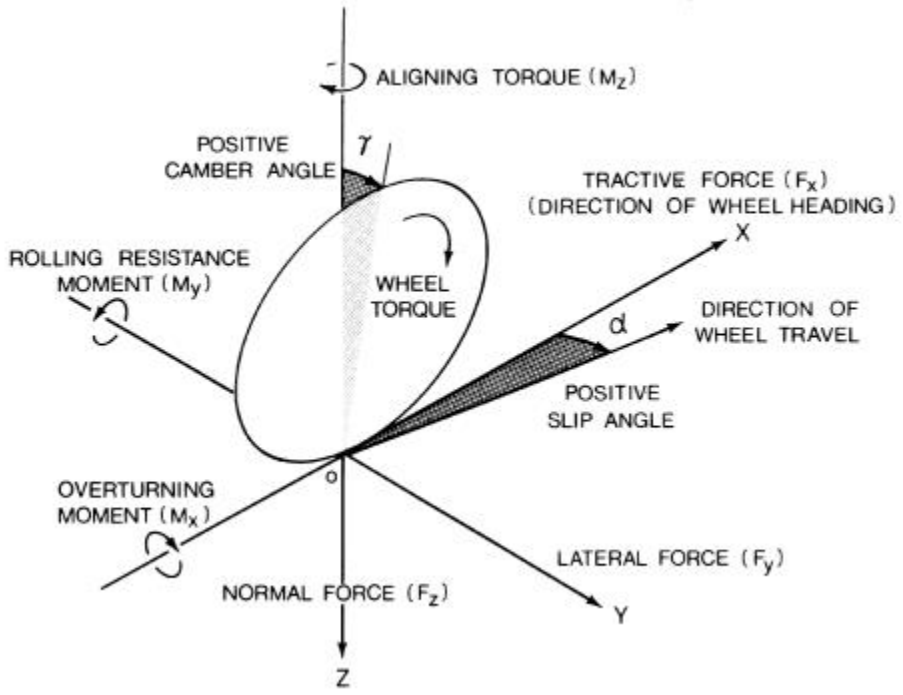

Figure 3.2: The coordinate frame for each of the tires.

Tire Velocity Calculator

Due to the fact that the tires are not all in the same position with respect to the center of rotation of the car, when the car yaws, the speeds are not the same for each tire. This works by taking the cross product between the yaw rate of the car and the distance to the tire from the center of gravity in both lateral and longitudinal coordinate tire directions. This yields the velocity of the tire in the body coordinates, with respect to the CG of the car. This velocity vector is then added to the velocity of the car in the X and Y directions, yielding the total velocity of the wheels. This is shown mathematically below for the front left wheel.

$$\begin{bmatrix} Vx \\ Vy \end{bmatrix}_{FL\ Tire} = \begin{bmatrix} Vx \\ Vy \end{bmatrix}_{CG} + \omega_z \times \begin{bmatrix} a & -T/z \end{bmatrix} \quad (17)$$

Where:

ω_z = yaw rate of the car $\left(\frac{rad}{sec}\right)$

Slip Angles and Slip Ratios

This subsystem calculates the slip angle of all four tires. It compares the angle the tire is traveling with the angle the tire is turned. This is the slip angle and shown below mathematically.

$$\alpha = \delta - \tan\left(\frac{Vy_{tire}}{Vx_{tire}}\right) \quad (18)$$

Where:

α = slip angle of the tires (rad)

δ = steering angle of the tires (rad)

The other calculation performed in this subsystem is the slip ratio calculations. This slip ratio is responsible for the longitudinal force generation of the tire and is the percent difference in speed between a free rolling tire and one with torque applied, as shown in equation(19).

$$\boldsymbol{\sigma_x = \frac{r_{tire} * \omega_{tire} - Vx_{tire}}{Vx_{tire}}} \quad (19)$$

Where:

σ_x = Slip Ratio of the tire

r_{tire} = rolling radius of the tire (m)

ω_{tire}= rotational speed of the tire (rad/sec)

Pacejka Tire Model

The two parts to the Pacejka model used in the 9 DOF model are the pure slip magic equations and the combined slip equations. The pure slip equation is the 1994 magic equation. In this model, the lateral force generation does not affect the longitudinal force, unlike the actual behavior of the tire. Inputs to this equation are normal force, slip angle, and slip ratio and its outputs are lateral, longitudinal force, and aligning torque. The combined slip equations were developed in 1996 and cause the lateral and longitudinal forces to effect each other. Using this equation, the lateral force peak is diminished if the longitudinal force is higher, or vice versa. There are six constants that determine the load forces and torques produced by the tire. Equation (20) is written generically because it is the same equation with different constants for *Fy*, *Fx*, and *Mz* calculations.

$$\boldsymbol{y = D * sin[C * \arctan\{B * x - E(B * x - actran(B * x))\}]} \quad (20)$$

With

$$\boldsymbol{Y(X) = y(x) + S_v} \quad (21)$$

$$\boldsymbol{x = X - S_h} \quad (22)$$

Where:

Y = The Output Variable, Lateral Force Fy, Longitudinal Force Fx, and aligning moment Mz

X = The Input Variable: slip angle or slip ratio

B = Stiffness Factor

C = Shape Factor

D = Peak Value

E = Curvature Factor

S_h = Horizontal Shift

S_V = Vertical Shift

The D values determines the peak force or torque generated by the tire at the specific normal loading condition. C is the shape factor and it controls the range of the sine function. The stiffness factor is B and it helps to determine the slope of the curve near the origin. The product of BCD determines the slope of the curve at the origin, this is also C_α. S_h and S_V are offsets and account for ply-steer, conical effects, and rolling resistance

that can cause a change in the forces generated by the tire. Finally, E adjusts the slope of the curve near the peak force where the tire is very nonlinear. This relation is shown in Figure 3.3.

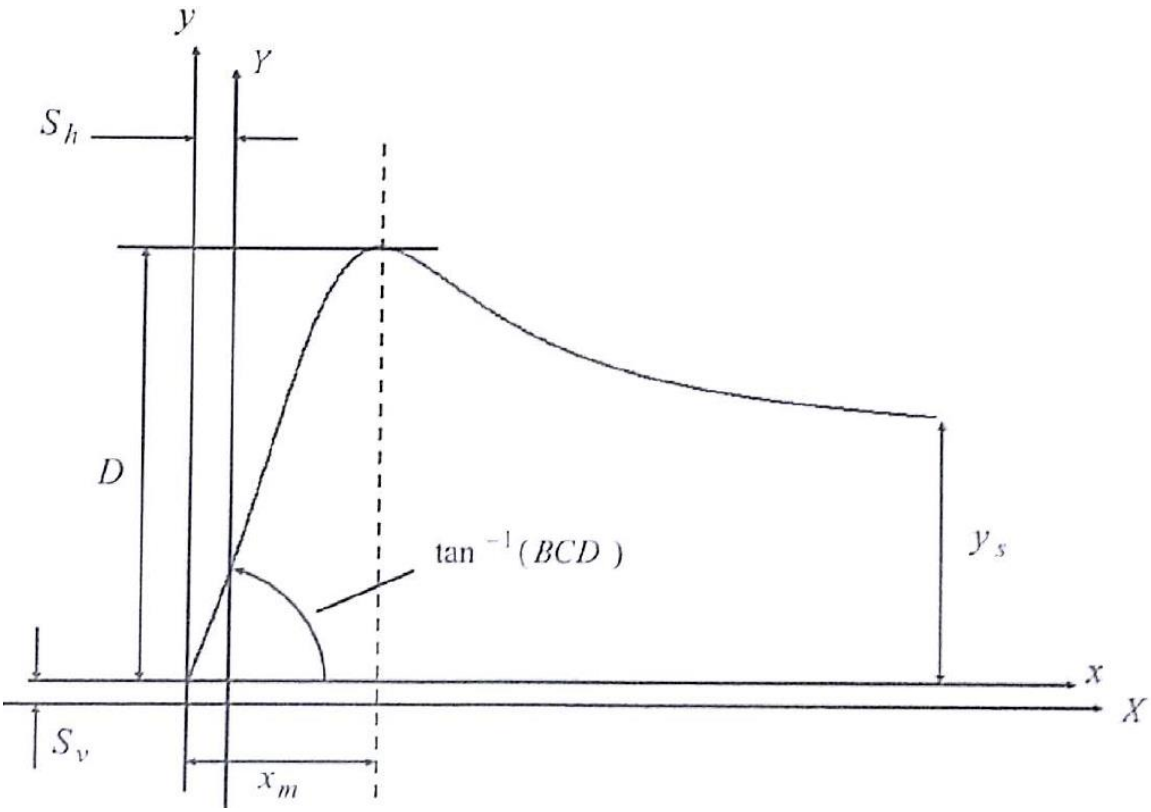

Figure 3.3: The relationship between the constants in the Pacejka Model.

The constants are normally represented by vectors so they can change with the normal loads applied to the tire. Most of the time, tires will generate more force with an increase in normal load, but there is an overall peak to the force possible. The shape of the curve also changes with normal loading (Rajamani, 2012).

Rotational Subsystem

The rotational subsystem is responsible for computing the rotational speed of the tires. It does this by summing all of the torques applied to the rotating assembly in this model. The first is the rolling resistance of the tire. Rolling resistance is the force required to maintain forward or rearward movement of the loaded pneumatic tire. The tread and underlying plies account for 2/3 of the rolling resistance of a tire while the remaining energy is absorbed by the sidewall and bead area (Tire Tech, 2017). The viscoelastic bending, stretching, and recovering is accounted for by the equation (23)

$$\overline{T_{rr}} = \overline{F_z} * \overline{\mu_{rr}} * r_{tire} \quad (23)$$

Where:

$\overline{T_{rr}}$ = torque due to rolling resistance (N*m)

$\overline{\mu_{rr}}$ = rolling resistance coefficient

Another thing that is accounted for in the rotational subsystem calculations is the drivetrain loss associated with the spinning wheel assemblies. This is a somewhat generic assumption that accounts for the frictional losses in the half-shafts and wheel bearings. From there, the sum of torques is applied to each of the wheels and once the inertia of the rotating assembly is divided out, the angular acceleration of the wheel is determined. First integral is applied and the wheel speed is established and used as an output for the slip ratio calculations.

The output of the wheel and tire assembly is the longitudinal and lateral force generated by the tires. Forces are fed into the sum of forces and moments subsystem for further calculations.

Sum of Forces and Moments

The longitudinal and lateral forces generated by the tires are in the coordinate system defined by the tire. In order to get the *Fx* and *Fy* to align with the vehicles coordinate system, a coordinate transform is necessary. A transformation matrix is used to change the forces to the body fixed coordinated. This process is shown in equation (24).

$$\begin{bmatrix} \boldsymbol{Fx} \\ \boldsymbol{Fy} \end{bmatrix}_{\boldsymbol{Body}} = \begin{bmatrix} \boldsymbol{\cos\delta} & \boldsymbol{-\sin\delta} \\ \boldsymbol{\sin\delta} & \boldsymbol{\cos\delta} \end{bmatrix}^{\boldsymbol{T}} * \begin{bmatrix} \boldsymbol{Fx} \\ \boldsymbol{Fy} \end{bmatrix}_{\boldsymbol{tire}} \quad (24)$$

With the forces in the body fixed coordinates, the torques caused by the tires can also be solved for using the cross product between the forces and the distances to the tires in X and Y. After the torques have been solved for, the vehicle's Izz inertia is divided out and the integral is taken. This gives the yaw rate of the vehicle. To calculate the acceleration of the vehicle, the force in the component directions is divided by the mass of the vehicle. This is the absolute acceleration of the coordinate frame in the body fixed coordinates. To find the true accelerations of the vehicle, equation (25) is applied.

$$\dot{\boldsymbol{V}}^{\boldsymbol{xy}}\big|_{\underline{\boldsymbol{XY}}} = \begin{bmatrix} \dot{\boldsymbol{V}}_{\boldsymbol{x}} - \boldsymbol{V}_{\boldsymbol{y}} * \boldsymbol{\omega}_{\boldsymbol{z}} \\ \dot{\boldsymbol{V}}_{\boldsymbol{y}} + \boldsymbol{V}_{\boldsymbol{x}} * \boldsymbol{\omega}_{\boldsymbol{z}} \end{bmatrix} \quad (25)$$

The accelerations and velocities are then used as an output for the sum of forces. The accelerations are used in the normal force calculations and the velocities and yaw rate are used in the coordinate transform group (Rajamani, 2012).

Coordinate Transform

Up until this point in the simulation, the forces have been with respect to the tires or the body of the car. In order to get the position of the car in global coordinates, another coordinate transform must be made. This system applies equation (24) but instead of using steering angle to perform the transform, yaw angle (ψ) is used. This will get the velocity of the car in the global coordinate system and an integral can be used to get the position of the car.

Rear Toe Controller

The rear steer calculations are comprised of four main sections, understeer calculations, error calculations, controls logic, and the Ackermann calculator.

Understeer Calculations

This system performs the understeer calculations for the controller. The inputs to the group are kinematic turning radius, yaw rate, front wheel steering angle, and the longitudinal velocity. The first thing to be computed is the actual turning radius of the car. This is done by applying equation (26).

$$\boldsymbol{r = \frac{V_x}{\omega_z}} \tag{26}$$

Where:

r = radius of the turning circle (m)

This equation is used because it will capture the sliding nature of the car since it accounts for both the velocity of the car and the rate at which it is rotating. Using this equation, the lateral acceleration of the car, in units of g, is found.

$$\boldsymbol{a_{y\,(g)} = \frac{Vx^2}{g*r}} \quad (27)$$

Where:

$a_{y\,(g)}$ = lateral acceleration (g)

Using the unit of g for the lateral acceleration is important because the standard notation of the understeer gradient is $\frac{deg}{g}$ (Reza, 2008). The understeer gradient is calculated using equation (28).

$$\boldsymbol{Kus = \left(\frac{\delta_f - \frac{L}{r_{kin}}}{a_{y(g)}}\right) * \left(\frac{180}{\pi}\right)} \quad \textbf{(28)}$$

Where:

Kus = understeer gradient (deg/g)

δ_f = front steering angle (rad)

r_{kin} = kinematic turning radius (m)

The kinematic turning radius is used in this equation because the $\frac{L}{r}$ part of the steering equation, (6), defines the low speed dynamics of the vehicle where the vehicle slip is negligible. This is a value that is simple to calculate in simulation; however, the

turning radius is very hard to calculate accurately due to sensor limitations in most production cars.

Error Calculations

The error calculation is primarily composed of the lateral acceleration lookup table. This is the table that allows for understeer control by comparing actual lateral acceleration of the car to the desired acceleration. In a traditional car, the understeer increases linearly until higher lateral g cause nonlinearities in the dynamics. This is shown in Figure 3.4.

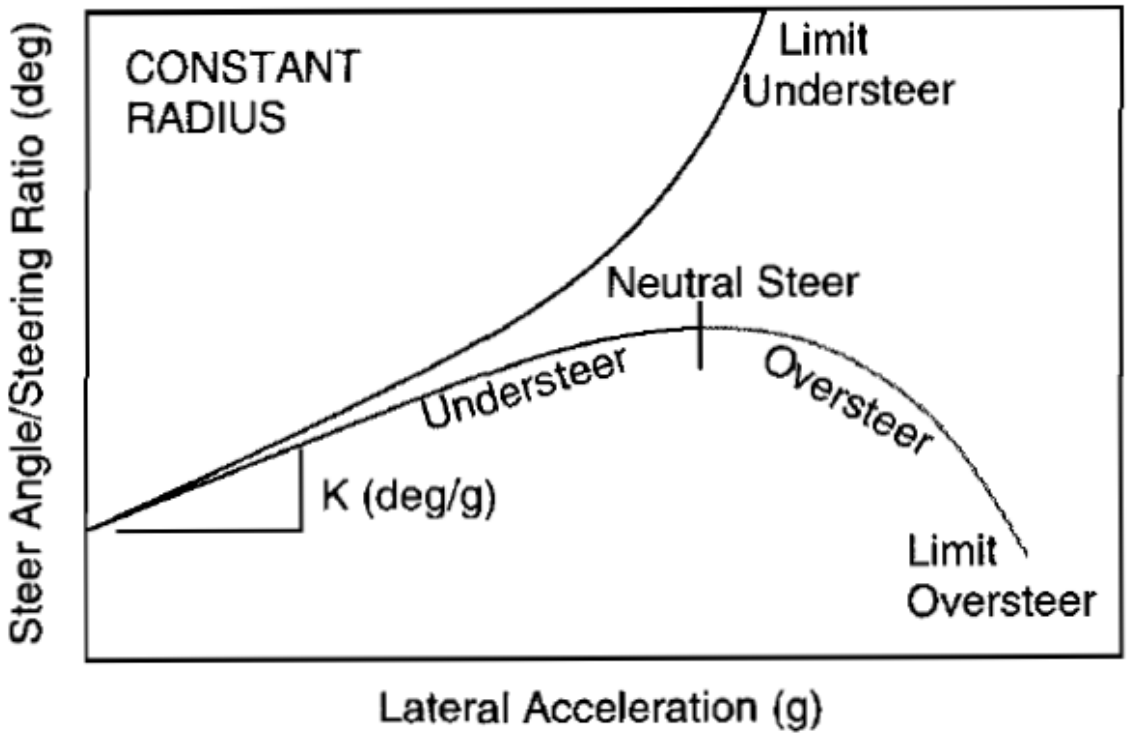

Figure 3.4: The influence of lateral acceleration on the understeer of a car.

Most production cars are designed to understeer as they approach limit grip because this is a stable condition. However, there are some conditions that tend to cause

oversteer and as previously stated, often times the understeer of a car is an afterthought of the suspension design (Gillespie, 1992).

To control the understeer of the car, the acceleration is controlled. This is because the acceleration is much easier to calculate in a production car then the understeer gradient. To increase or decrease the understeer gradient, the slope of the curve shown in figure is adjusted by changing the amount of lateral acceleration per given steering input. the actual lateral acceleration is compared to a two-dimensional lookup table containing the desired acceleration values for the range of speed and steering angles the vehicle is capable of. The table is determined by simulating the car with three different CG positions, 45% front, 50% front, and 55% front and a step steer input at a defined speed, causing the car to turn in a circle. Once steady state is achieved, the lateral acceleration and Kus are recorded. The lateral acceleration is shown for the 50% front case in table 3.1 and the others are shown in Appendix A1, B2, and B3.

Ay NS (m/s^2)		Vx																			
		2.00	4.68	7.37	10.05	12.74	15.42	18.11	20.79	23.47	26.16	28.84	31.53	34.21	36.89	39.58	42.26	44.95	47.63	50.32	53.00
Delta	-20.00	-0.6	-2.5	-5.9	-7.2	-7.3	-7.2	-7.1	-7.5	-7.5	-0.9	0.7	1.0	0.9	0.4	1.0	0.9	0.8	0.8	0.8	0.8
	-18.95	-0.5	-2.4	-5.6	-7.2	-7.4	-7.3	-7.4	-7.4	-6.9	-0.7	0.6	0.8	0.5	0.9	0.9	0.8	0.8	0.8	0.8	0.8
	-17.89	-0.4	-2.2	-5.3	-7.4	-7.4	-7.5	-7.6	-7.5	-3.7	-0.7	0.5	0.6	0.4	0.9	0.9	0.7	0.7	0.7	0.7	0.7
	-16.84	-0.4	-2.1	-5.1	-7.5	-7.5	-7.6	-7.6	-7.7	-6.4	-0.6	0.0	-0.3	-1.4	0.8	0.8	0.7	0.7	0.7	0.7	0.7
	-15.79	-0.3	-2.0	-4.8	-7.5	-7.4	-7.6	-7.7	-7.1	-2.2	-0.6	-0.5	-0.4	0.8	0.8	0.7	0.6	0.6	0.6	0.6	0.6
	-14.74	-0.4	-1.9	-4.6	-7.4	-7.2	-7.6	-7.7	-4.2	-0.8	-0.5	-0.5	-0.6	0.8	0.8	0.6	0.6	0.6	0.6	0.6	0.6
	-13.68	-0.3	-1.8	-4.1	-7.2	-7.2	-7.3	-6.8	-7.4	-0.7	-0.5	-0.5	0.7	0.7	0.7	0.6	0.6	0.5	0.5	0.5	0.5
	-12.63	-0.3	-1.6	-3.8	-6.9	-7.3	-6.3	-5.4	-5.7	-0.6	-0.5	-0.4	0.7	0.7	0.7	0.5	0.5	0.5	0.5	0.5	0.5
	-11.58	-0.3	-1.5	-3.6	-6.5	-7.5	-6.4	-7.5	-2.5	-0.6	-0.5	-0.3	0.6	0.6	0.6	0.5	0.5	0.4	0.4	0.4	0.4
	-10.53	-0.3	-1.3	-3.2	-6.0	-7.5	-6.7	-7.7	-1.2	-0.6	-0.4	0.6	0.6	0.6	0.6	0.5	0.4	0.4	0.4	0.4	0.4
	-9.47	-0.2	-1.3	-3.0	-5.4	-7.4	-7.1	-7.8	-1.2	-0.7	-0.6	0.5	0.5	0.5	0.5	0.5	0.4	0.4	0.4	0.3	0.3
	-8.42	-0.2	-1.1	-2.6	-4.8	-7.1	-7.5	-7.4	-2.6	-0.8	6.0	0.5	0.5	0.5	0.5	0.5	0.4	0.3	0.3	0.3	0.3
	-7.37	-0.1	-0.9	-2.3	-4.2	-6.5	-7.6	-6.9	-7.5	-0.9	-0.8	0.4	0.4	0.4	0.4	0.4	0.4	0.4	0.3	0.3	0.3
	-6.32	-0.1	-0.8	-2.0	-3.6	-5.7	-7.4	-7.6	-7.1	-6.4	-0.9	-0.3	0.4	0.4	0.4	0.4	0.4	0.4	0.4	0.4	0.4
	-5.26	-0.1	-0.7	-1.6	-3.0	-4.8	-6.7	-7.5	-7.2	-7.2	-7.1	-0.9	-0.3	0.3	0.3	0.3	0.3	0.3	0.3	0.3	0.3
	-4.21	-0.1	-0.5	-1.4	-2.5	-3.8	-5.5	-7.0	-7.6	-7.4	-7.1	-7.8	-5.5	-0.7	-0.2	-0.1	0.3	0.3	0.3	0.3	0.3
	-3.16	-0.1	-0.4	-1.0	-1.8	-2.8	-4.2	-5.7	-6.9	-7.6	-7.6	-7.4	-7.3	-7.4	-7.6	-6.1	-1.0	-0.2	4.7	0.0	0.2
	-2.11	0.0	-0.3	-0.7	-1.2	-1.9	-2.8	-3.7	-4.9	-6.1	-7.0	-7.5	-7.7	-7.8	-7.8	-7.7	-7.7	-7.6	-7.5	-7.1	-6.5
	-1.05	0.0	-0.1	-0.3	-0.6	-0.9	-1.4	-1.9	-2.4	-2.9	-3.7	-4.6	-5.3	-6.1	-6.8	-7.2	-7.4	-7.6	-7.8	-7.9	-7.9
	0.00	0.0	0.0	0.0	0.0	0.0	0.0	0.0	0.0	0.0	0.0	0.0	0.0	0.0	0.0	0.0	0.0	0.0	0.0	0.0	0.0
	1.05	0.0	0.1	0.3	0.6	0.9	1.4	1.9	2.4	2.9	3.7	4.6	5.3	6.1	6.8	7.2	7.4	7.6	7.8	7.9	7.9
	2.11	0.0	0.3	0.7	1.2	1.9	2.8	3.7	4.9	6.1	7.0	7.5	7.7	7.8	7.8	7.7	7.7	7.6	7.5	7.1	6.5
	3.16	0.1	0.4	1.0	1.8	2.8	4.2	5.7	6.9	7.6	7.6	7.4	7.3	7.4	7.6	6.1	1.0	0.2	-4.7	0.0	-0.2
	4.21	0.1	0.5	1.4	2.5	3.8	5.5	7.0	7.6	7.4	7.1	7.8	5.5	0.7	0.2	0.1	-0.3	-0.3	-0.3	-0.3	-0.3
	5.26	0.1	0.7	1.6	3.0	4.8	6.7	7.5	7.2	7.2	7.1	0.9	0.3	-0.3	-0.3	-0.3	-0.3	-0.3	-0.3	-0.3	-0.3
	6.32	0.1	0.8	2.0	3.6	5.7	7.4	7.6	7.1	6.4	0.9	0.3	-0.4	-0.4	-0.4	-0.4	-0.4	-0.4	-0.4	-0.4	-0.4
	7.37	0.1	0.9	2.3	4.2	6.5	7.6	6.9	7.5	0.9	0.8	-0.4	-0.4	-0.4	-0.4	-0.4	-0.4	-0.4	-0.3	-0.3	-0.3
	8.42	0.2	1.1	2.6	4.8	7.1	7.5	7.4	2.6	0.8	-6.0	-0.5	-0.5	-0.5	-0.5	-0.5	-0.4	-0.3	-0.3	-0.3	-0.3
	9.47	0.2	1.3	3.0	5.4	7.4	7.1	7.8	1.2	0.7	0.6	-0.5	-0.5	-0.5	-0.5	-0.5	-0.4	-0.4	-0.4	-0.3	-0.3
	10.53	0.3	1.3	3.2	6.0	7.5	6.7	7.7	1.2	0.6	0.4	-0.6	-0.6	-0.6	-0.6	-0.5	-0.4	-0.4	-0.4	-0.4	-0.4
	11.58	0.3	1.5	3.6	6.5	7.5	6.4	7.5	2.5	0.6	0.5	0.3	-0.6	-0.6	-0.6	-0.5	-0.5	-0.4	-0.4	-0.4	-0.4
	12.63	0.3	1.6	3.8	6.9	7.3	6.3	5.4	5.7	0.6	0.5	0.4	-0.7	-0.7	-0.7	-0.5	-0.5	-0.5	-0.5	-0.5	-0.5
	13.68	0.3	1.8	4.1	7.2	7.2	7.3	6.8	7.4	0.7	0.5	0.5	-0.7	-0.7	-0.7	-0.6	-0.6	-0.5	-0.5	-0.5	-0.5
	14.74	0.4	1.9	4.6	7.4	7.2	7.6	7.7	4.2	0.8	0.5	0.5	0.6	-0.8	-0.8	-0.6	-0.6	-0.6	-0.6	-0.6	-0.6
	15.79	0.3	2.0	4.8	7.5	7.4	7.6	7.7	7.1	2.2	0.6	0.5	0.4	-0.8	-0.8	-0.7	-0.6	-0.6	-0.6	-0.6	-0.6
	16.84	0.4	2.1	5.1	7.5	7.5	7.6	7.6	7.7	6.4	0.6	0.0	0.3	1.4	-0.8	-0.8	-0.7	-0.7	-0.7	-0.7	-0.7
	17.89	0.4	2.2	5.3	7.4	7.4	7.5	7.6	7.5	3.7	0.7	-0.5	-0.6	-0.4	-0.9	-0.9	-0.7	-0.7	-0.7	-0.7	-0.7
	18.95	0.5	2.4	5.6	7.2	7.4	7.3	7.4	7.4	6.9	0.7	-0.6	-0.8	-0.5	-0.9	-0.9	-0.8	-0.8	-0.8	-0.8	-0.8
	20.00	0.6	2.5	5.9	7.2	7.3	7.2	7.1	7.5	7.5	0.9	-0.7	-1.0	-0.9	-0.4	-1.0	-0.9	-0.8	-0.8	-0.8	-0.8

Table 3.1: The lateral acceleration output table for the 50% front weight distribution.

On this table, the sections colored in green and red are higher lateral accelerations. The outliers (the opposite colored sections) are because the car is unstable, beyond peak tire grip, and therefore should be ignored. The control map used for active rear toe combines the favorable portions of all three lateral acceleration surfaces. It is based off the 55% forward table because it is stable; however, it smooths out the

variations at higher speed. It also extrapolates the table into the region where the tires are saturated at high speed and turning. This region is not one that cars operate in but the table can account for it and it is better to try to control the car. Acceleration is used instead of the understeer gradient because the lateral acceleration of the car is less sensitive and is therefore easier to control. Also, on the actual car, the understeer is a harder thing to calculate because there are more measured values needed and more uncertainty in the calculations; but the lateral acceleration is calculated using the accelerometer and not derived from any data. The control surface along with the other tables, is shown in Appendix A1, B2, and B3.

Controls Strategy

There are two main controls strategies applied to the model in order to control the understeer of the car, PID and sliding mode. There are also two forms of sliding mode control applied to the model, a switching and a hyperbolic-tangent model.

The PID control is used in the rear toe controller for model validation and the linear region of the car. The controllers control loop is shown in Figure 3.5.

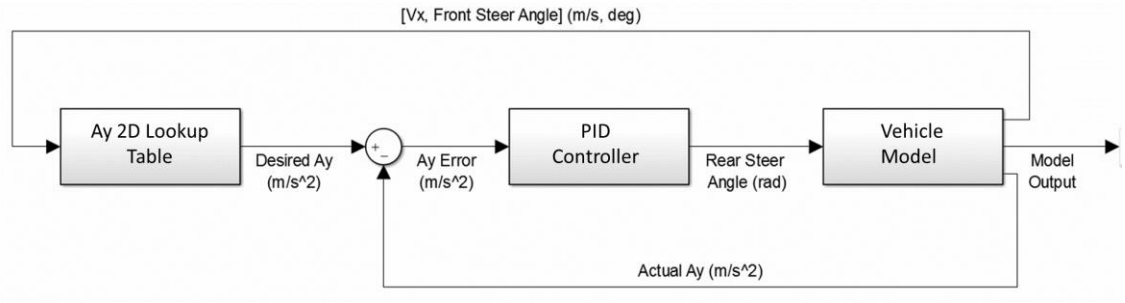

Figure 3.5: The Controls loop for the PID Controller ART system.

Because of the simplicity of the controller, it is a powerful controller for making sure the model is operating correctly. Simulink applies equation (29) for the PID control.

$$\boldsymbol{C_{par}(S) = \left[P + I\left(\frac{1}{s}\right) + D\left(\frac{Ns}{s+N}\right)\right]} \quad \textbf{(29)}$$

Where:

P = Proportional gain

I = Integral gain

D = Derivative gain

N = Filter Coefficient

This controller works well when the car is at low speeds and the nonlinear effects of the tires are minimal. An advantage this has over the more robust sliding mode is there is no chattering using this controller (Mathworks, 2017).

The first type of sliding mode control is the type 1 zeno controller. This controller is defined by a switching surface $g(x) = 0$. In this controller, there are also two functions, f_1 and f_2, shown in Figure 3.6.

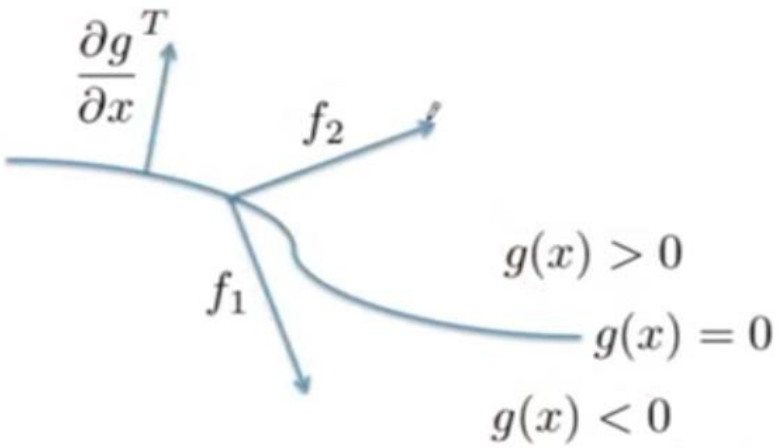

Figure 3.6: The f_1 and f_2 funtions and the switching surface.

Sliding along the switching surface occurs if the inner product between the gradient of $g(x)$ and f_2 is positive and the inner product between the gradient of $g(x)$ and f_1 is negative.

$$\frac{\partial g^T}{\partial x} * f_2 > 0 \ \textit{and} \ \frac{\partial g^T}{\partial x} * f_1 < 0 \ \text{at g(x)} = 0 \quad \textbf{(30)}$$

This multiplication of the derivative of g in the direction f is known as the Lie derivative and is notated as L_{fg}. The speed along the sliding surface is determined by equation (31).

$$\dot{x} = \sigma_1 f_1 + \sigma_2 f_2 \quad \textbf{(31)}$$

Sliding occurs when $g = 0 || \frac{dg}{dt} = 0$. Applying this to equation (31) yields the following.

$$\frac{dg}{dt} = \frac{dg}{dx}\dot{x} = \frac{dg}{dx}(\sigma_1 f_1 + \sigma_2 f_2) \quad \textbf{(32)}$$

$$\frac{dg}{dt} = 0 = \sigma_1 L_{f_1 g} + \sigma_2 L_{f_2 g} \quad (33)$$

$$\sigma_2 = -\sigma_1 \frac{L_{f_1 g}}{L_{2g}} \quad (34)$$

Since $\dot{x}$ must remain positive, σ_1 and σ_2 can be solved for and the following statements can be made.

$$\sigma_1, \sigma_2 \geq 0 \; and \; \sigma_1 + \sigma_2 = 1 \quad (35)$$

For the controls strategy of using sliding mode control to turn the rear wheels of a car, equation (35) sets what the gains for the positive and negative controller can be. As mentioned above, this controller is a type 1 zeno, meaning it switches an infinite number of times in a finite time interval (Zhang, Johansson, John, & Sastry). The switching nature of the sliding mode control allows it to following the sliding surface, shown in Figure 3.7.

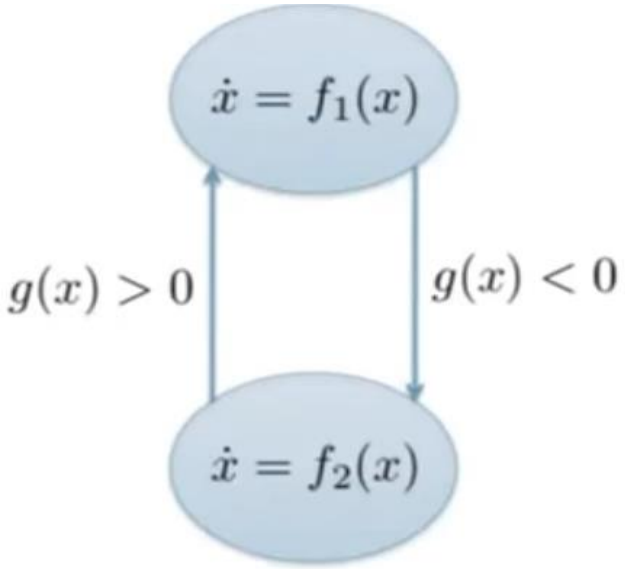

Figure 3.7: The switching nature of a type 1 Zeno sliding mode controller.

Using this strategy, it is possible to have a controller that compensates more in one direction than the other. For example, if the car has a tendency to oversteer, a smaller gain is needed to accomplish an oversteer maneuver and therefore the gain for the understeer can be higher (Egerstedt, 2000).

Due to the instant switching nature of this controller, it does suffer from chatter issues. To deal with this issue, a hyperbolic tangent is used. The hyperbolic tangent has a domain of $[-\infty, \infty]$, but its range is constrained to [-1,1]. It is asymptotic to its range, but the transition between the positive and negative ranges is a smooth transition shown in Figure 3.8

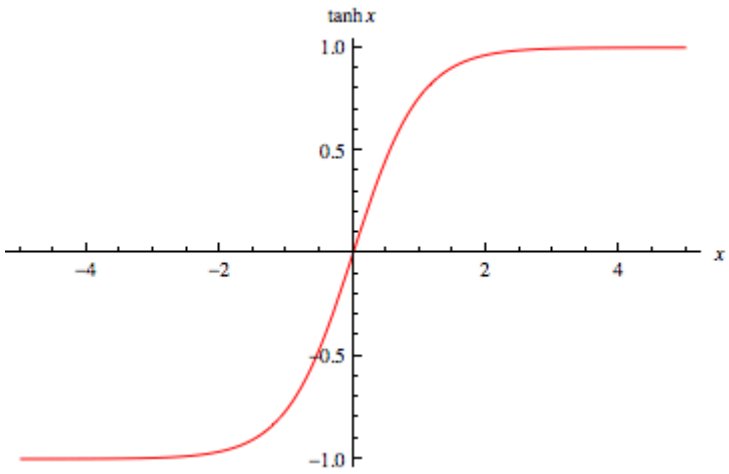

Figure 3.8: The hyperbolic tangent as y=tanh(x).

When this smooth center section is applied to a sliding mode controller, the control effort lowers as $g \rightarrow 0$ and smoothly increases as g increases. There is a gain placed before the hyperbolic tangent, this determines the boundary layer of the system by applying the following equation.

$$u = \eta \tanh\left(\frac{S}{BL}\right) \quad \textbf{(36)}$$

Where:

u = Control output

η = Gain on controller

S = Controls Input

BL = Boundary Layer of the controller

Using the boundary layer, errors under three times the boundary layer are reacted roughly linearly, however the function behaves like a signum above the boundary layer. This is very similar to the behavior of the equation shown in equation (10) (Deyer, 1979).

Unlike a PID controller, a sliding mode conller can not run off the remainder between the desired value and the actual value. If this is used, as error goes to 0, the control input also goes to 0, instead, a term S is used. Equation 37 shows how S is calculated.

$$S = \dot{\tilde{X}} + \lambda * \tilde{X} \quad \textbf{(37)}$$

With

$$\tilde{X} = Ay - Ay_{desired} \quad \textbf{(38)}$$

Where:

S = Input to the Sliding Mode Control

λ = The First Derivative of the Desired Lateral Acceleration

To implement the sliding mode controller, a different controls loop must be applied as shown in Figure 3.9.

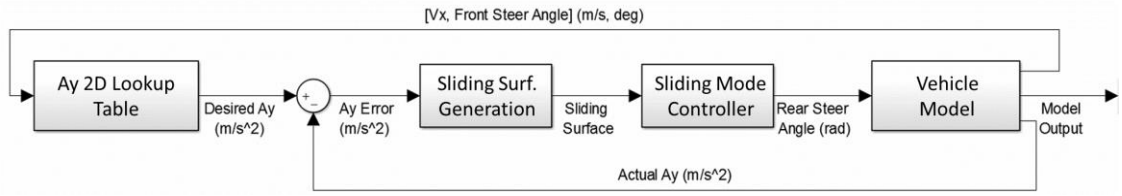

Figure 3.9: The controls loop for the sliding mode controlled ART.

The main difference between the controller's loop is the addition of the sliding surface generation. Without this block, the controller would be very ineffective at controlling the varying lateral acceleration.

Ackermann for Active Rear Toe

In order to maintain the ackermann steering for the rear toe of the car, independent control of the rear toe is implimented. This system maintains true ackermann steering in the rear wheels. It works by first computing the kinematic turning radius of the car, accounting for front wheel steering angle and the desired rear steering angle. The kinematic turning center is different then the actual steering center because it does not account for any slip in the tires. The two radii are similar for low speed dynamics, but the effects of the slip are apparent when comparing the kinematic radii to the one described in equation (26). The graphical representation of the kinematic turning center is shown in Figure 3.10.

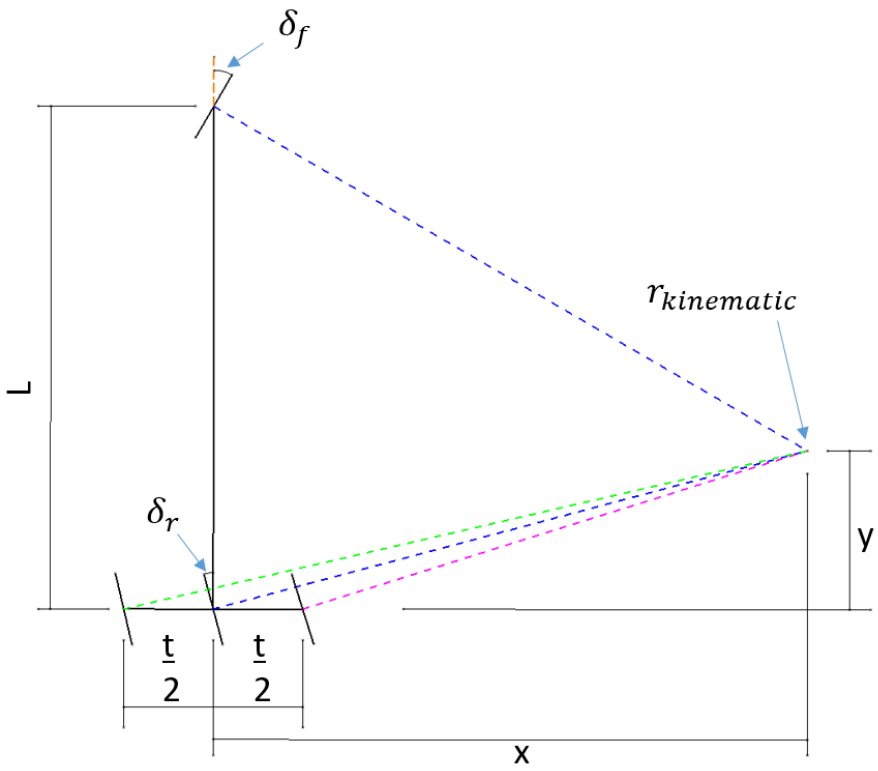

Figure 3.10: The graphic representation of the kinematic turning radius.

In order to calculate the kinematic turning radius, it is broken into its component directions, and solved for in equations (40) and (41). In order for the equations to be applicable in both positive and negative steering directions, the sign of the δ_f must be accounted for as shown in equation (39).

$$sgn = \begin{cases} -1 \; for \; \delta_f > 0 \\ 1 \; for \; \delta_f \leq 0 \end{cases} \tag{39}$$

$$X = \frac{L}{\tan(sgn * \delta_r) - \tan(sgn * \delta_f)} \tag{40}$$

$$Y = \tan(sgn * \delta_r) * X \tag{41}$$

With the component directions acounted for, the quadratic equation can be applied to determine the kinematic radius of the turn.

Since the rear wheels must turn at diffenent angles to achieve the ackermann steering, equations (42) and (43) are used to determine the necessary steering angles for the left and right wheels, δ_{rl} and δ_{rr} respectivly.

$$\boldsymbol{\delta_{rl} = -\tan^{-1}\left(\frac{Y}{x-\left(sgn*\left(\frac{t}{2}\right)\right)}\right)} \quad \textbf{(42)}$$

$$\boldsymbol{\delta_{rr} = -\tan^{-1}\left(\frac{Y}{x+\left(sgn*\left(\frac{t}{2}\right)\right)}\right)} \quad \textbf{(43)}$$

These two steering angles are the outputs of the rear toe controller. They are then used directly in the vehicle model to set the toe of rear wheels on the car. The Simulink block diagrams for the important systems are shown in Appendix A.

Chapter 4

Model Validation: ISO Standard Testing

In order to validate the 9 DOF model, physical testing is required. A 2007 Honda Accord on standard tires was used to perform the ISO4138:1996(E) test. This is a steady state circular driving test used to quantify the understeer of the car. The 4138 is especially important to this model because it needs to have proper understeer characteristics. For the ISO test to be valid, the measurement accuracy must remain in the tolerance specified in Table 4.1.

Table 4.1: The required tolerance for all the measurements in ISO4138.

Variable	Typical operating range	Recommended maximum error of the combined transducer and recorder system
Steering-wheel angle	− 360° to + 360°	± 2°, for angles < 180° ± 4°, for angles > 180°
Yaw velocity	− 50°/s to + 50°/s	± 0,5°/s
Sideslip angle	− 15° to + 15°	± 0,5°
Longidutinal velocity	0 m/s to 50 m/s	± 0,5 m/s
Lateral acceleration	− 15 m/s² to + 15 m/s²	± 0,15 m/s²
Steering-wheel torque	− 30 N·m to + 30 N·m	± 0,3 N·m
Roll angle	− 15° to + 15°	± 0,15°
NOTE — Transducers for measuring some of the listed variables are not widely available and are not in general use. Many such instruments are developed by users. If any system error exceeds the recommended maximum value, this and the actual maximum error shall be stated in the test report (see annex A).		

The required measurements to perform this test are steering position and lateral acceleration, the remaining measurements are optional but advised. In order to find the steering angle and keep the measurements within the required tolerance, an AMT-203 absolute encoder is turned using a 1:1 gear ratio on with a gear fixed around the steering I-shaft. This setup is shown in Figure 4.1.

Variable	Typical operating range	Recommended maximum error of the combined transducer and recorder system
Steering-wheel angle	− 360° to + 360°	± 2°, for angles < 180° ± 4°, for angles > 180°
Yaw velocity	− 50°/s to + 50°/s	± 0,5°/s
Sideslip angle	− 15° to + 15°	± 0,5°
Longidutinal velocity	0 m/s to 50 m/s	± 0,5 m/s
Lateral acceleration	− 15 m/s² to + 15 m/s²	± 0,15 m/s²
Steering-wheel torque	− 30 N·m to + 30 N·m	± 0,3 N·m
Roll angle	− 15° to + 15°	± 0,15°

NOTE — Transducers for measuring some of the listed variables are not widely available and are not in general use. Many such instruments are developed by users. If any system error exceeds the recommended maximum value, this and the actual maximum error shall be stated in the test report (see annex A).

Figure 4.1: The placement of the absolute encoder in the I-shaft. Note, the original setup used a 1:4 gear ratio as shown here.

The original encoder setup used a 1:4 gear ratio which caused truncation of the data under high speed turning events, so the fixture has been modified to have a 1:1 gear ratio. The encoder has an accuracy of .09^{o}, which is within the ISO standard and is able to deliver clean and accurate data (CUI INC, 2016). One of the uncertainties with this setup is the possible cyclic nature of the I-shaft's speed due to the phasing of the universal joints. Acceleration, rotational rate, and angular position measurements are taken using an Adafruit LSM9DS1 9-DOF IMU. This breakout board contains a LGA-24L sensor for the positional measurements. A benefit of having the angular position and acceleration data generated by the same sensor is the sensor accounts for gravitational acceleration and filters the offset out. This is good for this testing because the effects of body roll do not cause skewed data (ST: Life Augmented, 2015).

ISO4138 contains location requirements. First, the surface must be dry asphalt, concrete, or other high μsurface. The surface must also have a gradient of less than 2.5% at any location. The test itself begins at low speeds and a constant steering wheel position so the car turns in a circle with a minimum radius of 30m. The car slowly increases in speed so the transient effects of the car do not affect the dynamics of the suspension. According to the standard, if the steering angle differs by more than 10 degrees, it must be noted.

To calculate the angle of the tires with the steering wheel is turned, the steering wheel is turned and the angle of the road wheels are recorded as shown in Figure 4.2.

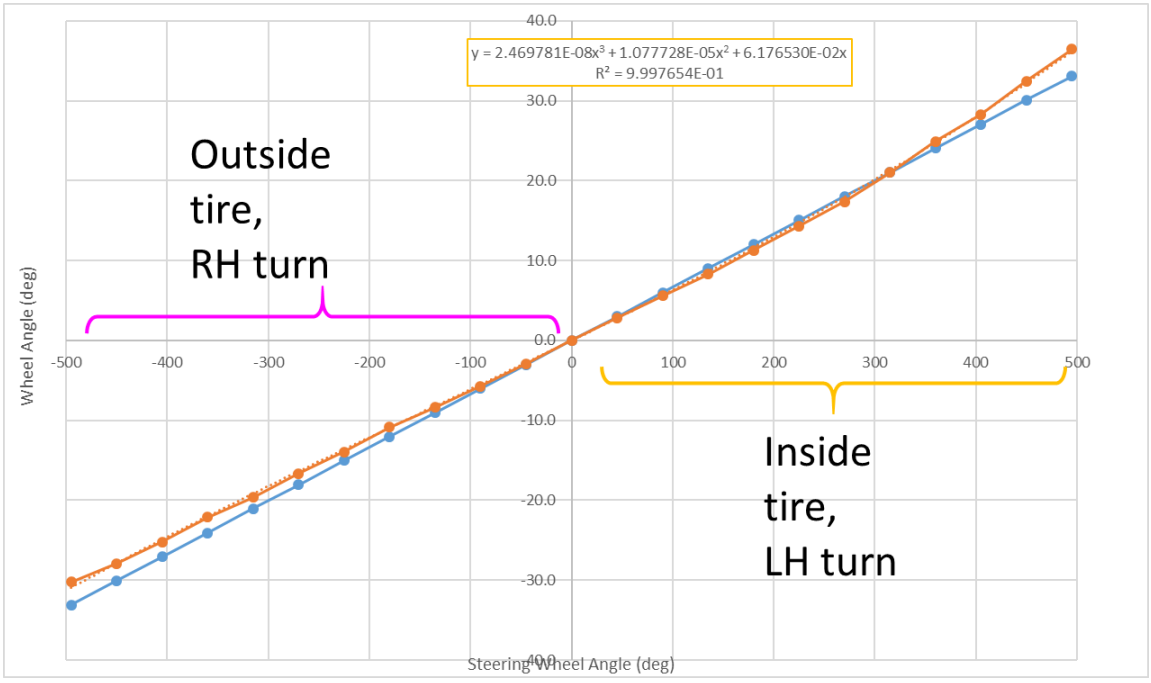

Figure 4.2: The relationship between degrees of and wheel angle to steering angle.

This relationship is then applied to the model to convert the test data to the road wheel angle on the car. As shown by the trend line, the steering relationship is almost linear.

The ISO test is conducted using a right hand turn. The GPS plot during the test is shown in Figure 4.3.

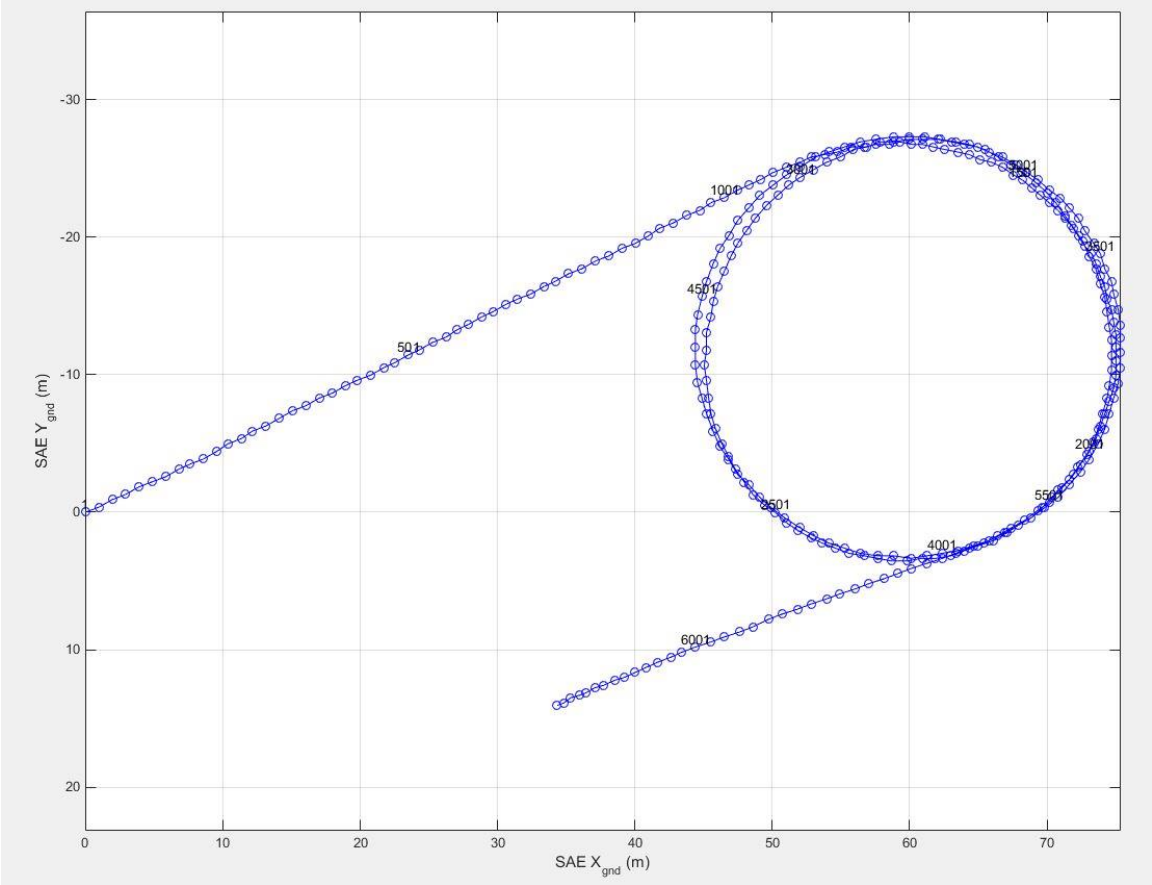

Figure 4.3: The vehicle position as gathered by the GPS unit (100hz).

The steering angle was held as steady as possible so human error and the vehicle's understeer both contribute to the drift in the GPS data. It could also come from the accuracy of the GPS system used. In order to validate the tire model, the data is repeated

and inverted for the steering and lateral acceleration of the ISO4138 test. The above mentioned steering wheel position is shown in Figure 4.4. Because the test is conducted in one direction, error and overtraining can occur during the optimization. Because of this, the test is run twice, the second time with inverted steering and lateral acceleration.

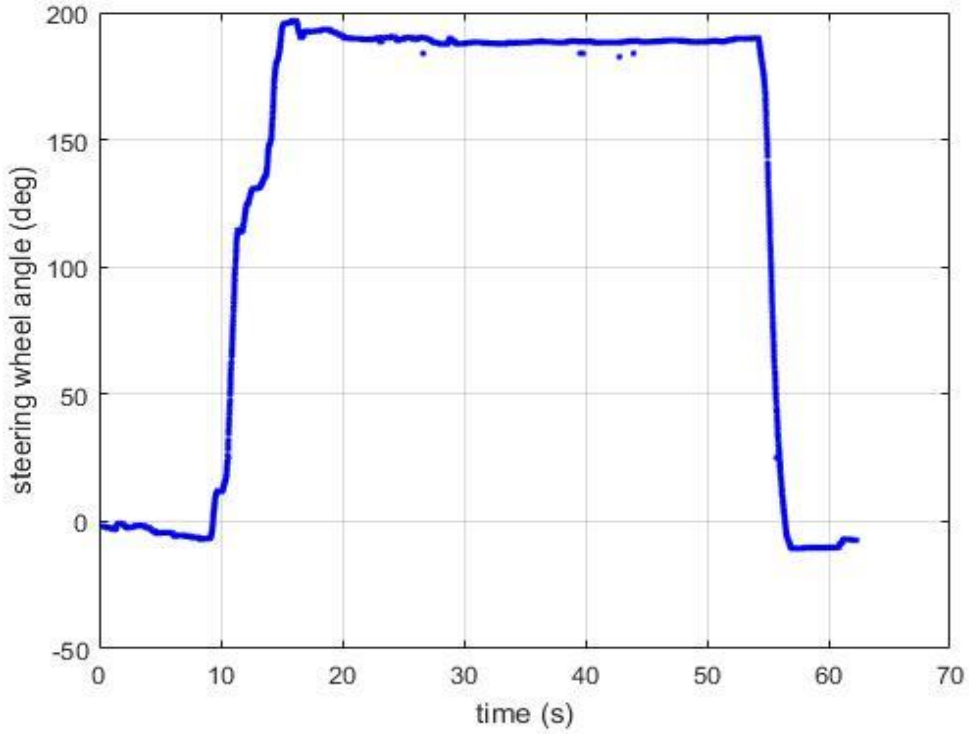

Figure 4.4: The handwheel steering angle from the ISO test.

The encoder had some erroneous, shown by the sudden dips in the data. These errors are insignificant to the simulation because of their very short duration. The vehicles speed was determined by the GPS unit. It is shown in Figure 4.5.

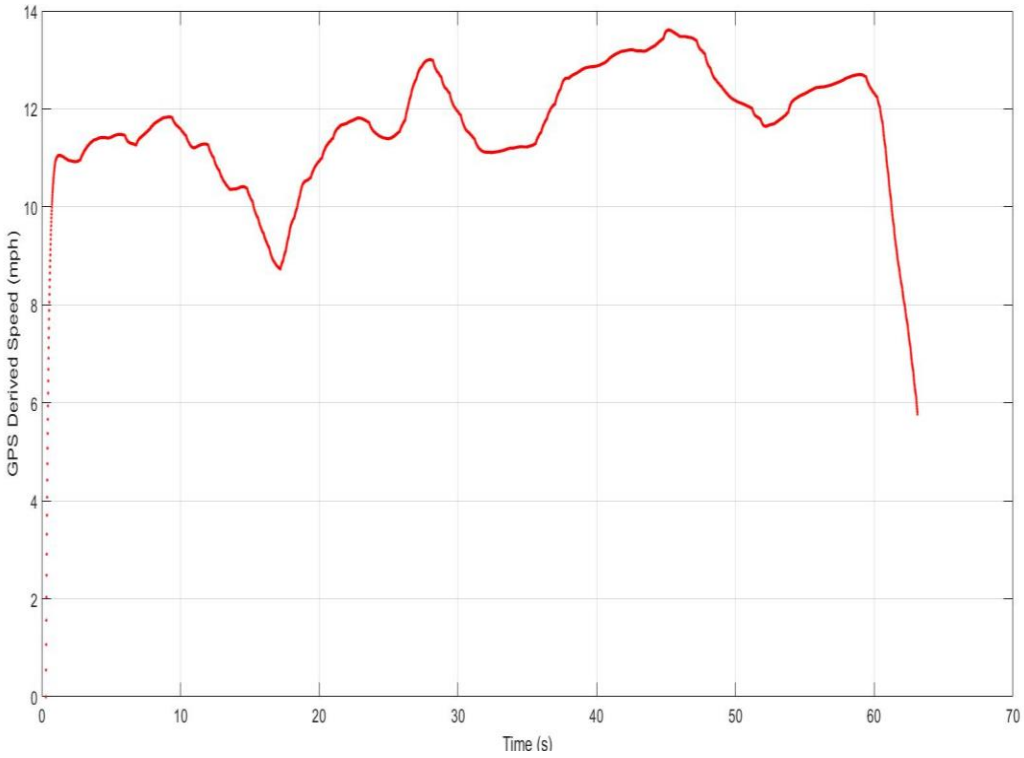

Figure 4.5: The GPS derived vehicle velocity.

. Because the test car only turned in the positive direction, the simulation was ran twice with the steering and acceleration inverted.

Model Validation: Tire Model Correlation

Tires are the only part of the car that produces a force that moves the car, therefore they are able to produce the largest change in the lateral and longitudinal capabilities of the car. There are also large fluctuations of the shape on the force curves generated by different types of tire. In order to optimize the tire model to correlate the model to the real world, it is first necessary to determine the cost function. Because the lateral force is necessary for the understeer controller, it was chosen as the variable to optimize. For this optimization function, the residual is shown in equation (44).

$$J = \int (\tilde{X})^2 \quad \textbf{(44)}$$

Where:

J = Cost Function

$\tilde{X}$ = Remainder of the Simulated and Actual Test Data

Fmincon is the chosen solver to optimize the tire function. This solver finds the constrained minimum of a scalar function of several variables using an initial starting estimate. It is generally referred to as a constrained nonlinear optimization and is in the nonlinear programming family. The function in this situation optimizes the D, B, C, and E Pacejka parameters are 4 different loading conditions, 2, 4, 6, and 8 kN in order to match the lateral acceleration of the test car (University of California at Berkley). The initial estimates, bounds, and termination tolerances are shown in Table 4.2.

Table 4.2: The initial estimate, upper and lower bounds, and termination tolerance for the FMINCON function.

FMINCON parameters	D (N)				B				C				E			
Normal Load (kN)	2	4	6	8	2	4	6	8	2	4	6	8	2	4	6	8
Initial Estimate	1500	3000	5000	6000	0.244	0.24	0.16	0.112	1.5	1.19	1.27	1.36	-0.132	-0.678	-1.61	-2.16
Lower Bound	1000	1000	1000	1000	0	0	0	0	0	0	0	0	-4	-4	-4	-4
Upper Bound	7000	7000	7000	7000	4	4	4	4	4	4	4	4	0	0	0	0
Function Falue Termination Tolerance:					0.001											
Termination Tolerance on X					0.001											

The initial estimate used is a nominal tire model. When it is used in the simulation, it produces the acceleration in Figure 4.6.

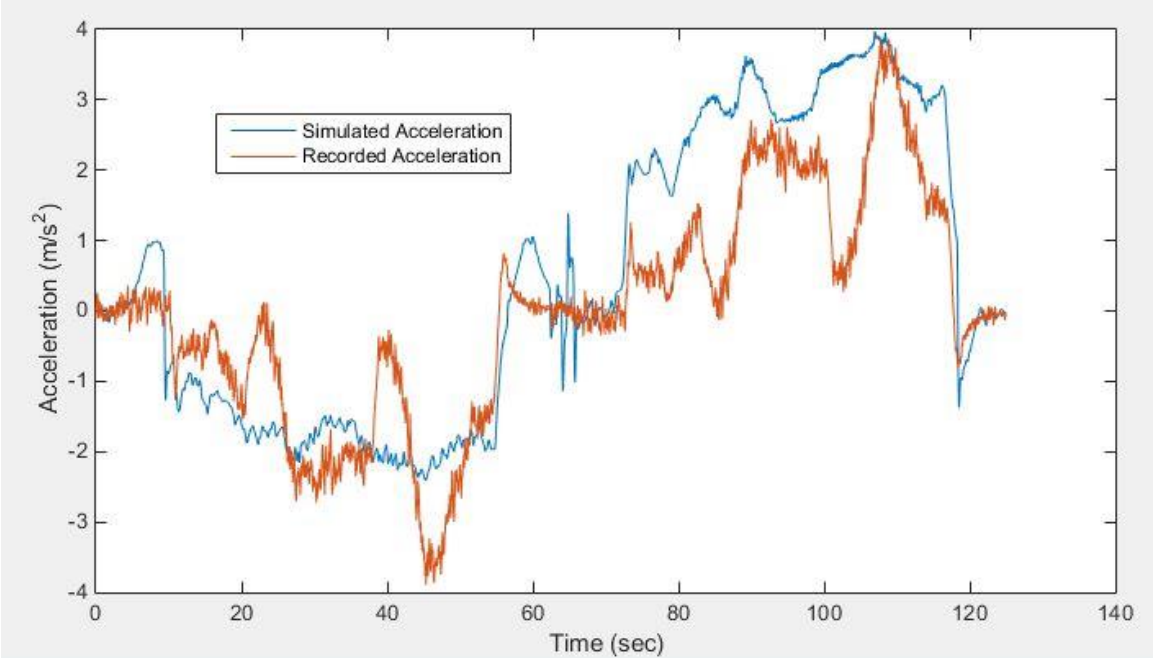

Figure 4.6: The simulated and recorder lateral acceleration.

There is poor agreement between the simulated and recorded data after 60 seconds, when the simulation is repeated and the steering and acceleration are negated. This shows that the original Pacejka coefficients caused the car to perform asymmetrically. This is shown in the offset in the error in Figure 4.7.

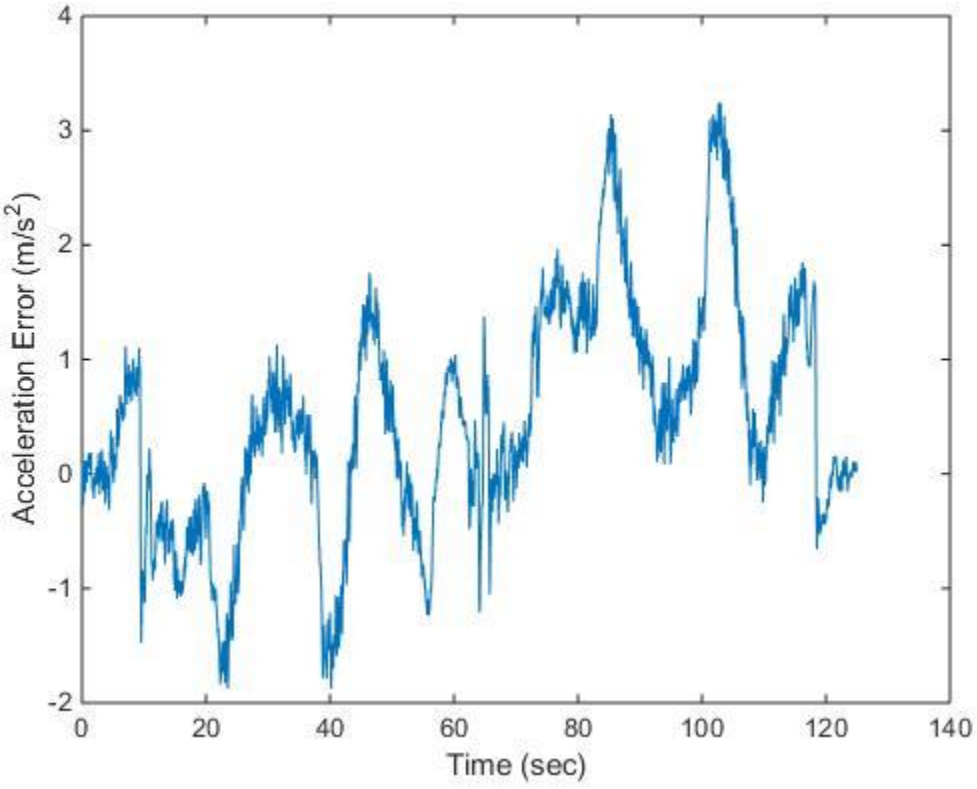

Figure 4.7: The error between the calculated and measured lateral acceleration.

The recorded data has large fluctuations in acceleration. Ideally this is a smooth increase as the speed steadily increases. However, due to the slow nature and limited testing space, cruise control could not be engaged therefore the speed is susceptible to human error. It is also possible to have fluctuations in the GPS derived speed due to the ~±2m tolerance. Another possible cause of the error is the body roll of the car. This would cause the lateral acceleration measurement to be skewed because of the angle of the car. The body roll of the car is shown in Figure 4.8.

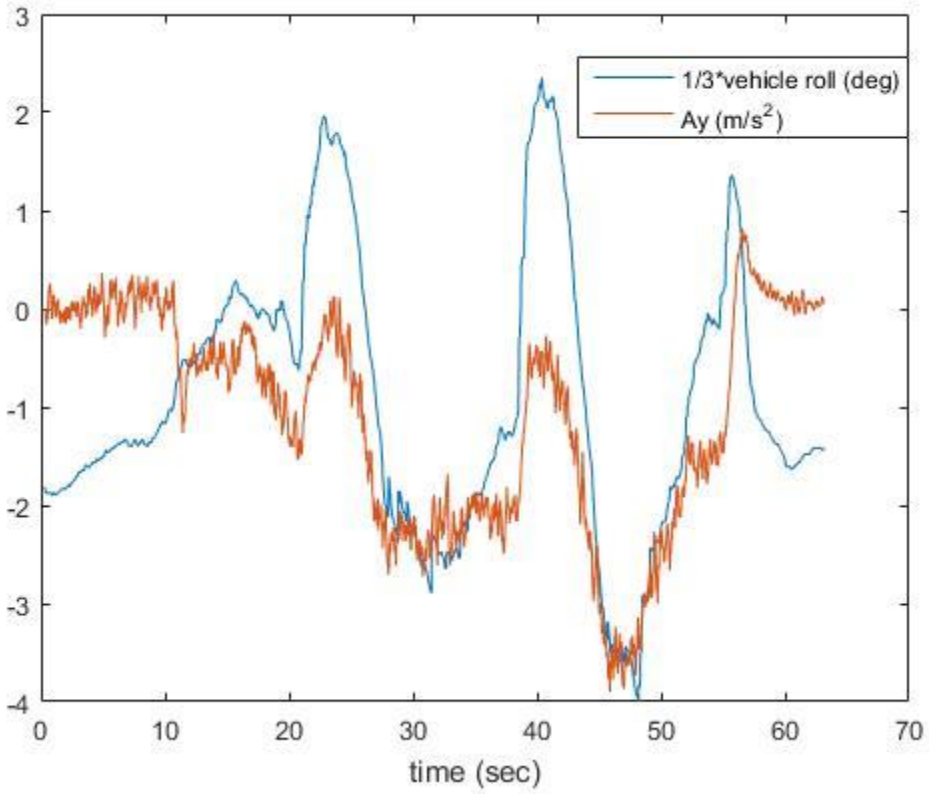

Figure 4.8: The body roll of the Honda Accord during the ISO testing.

7 DOF model is a rigid body, it accounts for weight transfer but because there is not suspension i.e. no damping, the weight transfers instantly. This also means that the simulation also does not account for roll and the effects of it. However, the real-world cars have a suspension and dampers. Based on Figure 4.8, the correlation between vehicle roll and lateral acceleration is shown. Due to the irregularities in the data and the generic tire coefficients, the tire model integral of the square of the remainder was $83\frac{m}{s}$, as shown in Figure 4.9.

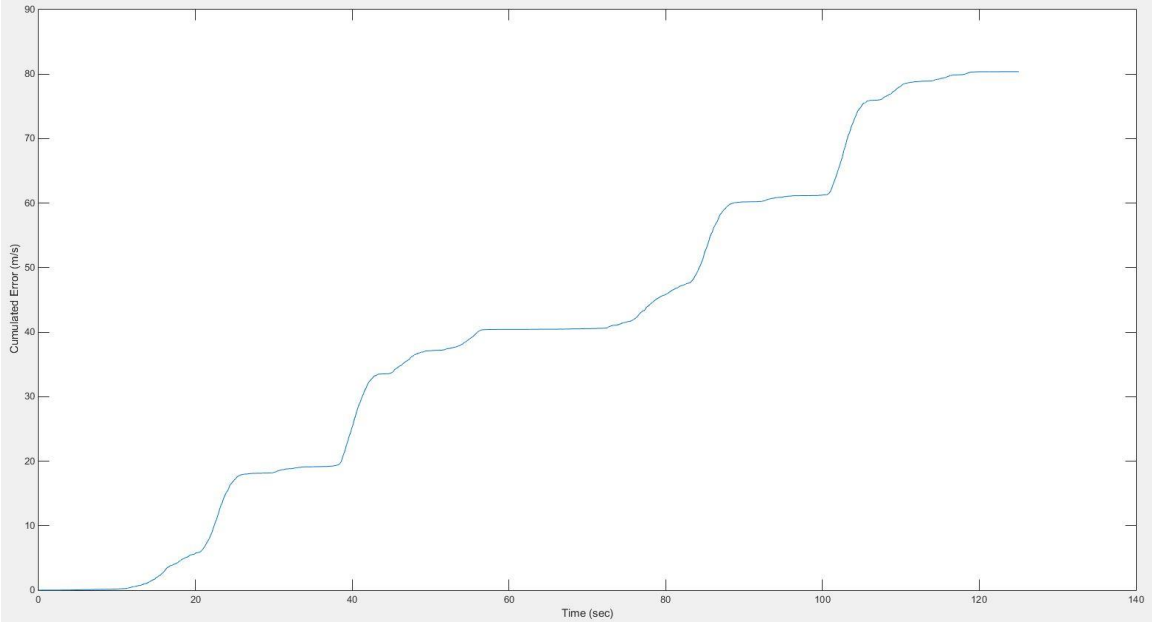

Figure 4.9: The cumulated error in the base tire model.

The error only increases because of the way the J function is written, with the integral of the square. The tire model did not accurately capture the dynamics of the model. It generated more force in the positive y direction than the negative. It also produced abnormal results in the middle section around 65 seconds into the simulation. The model after the FMINCON optimization script is shown in Figure 4.10.

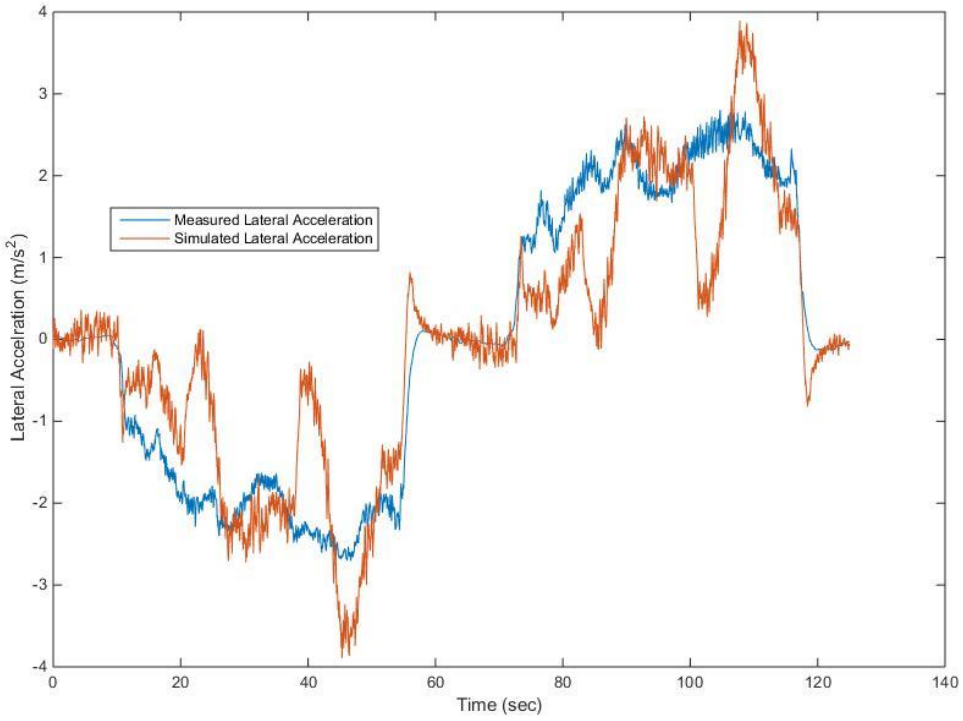

Figure 4.10: The optimized tire data and the measured acceleration data.

The optimized model is more symmetric than the previous tire model, allowing for reduction in the error. There is a higher amplitude on the noise in the model, but that is also shown in the accelerometer data. The cumulatives error is shown in Figure 4.11.

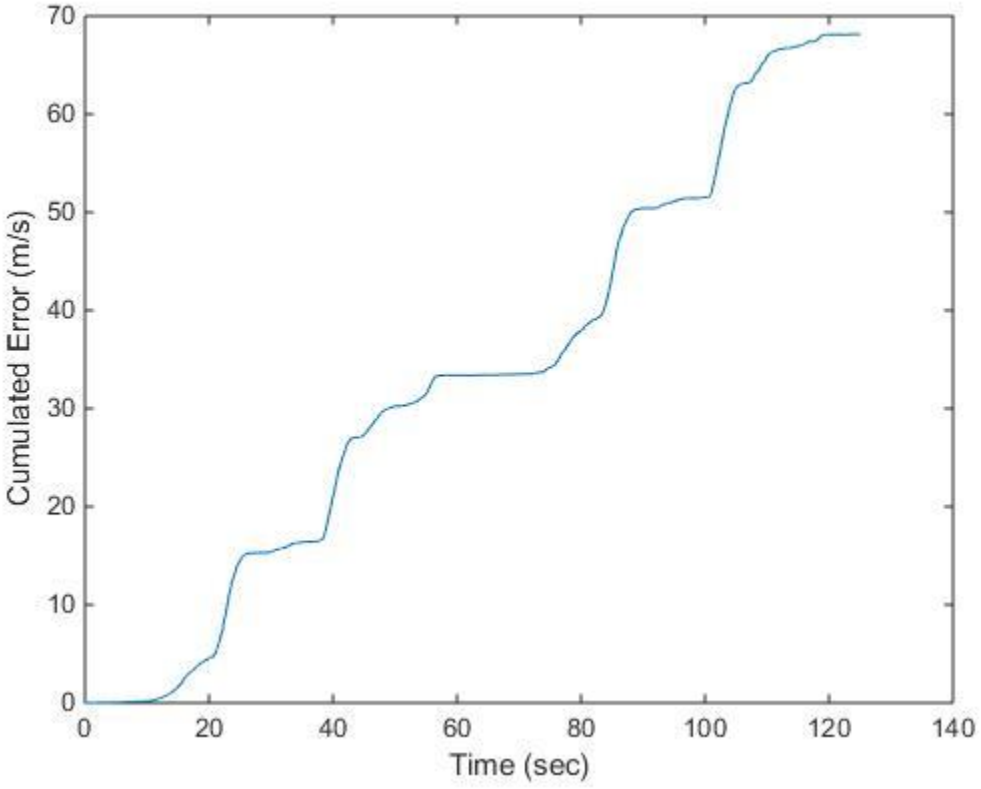

Figure 4.11: The cumulative error from the acceleration data, post FMINCON.

The cost function was reduced by 15 $\frac{m}{s}$. There is still error in the tire model but there may be multiple causes. First, the transient effects in the change in velocity will influence the tires that is not captured in this model. Another possible source of the error comes from the lack of the suspension in the 9DOF model, therefore it does not capture the camber gain that would be present at the large roll angles. Also, because the weight transfer is done through a rigid body, the effect of the springs and anti-roll bars is not captured in the model. Another possible source of error is the constant varying torque application caused by the sliding mode controlled stability control. This will cause a fluctuation in the slip ratio, which will cause a change in the lateral performance of the tire. The force slip plots are in Appendix A28 and B29.

ART Simulation Results

This section of the thesis discusses the results from the testing performed in simulation. The first test conducted is a step steer test, to show the effect of different steering positions and speeds to see how well the controller can reject the error and stay on the desired acceleration table. The second test is a ramp steer at a constant speed. This is one way of determining the understeer characteristics of the car and is a simple way to see the abilities of the ART to control the trait.

Step Steer Testing

The step steer test is conducted from 0-20 degrees of road wheel angle. In simulation, the steering angle increases linearly to the specified steering angle at a rate of $8\,\frac{deg}{sec}$. There is high speed vehicle instability caused by the instantaneous change in steering angle that Simulink is capable of, therefor the gain is needed. The testing speed is held constant using a sliding mode controller to deliver torque to the front wheels based off the initial conditions for the vehicle speed. The speed of the simulation increases from $2\frac{m}{s}$ to $53\frac{m}{s}$. There are 15 increments of both steering angle and vehicles speed, per control type, per CG position. The simulation is run for 120 seconds to ensure that the vehicle is reached a steady state condition. To minimize the effect of controller steady state oscillation, the last 50 data points are averaged to form the results. There are also three different data sets generated by the simulation. First is the error from the desired acceleration table. The second data set is the lateral acceleration produced by the car. The final table is the vehicle slip angle, beta. Beta is a good metric to show the

instability of the vehicle, larger slip angles mean the car is sliding more or osculation. The test automatically stops at 70 degrees of body slip.

Actual CG, No ART

For the following tests, the CG is in the same position (53% front) as the Honda Accord used to validate the tire model. The control test is used to establish the baseline. For the control test, ART is turned off so the effects of the vehicle's passive dynamics can be observed and recorded. The error between the actual lateral acceleration and the desired lateral acceleration is shown in Figure 4.12.

Error (m/s^2)		Vx (m/s)														
		2.00	5.64	9.29	12.93	16.57	20.21	23.86	27.50	31.14	34.79	38.43	42.07	45.71	49.36	53.00
Delta (deg)	0.00	0.00	0.00	0.00	0.01	0.01	0.01	0.02	0.02	0.03	0.03	0.04	0.04	0.05	0.05	0.06
	1.43	0.01	0.05	0.25	0.60	1.15	1.84	2.62	2.81	2.67	2.44	1.73	-1.87	1.99	2.61	2.18
	2.86	0.01	0.12	0.45	1.08	2.01	2.18	1.36								
	4.29	0.01	0.19	0.68	1.54	1.74	-5.53									
	5.71	0.02	0.18	0.83	1.86	-5.48										
	7.14	-0.01	0.27	1.03	-5.18											
	8.57	0.05	0.32	1.21	-5.66											
	10.00	0.04	0.31	1.40	-0.93											
	11.43	0.06	0.36	1.71	-0.88											
	12.86	0.07	0.42	-4.86	-1.23											
	14.29	0.04	0.40	-5.12	-1.75											
	15.71	0.02	0.47	-5.20	-2.18											
	17.14	0.01	0.54	-5.49	-2.38											
	18.57	0.10	0.55	-0.18	-2.54											
	20.00	0.13	0.64	-0.61	-2.74											

Figure 4.12: The error heat map for the Actual CG No ART Case w/ 1g Curve.

On the above surface, the areas colored in yellow are more desired for their low error. The red line signifies the steering and speed combination that yields a 1G turn. This means that all the data above the line is beyond the peak grip levels of the tire. This means that control authority is greatly diminished. This result is as expected because it shows the lowest error at low speeds and higher turning and at higher speeds and lower turning angles. The data tables from this test along with all of the following tests are found in Appendix A.

Actual CG, PID Control

As with the previous test, the CG is in the same spot at the production car; however, the ART controller is engaged using PID to control the rear toe. The error surface for this is shown in Figure 4.13.

Error (m/s^2)	Vx (m/s)														
	2.00	5.64	9.29	12.93	16.57	20.21	23.86	27.50	31.14	34.79	38.43	42.07	45.71	49.36	53.00
0.00	0.00	0.00	0.00	0.01	0.01	0.01	0.02	0.02	0.03	0.03	0.04	0.04	0.05	0.05	0.06
1.43	-0.56	0.84	-0.97	-1.90	2.35	-4.49	-4.19	-4.26	-4.39	3.36	2.76	3.06	-8.20	-7.99	-8.38
2.86	0.37	-0.61	1.42	-0.07	-4.60	-4.43	1.97	-5.63	1.16	1.62	1.50	0.85	-10.01	-10.67	-10.87
4.29	0.04	0.51	0.13	-4.64	-4.57	-5.28									
5.71	0.53	0.27	0.66	-4.54	-5.04										
7.14	-0.44	-0.74	0.46	-4.73											
8.57	0.39	0.06	-1.21	-0.06											
10.00	0.07	-0.17	-1.14	-0.58											
11.43	-0.40	-0.82	-4.32	-1.30											
12.86	0.46	-0.72	-4.57	-1.99											
14.29	-0.05	-0.47	-4.89	-2.59											
15.71	0.23	0.63	-4.70	-3.13											
17.14	0.25	0.85	-5.40	-3.44											
18.57	-0.33	0.79	-0.40	-3.69											
20.00	0.51	0.08	-1.16	-3.96											

Delta (deg)

Figure 4.13: The error heat map for the Actual CG PID Case w/ 1g Curve.

The PID is ineffective at controlling the understeer of the car due to the large error and variation in the results. Because of the nonlinearities in the system, the controller has issues driving the error to 0. There are unpredictable instabilities shown in the error as well as in the slip angle data as shown in Table 4.3.

Table 4.3: Beta for the Actual CG with PID control.

Beta (deg)		Vx (m/s)														
		2.00	5.64	9.29	12.93	16.57	20.21	23.86	27.50	31.14	34.79	38.43	42.07	45.71	49.36	53.00
Delta (deg)	0.00	-0.03	-0.03	-0.03	-0.03	-0.03	-0.03	-0.04	-0.04	-0.04	-0.04	-0.05	-0.05	-0.05	-0.05	-0.05
	1.43	0.75	0.37	0.18	2.38	-1.25	-61.59	-62.56	-63.51	-63.75	62.71	62.18	64.17	-64.40	-63.22	-64.14
	2.86	1.24	2.69	1.45	2.68	-61.69	-63.18	60.44	-62.82	60.84	62.60	62.94	63.43	-63.80	-64.03	-63.77
	4.29	3.24	3.38	1.42	-60.98	-63.15	-62.32									
	5.71	3.66	4.21	3.78	-62.05	-62.93										
	7.14	3.56	5.16	2.48	-62.83											
	8.57	4.35	4.26	3.41	-8.17											
	10.00	6.29	6.69	3.83	-5.87											
	11.43	6.84	5.94	-61.51	-5.94											
	12.86	6.74	6.65	-61.71	-5.64											
	14.29	7.23	7.13	-62.04	-5.40											
	15.71	7.97	9.20	-62.14	-5.21											
	17.14	8.73	8.85	-62.65	-5.08											
	18.57	10.04	9.26	-2.98	-5.00											
	20.00	10.85	11.28	-2.58	-4.96											

There is the section at moderate steering and speed where the vehicle is unstable, then it reduces its slip angles up until limit grip is achieved, after that point the tires are saturate and ART is ineffective at controlling the vehicle. The other tables associated with this CG position and PID controlled ART are shown in Appendix A.

Actual CG, Zeno SMC Case

The Type 1 Zeno sliding mode controller has improved control ability over the PID control and produces a smoother error plot than the PID controlled ART. Its error plot is shown in Figure 4.14.

Error (m/s^2)		Vx (m/s)													
		2.00	5.64	9.29	12.93	16.57	20.21	23.86	27.50	31.14	34.79	38.43	42.07	45.71	49.36	53.00
Delta (deg)	0.00	0.00	0.00	0.00	0.01	0.01	0.01	0.02	0.02	0.03	0.03	0.04	0.04	0.05	0.05	0.06
	1.43	-0.07	0.20	0.64	1.71	3.50	3.64	-2.37	-0.59	2.11	-2.45	-5.50	-9.34	-10.24	-9.18	-8.19
	2.86	-0.15	0.22	0.96	2.29	3.02	-5.03	-5.41	-5.80	-6.18	-6.56	-6.93	3.23	-7.71	-7.98	-8.22
	4.29	-0.41	0.31	1.25	2.67	-5.20	-5.71									
	5.71	-0.62	0.32	1.42	-5.01	-5.71										
	7.14	-0.45	0.42	1.62	-5.34											
	8.57	0.91	0.48	1.79	-5.61											
	10.00	0.31	0.47	-4.66	-5.94											
	11.43	-0.48	0.53	-4.79	-0.57											
	12.86	1.44	0.59	-4.87	-1.11											
	14.29	-1.04	0.56	-5.17	-1.75											
	15.71	1.25	0.63	-5.38	-2.20											
	17.14	0.30	0.70	-5.35	-2.47											
	18.57	-0.17	0.70	-5.62	-2.71											
	20.00	1.00	0.79	-0.28	-3.31											

Figure 4.14: The error heat map for the Actual CG Zeno SMC Case w/ 1g Curve.

Although the error is comparable to the non-ART case, the error slowly builds as the steering and acceleration increase. Once this happens, the controller is ineffective at controlling the understeer and the slip angle becomes more unstable and eventually leads to spins at higher speeds and steering angles as shown in the tables in Appendix A.

Actual CG, Tanh SMC Case

There is a marginal improvement using the tanh variant on the sliding mode controller. This could possibly be due to the reduced chatter that comes from using the hyperbolic tangent instead of the signum function. The surface plot for the error is shown in Figure 4.15.

Error (m/s^2)		Vx (m/s)														
		2.00	5.64	9.29	12.93	16.57	20.21	23.86	27.50	31.14	34.79	38.43	42.07	45.71	49.36	53.00
Delta (deg)	0.00	0.00	0.00	0.00	0.01	0.01	0.01	0.02	0.02	0.03	0.03	0.04	0.04	0.05	0.05	0.06
	1.43	0.01	0.05	0.25	0.63	1.23	2.01	2.82	3.19	1.68	2.43	1.74	-0.70	-2.21	2.49	3.41
	2.86	0.01	0.12	0.45	1.13	2.10	-5.02	-5.52	-6.02	2.09	2.36	1.80	2.07	1.92	-7.88	0.40
	4.29	0.02	0.19	0.69	1.58	-5.15	-5.67									
	5.71	0.02	0.18	0.84	1.91	-5.73										
	7.14	0.00	0.27	1.03	1.51											
	8.57	0.05	0.31	1.20	-0.41											
	10.00	0.05	0.30	1.37	-0.48											
	11.43	0.06	0.36	1.60	-0.64											
	12.86	0.08	0.41	-4.98	-1.22											
	14.29	0.05	0.39	-5.21	-1.55											
	15.71	0.03	0.45	0.77	-2.10											
	17.14	0.02	0.52	0.71	-2.25											
	18.57	0.11	0.52	0.30	-2.49											
	20.00	0.15	0.61	-0.15	-2.72											

Figure 4.15: The error heat map for the Actual CG Tanh SMC Case w/ 1g Curve.

The controller shows the ability to control the understeer of the car at most steering conditions up to ~31$\frac{\boldsymbol{m}}{\boldsymbol{s}}$. There is a section at mid speed and mid steering where the car becomes unstable as shown in Table 4.4.

Table 4.4: Beta for the Actual CG case using tanh SMC ART.

Beta (deg)		Vx (m/s)														
		2.00	5.64	9.29	12.93	16.57	20.21	23.86	27.50	31.14	34.79	38.43	42.07	45.71	49.36	53.00
Delta (deg)	0.00	-0.03	-0.03	-0.03	-0.03	-0.03	-0.03	-0.04	-0.04	-0.04	-0.04	-0.05	-0.05	-0.05	-0.05	-0.05
	1.43	0.71	0.59	0.35	-0.03	-0.60	-1.50	-3.03	-4.92	-2.55	-6.37	-12.89	-21.62	-27.02	67.89	66.19
	2.86	1.45	1.22	0.72	-0.17	-2.06	-63.95	-62.06	-61.90	68.35	66.56	69.39	67.29	66.45	-63.42	66.57
	4.29	2.20	1.84	1.06	-0.71	-62.32	-61.92									
	5.71	2.94	2.46	1.34	-2.30	-61.89										
	7.14	3.69	3.08	1.53	-6.75											
	8.57	4.43	3.70	1.59	-9.19											
	10.00	5.18	4.30	1.39	-0.27											
	11.43	5.92	4.91	0.66	-6.51											
	12.86	6.66	5.50	-61.47	-0.69											
	14.29	7.40	6.08	-61.49	-2.95											
	15.71	8.14	6.65	-5.27	-0.73											
	17.14	8.86	7.22	0.92	-1.03											
	18.57	9.58	7.77	-0.41	-0.51											
	20.00	10.29	8.31	1.76	-0.31											

This instability can be removed either through more tuning of the controller or using stability control to augment the deficiencies of ART. As before, once the tires become saturated, ART has very little effect. The remaining data tables are shown in Appendix A.

Rear CG Condition, No ART

The oversteer condition is meant to simulate a CG shift in the car. For example, if the CG is more rearwards on a different specification for the same car. In this case, the CG moves rearwards by 8%, 45% forward weight distribution. The desired lateral acceleration table is the same as the 53% front table. The error to the desired table is shown as a surface in Figure 4.16.

Error (m/s^2)		Vx (m/s)														
		2.00	5.64	9.29	12.93	16.57	20.21	23.86	27.50	31.14	34.79	38.43	42.07	45.71	49.36	53.00
Delta (deg)	0.00	0.00	0.00	0.00	-0.01	-0.02	-0.02	-0.03	-0.04	-0.06	-0.07	-0.09	-0.11	-0.11	-0.10	-0.22
	1.43	0.01	0.05	0.26	0.68	1.40	2.45	3.03	2.85	2.49	2.21	1.84	1.55	1.49	1.27	0.73
	2.86	0.01	0.12	0.49	1.27	2.35	2.04	1.17	0.50	0.17	-0.69	-4.53	-1.86	-2.27	-2.29	-13.09
	4.29	0.01	0.20	0.74	1.84	1.56	0.36									
	5.71	0.02	0.19	0.93	1.80	0.38										
	7.14	-0.01	0.28	1.16	1.06											
	8.57	0.05	0.33	1.37	0.31											
	10.00	0.04	0.33	1.55	-0.48											
	11.43	0.06	0.38	1.57	-1.02											
	12.86	0.07	0.44	1.23	-1.64											
	14.29	0.04	0.42	0.74	-2.18											
	15.71	0.02	0.49	0.31	-2.68											
	17.14	0.01	0.57	-0.12	-2.97											
	18.57	0.09	0.58	-0.64	-3.22											
	20.00	0.13	0.68	-1.18	-3.53											

Figure 4.16: The error surface for the No ART on the 45% front CG simulation w/ 1G Curve.

When compared to the initial control case, the low speed dynamics are very similar at low speed/high steering and high speed/low steering. As the slip angles increase, the different loading begins to have an effect. The understeer car become unstable faster as shown in the fluctuation of error shown by the surface. This is conducive of a car with oversteer tendency. The remaining data tables are shown in Appendix A.

Rear CG Condition, PID Controller

In similar fashion to the previous PID controller case, the controller is not effective at controlling the understeer of the car. At many locations on the surface, the error is worse than the control case without ART as shown in Figure 4.17.

Error (m/s^2)		Vx (m/s)														
		2.00	5.64	9.29	12.93	16.57	20.21	23.86	27.50	31.14	34.79	38.43	42.07	45.71	49.36	53.00
Delta (deg)	0.00	0.00	0.00	0.00	-0.01	-0.02	-0.02	-0.03	-0.04	-0.06	-0.07	-0.09	-0.11	-0.14	-0.18	-0.22
	1.43	-0.27	0.21	-0.53	2.23	2.80	2.87	2.41	2.25	5.06	1.83	1.69	1.62	1.73	2.03	1.97
	2.86	0.29	-1.35	0.33	1.81	-4.35	-0.48	-0.12	2.10	1.66	1.00	0.84	0.25	-0.18	-0.33	-0.52
	4.29	-0.17	-1.21	1.28	-3.30	1.75	-3.47									
	5.71	0.66	-0.92	0.78	-1.43	1.94										
	7.14	0.40	-1.01	1.21	1.05											
	8.57	-0.49	1.06	0.51	0.39											
	10.00	-0.45	-1.39	1.42	-1.68											
	11.43	-0.45	0.43	-4.54	-1.93											
	12.86	-0.52	0.23	-0.22	-2.72											
	14.29	0.21	-1.33	0.81	-3.42											
	15.71	0.54	-0.49	0.33	-4.07											
	17.14	-0.03	-0.91	-1.78	-4.48											
	18.57	-0.45	-1.20	-2.24	-4.82											
	20.00	-0.36	-0.01	-3.20	-5.16											

Figure 4.17: The error surface for the 45% front CG PID Case w/ 1G Curve.

One possible cause for this decrease in performance is the controller's gain are not updated before the weight shifted rearwards. The two sliding mode controllers can account for this change due to their robust nature. This is a case where an adaptive controller may be very effective at updating the gains. During the testing, the car had a yaw oscillation as the speed increased; however, except for a few outliers the slip angle did not get above 10 degrees until the tires became saturated.

Oversteer Condition, Zeno SMC Case

The zeno SMC produces an error that is slightly higher than the no ART case; however, it is slower to generate the error as shown in Figure 4.18.

Error (m/s^2)	Vx (m/s)														
Delta (deg)	2.00	5.64	9.29	12.93	16.57	20.21	23.86	27.50	31.14	34.79	38.43	42.07	45.71	49.36	53.00
0.00	0.00	0.00	0.00	-0.01	-0.02	-0.02	-0.03	-0.04	-0.06	-0.07	-0.09	-0.11	-0.14	-0.18	-0.22
1.43	-0.01	0.01	0.62	1.78	4.33	4.06	3.58	3.09	2.68	2.38	1.99	1.66	1.47	1.24	1.01
2.86	0.02	0.21	0.97	2.45	2.87	2.18	1.26	0.43	-0.07	-0.47	-8.92	-0.49	-3.32	-0.34	-0.96
4.29	0.02	0.30	1.29	2.61	1.76	0.44									
5.71	0.03	0.31	1.49	2.10	5.46										
7.14	0.00	0.42	1.70	1.27											
8.57	0.06	0.47	1.88	0.43											
10.00	0.06	0.47	1.98	-0.28											
11.43	1.34	0.54	1.94	-0.97											
12.86	-1.61	0.59	1.60	-1.58											
14.29	1.20	0.57	1.16	-2.21											
15.71	1.47	0.64	0.68	-2.79											
17.14	-0.35	0.71	0.28	-3.15											
18.57	0.83	0.71	-0.24	-3.49											
20.00	0.73	0.80	-0.82	-3.36											

Figure 4.18: The error surface for the 45% front CG Zeno SMC Case w/ 1G Curve.

The Zeno controller is able to push the boundaries of error to beyond what the passive OS car is capable of. It's performance also gradually decreases which is easier for the handoff to more traditional means of stability control. The slip angle also remains stable as shown in Figure 4.19.

Beta (deg)	Vx (m/s)														
Delta (deg)	2.00	5.64	9.29	12.93	16.57	20.21	23.86	27.50	31.14	34.79	38.43	42.07	45.71	49.36	53.00
0.00	-0.03	-0.02	-0.02	-0.02	-0.02	-0.01	-0.01	0.00	0.00	0.01	0.02	0.03	0.04	0.06	0.08
1.43	0.20	0.17	-0.31	-1.38	-4.51	-9.98	-3.79	-11.03	-6.66	-7.00	-7.16	-7.16	-7.20	-7.15	-7.31
2.86	1.06	0.69	-0.29	-2.23	-4.97	-5.66	-5.94	-5.45	-5.65	-5.81	-62.34	-6.45	-4.06	63.19	63.40
4.29	1.69	1.13	-0.23	-3.58	-5.61	-5.68									
5.71	2.31	1.56	-0.23	-4.38	-4.89										
7.14	2.95	2.01	-0.33	-4.35											
8.57	3.58	2.46	-0.66	-3.69											
10.00	4.21	2.91	-1.36	-4.36											
11.43	3.99	3.36	-2.22	-2.95											
12.86	5.45	3.81	-2.10	-2.94											
14.29	4.16	4.25	-2.34	-2.54											
15.71	7.16	4.68	-1.12	-2.16											
17.14	4.58	5.11	-0.72	-1.89											
18.57	10.77	5.54	-0.49	-1.64											
20.00	6.01	5.96	-0.02	-7.66											

Figure 4.19: The slip angle for the 45% front CG Zeno SMC case.

Except for a few outliers, the car remains stable and very little oscillation until the tires become more saturated and the ability to control the angle is greatly reduced. This is

a very favorable condition for the car because it allows for more driver confidence at higher lateral accelerations.

Oversteer Condition, Tanh SMC Case

The Tanh sliding mode controller performed well. It still had error, but it was comparable or in some conditions, lower than the 50% CG and no ART. It has an error shown in Figure 4.20.

Error (m/s^2)		Vx (m/s)														
		2.00	5.64	9.29	12.93	16.57	20.21	23.86	27.50	31.14	34.79	38.43	42.07	45.71	49.36	53.00
Delta (deg)	0.00	0.00	0.00	0.00	-0.01	-0.02	-0.02	-0.03	-0.04	-0.06	-0.07	-0.09	-0.11	-0.14	-0.18	-0.23
	1.43	0.01	0.05	0.27	0.71	1.49	2.61	3.10	2.88	2.39	2.15	2.00	1.79	1.45	0.97	0.60
	2.86	0.01	0.12	0.49	1.32	2.40	2.09	1.39	-0.22	-0.33	-0.24	-0.28	-1.24	-6.75	-3.38	-8.65
	4.29	0.02	0.19	0.75	1.86	1.66	0.00									
	5.71	0.02	0.18	0.93	1.87	0.39										
	7.14	0.00	0.28	1.15	1.22											
	8.57	0.05	0.32	1.35	0.51											
	10.00	0.05	0.32	1.51	-0.29											
	11.43	0.06	0.37	1.61	-0.77											
	12.86	0.08	0.43	1.46	-1.52											
	14.29	0.05	0.41	1.08	-1.98											
	15.71	0.03	0.47	0.72	-2.59											
	17.14	0.02	0.54	0.32	-2.88											
	18.57	0.11	0.55	-0.15	-3.18											
	20.00	0.14	0.64	-0.67	-3.52											

Figure 4.20: The error surface for the 45% front CG Tanh SMC case.

The controller becomes less effective and more unstable as the loads increase on the tires. This is shown in the fluctuation of the surface in the above figure.

Time Series Results

The time series results for the tests yield a better understanding for the ability for the rear toe to control the understeer and acceleration of the car. All the following results are the for 55% rear CG case with 5 degree of steering angle at the wheels. The first figure, Figure 4.21, shows the lateral acceleration for the car at 15m/s.

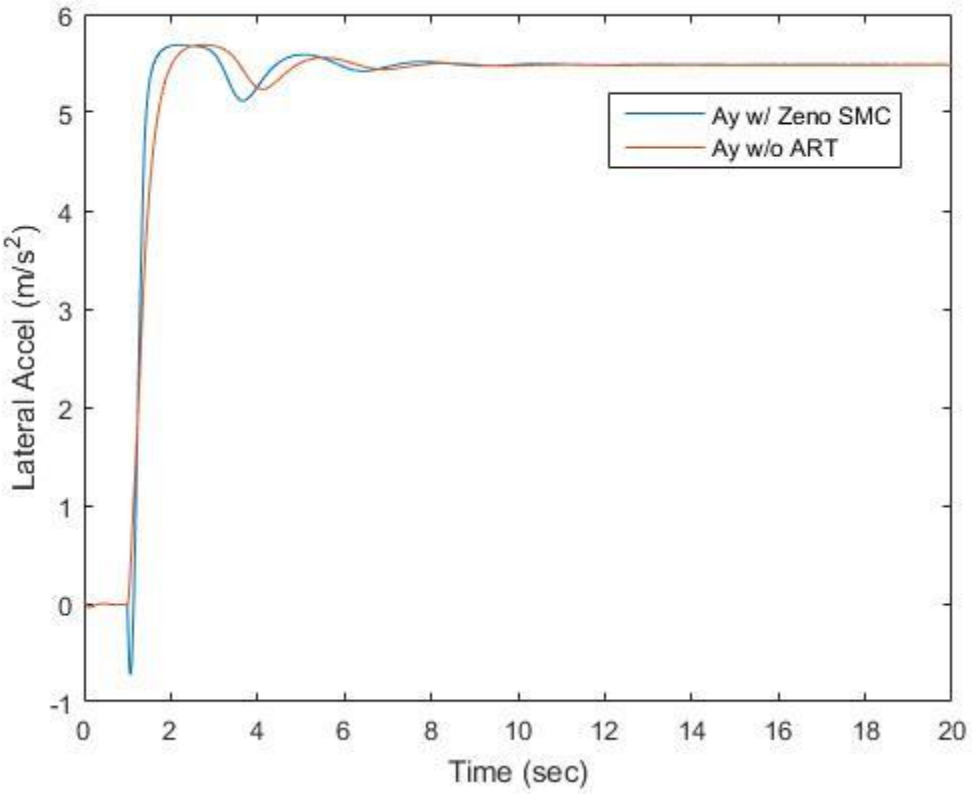

Figure 4.21: The lateral acceleration for a step steer input at 15m/s.

This accurately demonstrates the limitations of active rear to in that it cannot increase the maximum performance of the car. This is set by the tires and the suspension and changing the rear steer angle does not have an effect of the ability to control the lateral acceleration. Something to note is the ability to change acceleration is improved with the active rear toe, note the increased slope of the acceleration plot for the car with the Zeno ART when compared to the non-ART car. At lower speeds, under the maximum performance of the car, the abilities of ART become more apparent as Figure 4.22 shows.

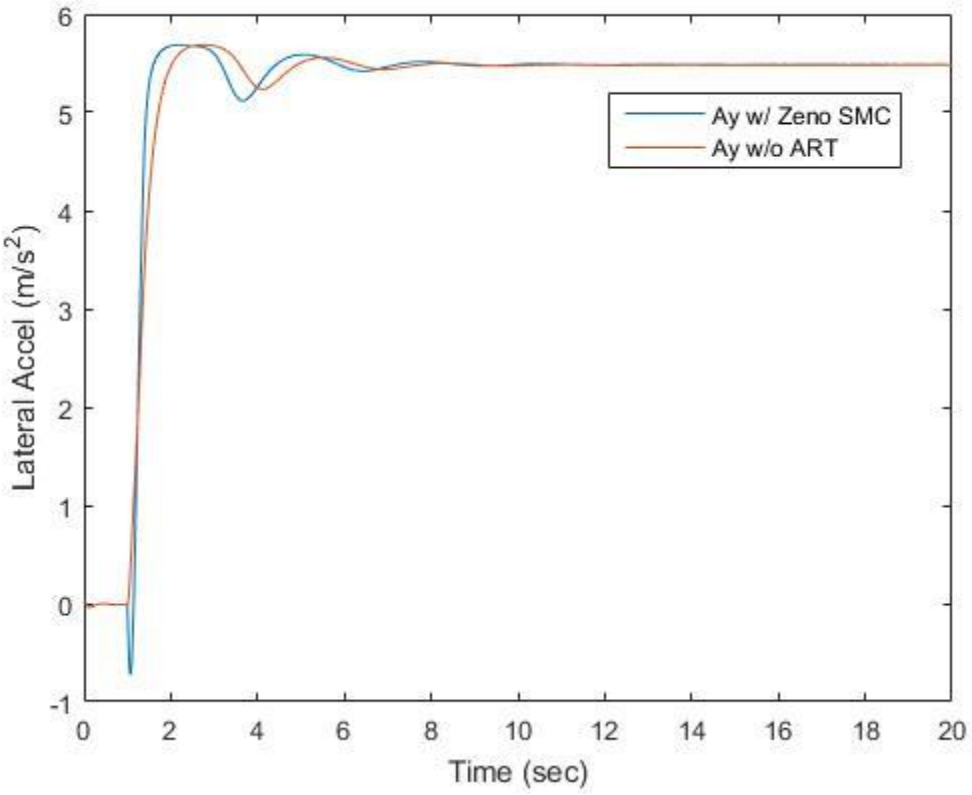

Figure 4.22: The lateral acceleration of the car at 10 m/s.

With the same 5-degree steer angle but at a lower speed, the effect of ART to control the lateral acceleration. For this condition, the ART has changed the lateral acceleration of the car by ~.75m/s.

A consequence of controlling the lateral acceleration through the ART is the slip angle of the car is also controlled. Even at the 15 m/s case, there is still a difference in beta for the cars as Figure 4.23 shows.

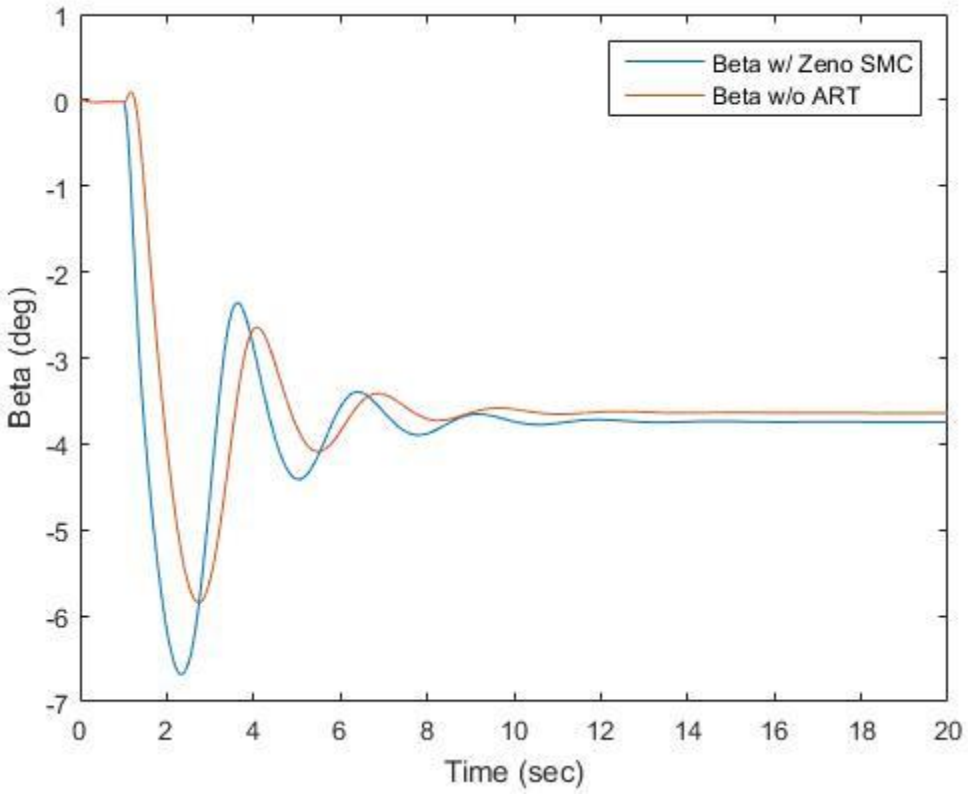

Figure 4.23: The slip angle for the car at 15m/s and 5 deg. of steep steer input.

The active rear toe also increases the frequency of the yaw oscillation of the vehicle. This difference in slip angle is even larger at the lower speed condition, as Figure 4.24 shows.

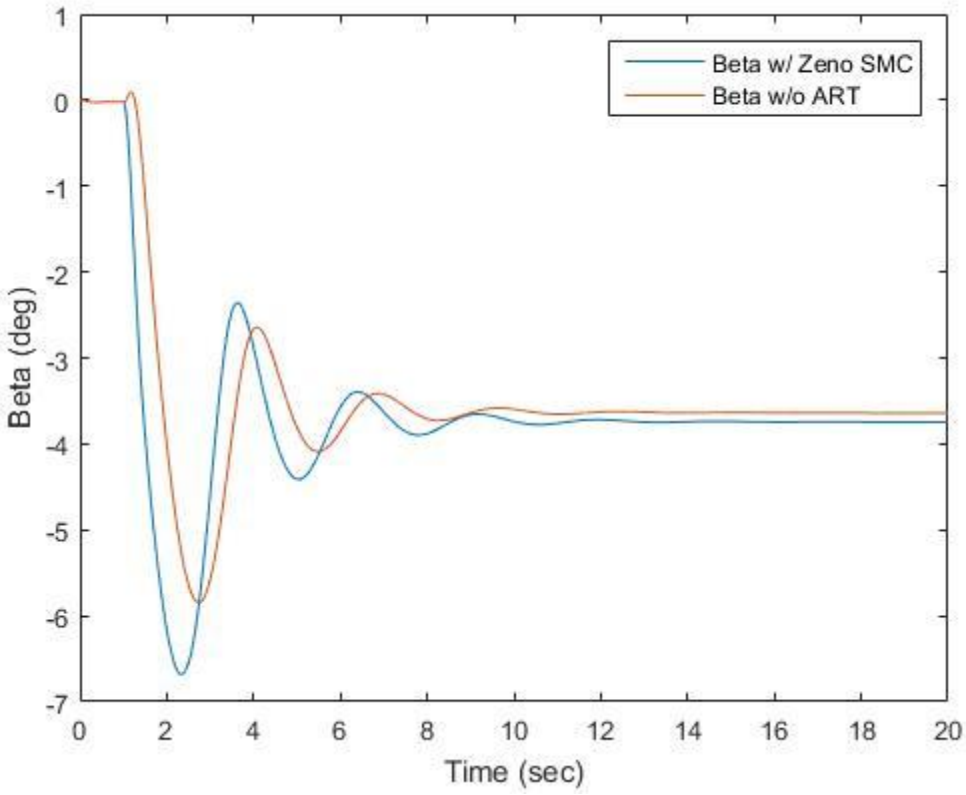

Figure 4.24: The slip angle at 10m/s and 5 deg. of steering input.

The slip angel now differs by ~1.25 degrees because of the car rotating more to achieve the higher lateral acceleration requested by the controller.

Chapter 5

Conclusion

There are three main conclusions that can be drawn from this thesis. First, Active Rear Toe is a viable method for dynamically changing the handling characteristics of a vehicle in real time. Second, a nonlinear controls approach, such as sliding mode control is necessary for effective ART control. Chapter 4 results showed the PID approach was not effective. Third, the understeer gradient is commonly used to discuss handling characteristics but was a very sensitive parameter to control directly. Lateral acceleration was found to be a much easier parameter to control, and because of its direct effect on the understeer gradient, it was still able to control Kus.

PID control does not show the ability to control Kus effectively. There is too much variation in the results for it to be a usable controller in its current design. However, the effective range of the PID control could be increased with the use of three more 2D lookup tables, one for each of the gains in the controller. Using this gain scheduling, the performance of the PID controller can be expanded. There will also need to be the ability to adjust the gain depending on grip levels which can be harder to predict, if the road surface becomes wet or μ decreases.

Robust control strategies like type 1 zeno and tanh sliding mode control can allow for changing conditions. They can account for changing μ or aftermarket tire selection, both of which will change the performance of the car and therefore effect the controller. One hindrance of using sliding mode control is that the controller works by controlling high frequency oscillations which may not happen due to incapable of happening due to

actuator limitations. The zeno controller is defined by switching an infinite number of times in a finite amount of time which is impossible in the real world due to actuator and other physical limitations. Using the step steer OS case and a $\pm 12\ \frac{deg}{sec}$, the surface shown in Figure 5.1 is generated.

Error		Vx														
		2.00	5.64	9.29	12.93	16.57	20.21	23.86	27.50	31.14	34.79	38.43	42.07	45.71	49.36	53.00
Delta	0.00	0.00	0.00	0.00	0.00	0.00	0.00	0.00	0.01	0.01	0.01	0.02	0.03	0.05	0.09	0.15
	1.43	0.10	0.02	0.57	1.45	3.42	4.56	6.36	6.04	6.38	6.39	6.37	6.30	6.31	5.80	-2.62
	2.86	0.11	0.86	1.27	3.26	6.21	6.41	6.29	6.34	6.22	5.63	5.24	-3.78	-3.71	4.16	3.75
	4.29	0.03	0.87	1.75	5.43	6.47	6.26									
	5.71	0.12	1.16	3.44	6.40	5.97										
	7.14	0.29	1.61	4.67	6.36											
	8.57	0.19	1.76	5.23	6.54											
	10.00	0.27	2.62	5.92	6.17											
	11.43	0.25	2.41	6.50	5.96											
	12.86	0.32	2.63	6.56	5.72											
	14.29	0.37	3.57	6.44	5.47											
	15.71	0.42	2.85	6.89	5.52											
	17.14	0.45	4.00	5.84	5.04											
	18.57	0.48	4.03	5.54	4.02											
	20.00	0.50	4.16	5.43	4.19											

Figure 5.1: The error plot for OS case Tanh SMC case with a rate limit.

There is more error in this surface then the other SMC controlled cases, but that is expected due to the nature of the sliding mode controller. The other issue with the sliding controls is oscillation may be noticeable to the occupants. A rapidly changing Kus does not bode well for the confidence of the driver. The controller also is ineffective at changing to maximum acceleration of the car. That value is set by the tire, therefore changing the rear steer angle has no effect in increasing the acceleration, only decreasing it. It does show the ability to increase the gain of acceleration, but the peak is unchanged, note Figure 4.21.

Model Limitations

As stated before, the majority of the data is done without actuator limitations. Before this system is implemented, it is imperative that a proper actuator model is generated. In order to do this, the trail, kingpin axis, and toe link position would need to be known to generate how much load the toe link sees. From there, a lookup table can show maximum speed at that loading condition. Once the proper actuator limitations have been accounted for, it is possible to generate a more advanced rear toe controller. As stated when discussing the possibilities of the ZF system, one could toe out the rear wheels to induce a yaw rate, or write code to minimize toe when driving on highways to minimize the rolling resistance of the tires. Another large step in the advancement of this model is to account for a suspension with springs and dampers. This will allow for the transients to be accounted for so the model can be tested in more circumstances. It will also allow for the user to account for bump-toe characteristics, camber gain, and more accurate weight transfer.

Areas for Further Study

One possible area for further study is to apply an adaptive controls strategy to the problem of controlling Kus, working in conjunction with a sliding mode controller. This would update the gains for the sliding mode controller to adjust for differing CG positions, grip levels, and variations in vehicle suspension/packaging. It would allow for a more robust model that acts quickly. Adaptive control ensures control of over a larger range of variability then just the sliding mode controller is capable of.

The next area of focus will be the transition between the control authority granted by ART to a more traditional stability control system. The data has shown a definite limit to the controls ability of ART. Once the tires become saturated, the controls authority greatly diminishes. This is where a system that controls by removing energy will be useful like independent Fx control of the wheels. With the addition of ART to a car, the controls will often become over-actuated, but with a proper controls strategy, the stability, comfort, and performance of the car can be tuned to meet the demands of the modern chassis system.

References

Abe, M. (1999). Vehicle dynamics and control for improcing handling and actirve safety: from four-wheel steering to direct yaw moment control. *Proc Instn Mech Engrs Vol 213 Part K*, 87-101.

Araki, M. (n.d.). *Control Systems, Robotics, and Automation, Vol.II - PID Control.* Encyclopedia of Life Support Systems.

CUI INC. (2016). *ATM20 Modular Absolute Encoder Datasheet.*

Deyer. (1979). *Standard Mathematical Tables.* Boca Raton: CRC Press.

Egerstedt, M. (2000, March). Lecture Notes in Computer Science: Hybrid Systems III: Computation and Control. *Behavior Based Robotics Using Hybrid Automata*, pp. 103-116.

Gillespie, T. (1992). *Fundamentals of Vehicle Dynamics.* Warrendale: Society of Automotive Engineers.

Louis, L., & Schramm, D. (2012). Nonlinear State Estimation of Tire-Road Contact Forces using a 14 DoF. *Applied Mechanics and Materials Vol. 165*, 155-159.

Mathworks. (2017, 02 09). *PID Controller, Discrete PID Controller*. Retrieved from mathworks: https://www.mathworks.com/help/simulink/slref/pidcontroller.html

Milliken, W. F. (2000). Maurice Olley. *SAE Automotive Dynamics and Stability Conference.* Troy: Milliken Research Associates, Inc.

Milliken, W., & Milliken, D. (1995). *Race Car Vehicle Dynamics.* 1997: Society of Automotive Engineers.

Pacejka, H. (2012). *Tire and Vehicle Dynamics.* Butterworth-Heinemann.

Rajamani, R. (2012). *Vehicle Dynamics and Control 2nd Ed.* New York: Springer.

Ren, H., Shim, T., Ryu, J., & Chen, S. (2014). Development of Effective Bicycle Model for Wide Ranges of Vehicle. *SAE Technical Paper 2014-01-0841*.

Reza, J. (2008). *Vehicle Dynamics: Theory and Applications.* New York: Springer.

SAE International. (2008). *J670 JAN2008.* SAE International.

Severson, A. (2015, June 12). *Four-wheel steering demystified*. Retrieved from Autoweek: http://autoweek.com/article/car-life/four-wheel-steering-demystified

Slotine, J.-J. E., & Wieping, L. (1991). *Applied Nonlinear Control.* Upper Saddle River: Prentice Hall.

ST: Life Augmented. (2015). *LSM9DS1 Datasheet.*

Tire Tech. (2017, February 06). *Tire Rolling Resistance Part 2: Defining Rolling Resistance*. Retrieved from tirerack.com: http://www.tirerack.com/tires/tiretech/techpage.jsp?techid=175

University of California at Berkley. (n.d.). *Optimization Toolbox: fmincon.* Berkley.

Utkin, V., Guldner, J., & Shi, J. (2009). *Sliding Mode Control in Electro-Mechanical Systems, 2nd Edition.* Boca Raton: CRC Press.

Wiesenthal, M., Collenberg, H., & Krimmel, H. (2008). Active Rear Axle Kinematics AKC - A Contribution to Driving Dynamics, Safety, and Comfort. *17th Annual Colloquium on Vehicle and Engine Technology*, 1-16.

Wong, J. (2001). *Theory of Ground Vehicles.* New York: John Wiley & Sons, Inc.

Zhang, J., Johansson, K., John, L., & Sastry, S. (n.d.). *Dynamical Systems Revisited: Hybrid Systems with Zeno Executions.* Berkeley: University of California, Berkeley.

Appendix A

B1: The Desired Understeer Table for the Active Rear Toe Controller

B2: The Lateral Acceleration table for the 45% forward condition

B3: The Lateral Acceleration table for the 55% forward condition

B4, B5 and B6: Error, Ay, and Beta Tables for the Actual CG Control Case.

B7, B8, and B9: Error, Ay, and Beta Table for the Actual CG PID Case.

B10, B11 and B12: Error, Ay, and Beta Table for the Actual CG Zeno SMC Case.

B13, B14, and B15: Error, Ay, and Beta Table for the Actual CG Tanh Case.

B16, B17, and B18: Error, Ay, and Beta Table for the 45% Rear CG Control Case.

B19, B20, and B21: Error, Ay, and Beta Table for the 45% Rear CG PID Case.

B22, B23, and B24: Error, Ay, and Beta Table for the 45% Rear CG Zeno Case.

B25, B26, and B27: Error, Ay and Beta Table for the 45% Rear CG Tanh Case.

B28: Longitudinal Force Slip Plot.

B29: Lateral Force Slip Plot.

B30: Top Level View of the Simulink Block Diagram

B31, B32, and B33: The Controls logic used for the Sliding mode controller

B34: The Vehicle Model

B35 and B36: The Wheels and Tire Subsystem and Combined Slip Pacejka Model

Ay Desired (m/s^2)		Vx																		
		2.00	4.68	7.37	10.05	12.74	15.42	18.11	20.79	23.47	26.16	28.84	31.53	34.21	36.89	39.58	42.26	44.95	47.63	50.32	53.00
Delta	-20.00	-0.39	-2.22	-4.99	-7.09	-7.22	-7.07	-7.06	-7.09	-7.22	-6.70	-6.18	-5.66	-5.15	-4.63	-4.11	-3.59	-3.07	-2.56	-2.04	-1.52
	-18.95	-0.35	-2.16	-4.77	-6.98	-7.30	-7.14	-7.13	-7.16	-7.24	-7.15	-6.25	-5.83	-5.34	-4.87	-4.35	-3.88	-3.42	-2.93	-2.34	-1.83
	-17.89	-0.47	-2.10	-4.56	-6.81	-7.39	-7.23	-7.19	-7.18	-7.26	-7.21	-6.32	-6.01	-5.54	-5.12	-4.60	-4.17	-3.77	-3.30	-2.63	-2.15
	-16.84	-0.41	-1.93	-4.28	-6.66	-7.48	-7.32	-7.26	-7.19	-7.28	-7.28	-6.39	-6.18	-5.74	-5.37	-4.84	-4.46	-4.11	-3.67	-2.93	-2.47
	-15.79	-0.40	-1.86	-4.10	-6.47	-7.52	-7.40	-7.25	-7.14	-7.30	-7.34	-6.47	-6.35	-5.94	-5.61	-5.09	-4.74	-4.46	-4.04	-3.23	-2.78
	-14.74	-0.29	-1.78	-3.90	-6.23	-7.38	-7.50	-7.32	-7.11	-7.32	-7.40	-6.54	-6.52	-6.14	-5.86	-5.33	-5.03	-4.80	-4.41	-3.53	-3.10
	-13.68	-0.39	-1.64	-3.59	-5.85	-7.21	-7.56	-7.38	-7.15	-7.34	-7.46	-6.61	-6.69	-6.33	-6.11	-5.58	-5.32	-5.15	-4.78	-3.83	-3.41
	-12.63	-0.23	-1.47	-3.31	-5.46	-6.97	-7.56	-7.50	-7.37	-7.68	-7.53	-6.68	-6.86	-6.53	-6.35	-5.82	-5.61	-5.50	-5.15	-4.12	-3.73
	-11.58	-0.24	-1.35	-3.08	-4.99	-6.66	-7.53	-7.61	-7.62	-7.81	-7.79	-6.75	-7.03	-6.73	-6.60	-6.07	-5.90	-5.84	-5.52	-4.42	-4.04
	-10.53	-0.24	-1.29	-2.77	-4.67	-6.43	-7.23	-7.61	-7.72	-7.89	-7.95	-6.82	-7.20	-6.93	-6.85	-6.31	-6.19	-6.19	-5.89	-4.72	-4.36
	-9.47	-0.20	-1.13	-2.50	-4.30	-5.91	-7.00	-7.52	-7.67	-7.95	-7.98	-6.89	-7.38	-7.13	-7.09	-6.56	-6.48	-6.53	-6.26	-5.02	-4.67
	-8.42	-0.18	-0.98	-2.19	-3.80	-5.40	-6.62	-7.31	-7.49	-7.82	-8.00	-6.96	-7.55	-7.33	-7.34	-6.80	-6.76	-6.88	-6.63	-5.31	-4.99
	-7.37	-0.19	-0.82	-1.95	-3.29	-4.84	-6.04	-6.88	-7.26	-7.46	-7.94	-7.93	-7.72	-7.52	-7.59	-7.05	-7.05	-7.23	-7.00	-5.61	-5.30
	-6.32	-0.15	-0.77	-1.71	-2.83	-4.15	-5.38	-6.30	-6.88	-7.17	-7.31	-7.89	-7.89	-7.72	-7.83	-7.29	-7.34	-7.57	-7.37	-5.91	-5.62
	-5.26	-0.12	-0.62	-1.37	-2.33	-3.44	-4.51	-5.56	-6.18	-6.69	-6.99	-6.99	-7.54	-7.92	-7.60	-7.53	-7.50	-7.92	-7.75	-6.21	-5.93
	-4.21	-0.10	-0.47	-1.06	-1.84	-2.76	-3.63	-4.55	-5.37	-5.92	-6.28	-6.53	-6.69	-6.67	-7.27	-7.78	-7.65	-7.50	-7.00	-6.51	-6.25
	-3.16	-0.07	-0.34	-0.84	-1.37	-2.04	-2.72	-3.37	-3.99	-4.75	-5.24	-5.59	-5.86	-6.05	-6.12	-6.04	-6.29	-6.97	-7.48	-7.54	-7.08
	-2.11	-0.04	-0.26	-0.51	-0.91	-1.29	-1.72	-2.13	-2.63	-3.06	-3.52	-4.02	-4.37	-4.68	-4.93	-5.12	-5.25	-5.33	-5.32	-5.33	-5.51
	-1.05	-0.03	-0.14	-0.25	-0.44	-0.63	-0.83	-1.02	-1.23	-1.41	-1.59	-1.81	-2.02	-2.18	-2.41	-2.61	-2.84	-3.04	-3.36	-3.52	-3.63
	0.00	0.00	0.00	0.00	0.00	0.00	0.00	0.00	0.00	0.00	0.00	0.00	0.00	0.00	0.00	0.00	0.00	0.00	0.00	0.00	0.00
	1.05	0.03	0.14	0.25	0.44	0.63	0.83	1.02	1.23	1.41	1.59	1.81	2.02	2.18	2.41	2.61	2.84	3.04	3.36	3.52	3.63
	2.11	0.04	0.26	0.51	0.91	1.29	1.72	2.13	2.63	3.06	3.52	4.02	4.37	4.68	4.93	5.12	5.25	5.33	5.32	5.33	5.51
	3.16	0.07	0.34	0.84	1.37	2.04	2.72	3.37	3.99	4.75	5.24	5.59	5.86	6.05	6.12	6.04	6.29	6.97	7.48	7.54	7.08
	4.21	0.10	0.47	1.06	1.84	2.76	3.63	4.55	5.37	5.92	6.28	6.53	6.69	6.67	7.27	7.78	7.65	7.50	7.00	6.51	6.25
	5.26	0.12	0.62	1.37	2.33	3.44	4.51	5.56	6.18	6.69	6.99	6.99	7.54	7.92	7.60	7.53	7.50	7.92	7.75	6.21	5.93
	6.32	0.15	0.77	1.71	2.83	4.15	5.38	6.30	6.88	7.17	7.31	7.89	7.89	7.72	7.83	7.29	7.34	7.57	7.37	5.91	5.62
	7.37	0.19	0.82	1.95	3.29	4.84	6.04	6.88	7.26	7.46	7.94	7.93	7.72	7.52	7.59	7.05	7.05	7.23	7.00	5.61	5.30
	8.42	0.18	0.98	2.19	3.80	5.40	6.62	7.31	7.49	7.82	8.00	6.96	7.55	7.33	7.34	6.80	6.76	6.88	6.63	5.31	4.99
	9.47	0.20	1.13	2.50	4.30	5.91	7.00	7.52	7.67	7.95	7.98	6.89	7.38	7.13	7.09	6.56	6.48	6.53	6.26	5.02	4.67
	10.53	0.24	1.29	2.77	4.67	6.43	7.23	7.61	7.72	7.89	7.95	6.82	7.20	6.93	6.85	6.31	6.19	6.19	5.89	4.72	4.36
	11.58	0.24	1.35	3.08	4.99	6.66	7.53	7.61	7.62	7.81	7.79	6.75	7.03	6.73	6.60	6.07	5.90	5.84	5.52	4.42	4.04
	12.63	0.23	1.47	3.31	5.46	6.97	7.56	7.50	7.37	7.68	7.53	6.68	6.86	6.53	6.35	5.82	5.61	5.50	5.15	4.12	3.73
	13.68	0.39	1.64	3.59	5.85	7.21	7.56	7.38	7.15	7.34	7.46	6.61	6.69	6.33	6.11	5.58	5.32	5.15	4.78	3.83	3.41
	14.74	0.29	1.78	3.90	6.23	7.38	7.50	7.32	7.11	7.32	7.40	6.54	6.52	6.14	5.86	5.33	5.03	4.80	4.41	3.53	3.10
	15.79	0.40	1.86	4.10	6.47	7.52	7.40	7.25	7.14	7.30	7.34	6.47	6.35	5.94	5.61	5.09	4.74	4.46	4.04	3.23	2.78
	16.84	0.41	1.93	4.28	6.66	7.48	7.32	7.26	7.19	7.28	7.28	6.39	6.18	5.74	5.37	4.84	4.46	4.11	3.67	2.93	2.47
	17.89	0.47	2.10	4.56	6.81	7.39	7.23	7.19	7.18	7.26	7.21	6.32	6.01	5.54	5.12	4.60	4.17	3.77	3.30	2.63	2.15
	18.95	0.35	2.16	4.77	6.98	7.30	7.14	7.13	7.16	7.24	7.15	6.25	5.83	5.34	4.87	4.35	3.88	3.42	2.93	2.34	1.83
	20.00	0.39	2.22	4.99	7.09	7.22	7.07	7.06	7.09	7.22	6.70	6.18	5.66	5.15	4.63	4.11	3.59	3.07	2.56	2.04	1.52

Ay OS (m/s^2)		Vx (m/s)																		
		2.00	4.68	7.37	10.05	12.74	15.42	18.11	20.79	23.47	26.16	28.84	31.53	34.21	36.89	39.58	42.26	44.95	47.63	50.32	53.00
Delta (deg)	-20.00	-0.47	-2.63	-6.59	-7.66	-7.41	-7.26	-7.33	-7.58	-7.49	-1.44	0.74	0.88	0.88	0.85	0.89	0.74	0.73	0.73	0.72	0.72
	-18.95	-0.45	-2.50	-6.28	-7.72	-7.52	-7.43	-7.55	-7.59	-7.67	-0.75	0.72	0.83	0.84	-0.34	0.81	0.70	0.69	0.69	0.68	0.68
	-17.89	-0.42	-2.36	-5.94	-7.75	-7.63	-7.59	-7.67	-7.64	-4.63	-0.64	0.66	0.78	0.79	0.81	0.70	0.65	0.65	0.64	0.64	0.64
	-16.84	-0.40	-2.22	-5.60	-7.82	-7.71	-7.71	-7.75	-7.75	-4.91	-0.57	0.58	0.73	0.73	0.77	0.64	0.61	0.61	0.60	0.60	0.60
	-15.79	-0.37	-2.09	-5.25	-7.96	-7.73	-7.78	-7.80	-7.75	-6.84	-0.52	0.47	0.71	-0.39	0.73	0.59	0.57	0.56	0.56	0.56	0.55
	-14.74	-0.35	-1.94	-4.91	-8.07	-7.64	-7.78	-7.81	-6.72	-3.48	-0.47	0.37	0.66	0.69	0.69	0.55	0.53	0.52	0.52	0.51	0.51
	-13.68	-0.32	-1.81	-4.55	-8.08	-7.40	-7.60	-7.53	-3.34	-0.70	-0.44	0.36	0.34	0.64	0.65	0.50	0.48	0.48	0.47	0.47	0.47
	-12.63	-0.30	-1.67	-4.21	-7.98	-7.41	-7.03	-6.41	-7.38	-0.54	-0.40	0.54	-0.39	0.60	0.60	0.46	0.44	0.43	0.43	0.43	0.43
	-11.58	-0.27	-1.53	-3.86	-7.62	-7.85	-6.51	-5.27	-6.78	-0.47	-0.36	0.54	0.57	0.56	0.56	0.43	0.40	0.39	0.39	0.39	0.38
	-10.53	-0.25	-1.39	-3.50	-6.90	-8.01	-7.27	-7.04	-4.54	-0.42	-0.32	-0.44	0.52	0.52	0.52	0.42	0.36	0.35	0.35	0.34	0.34
	-9.47	-0.22	-1.25	-3.14	-6.15	-8.08	-7.87	-7.82	-2.70	-0.40	-0.27	-0.36	0.48	0.47	0.47	0.43	0.33	0.31	0.30	0.30	0.30
	-8.42	-0.20	-1.11	-2.79	-5.42	-8.11	-7.96	-7.79	-2.73	-0.39	-0.23	-0.31	0.44	0.43	0.43	0.43	0.34	0.28	0.27	0.26	0.26
	-7.37	-0.17	-0.97	-2.44	-4.72	-7.92	-8.00	-7.93	-4.99	-0.44	-0.22	-0.30	0.40	0.39	0.39	0.39	0.33	0.25	0.23	0.22	
	-6.32	-0.15	-0.83	-2.09	-4.03	-6.99	-8.08	-7.99	-7.25	-0.81	-0.29	-0.31	0.37	0.35	0.35	0.35	0.34	0.34	0.34	0.30	0.22
	-5.26	-0.12	-0.69	-1.75	-3.35	-5.66	-8.02	-8.03	-8.00	-6.93	-0.72	-0.32	-0.28	0.32	0.31	0.31	0.30	0.30	0.30	0.30	0.30
	-4.21	-0.10	-0.56	-1.40	-2.67	-4.46	-7.29	-8.09	-8.04	-7.97	-7.43	-3.87	-0.42	-0.27	-0.12	0.27	0.27	0.27	0.26	0.26	0.26
	-3.16	-0.07	-0.42	-1.05	-1.99	-3.32	-5.13	-7.80	-8.08	-8.05	-8.03	-7.74	-7.54	-6.46	-1.69	-6.74	-0.06	-0.06	-0.03	0.23	0.24
	-2.11	-0.05	-0.28	-0.70	-1.33	-2.19	-3.35	-4.92	-7.64	-7.95	-8.06	-8.04	-8.05	-7.93	-7.57	-7.19	-7.00	-6.22	-5.71	-7.32	-0.03
	-1.05	-0.02	-0.14	-0.35	-0.66	-1.09	-1.65	-2.36	-3.32	-4.63	-7.30	-7.79	-7.86	-8.01	-8.01	-7.98	-7.98	-8.00	-8.00	-7.92	-7.76
	0.00	0.00	0.00	0.00	0.00	0.00	0.00	0.00	0.00	0.00	0.00	0.00	0.00	0.00	0.00	0.00	0.00	0.00	0.00	0.00	0.00
	1.05	0.02	0.14	0.35	0.66	1.09	1.65	2.36	3.32	4.63	7.30	7.79	7.86	8.01	8.01	7.98	7.98	8.00	8.00	7.92	7.76
	2.11	0.05	0.28	0.70	1.33	2.19	3.35	4.92	7.64	7.95	8.06	8.04	8.05	7.93	7.57	7.19	7.00	6.22	5.71	7.32	0.03
	3.16	0.07	0.42	1.05	1.99	3.32	5.13	7.80	8.08	8.05	8.03	7.74	7.54	6.46	1.69	6.74	0.06	0.06	0.03	-0.23	-0.24
	4.21	0.10	0.56	1.40	2.67	4.46	7.29	8.09	8.04	7.97	7.43	3.87	0.42	0.27	0.12	-0.27	-0.27	-0.27	-0.26	-0.26	-0.26
	5.26	0.12	0.69	1.75	3.35	5.66	8.02	8.03	8.00	6.93	0.72	0.32	0.28	-0.32	-0.31	-0.31	-0.30	-0.30	-0.30	-0.30	-0.30
	6.32	0.15	0.83	2.09	4.03	6.99	8.08	7.99	7.25	0.81	0.29	0.31	-0.37	-0.35	-0.35	-0.35	-0.34	-0.34	-0.34	-0.30	-0.22
	7.37	0.17	0.97	2.44	4.72	7.92	8.00	7.93	4.99	0.44	0.22	0.30	-0.40	-0.39	-0.39	-0.39	-0.39	-0.33	-0.25	-0.23	-0.22
	8.42	0.20	1.11	2.79	5.42	8.11	7.96	7.79	2.73	0.39	0.23	0.31	-0.44	-0.43	-0.43	-0.43	-0.34	-0.28	-0.27	-0.26	-0.26
	9.47	0.22	1.25	3.14	6.15	8.08	7.87	7.82	2.70	0.40	0.27	0.36	-0.48	-0.47	-0.47	-0.43	-0.33	-0.31	-0.30	-0.30	-0.30
	10.53	0.25	1.39	3.50	6.90	8.01	7.27	7.04	4.54	0.42	0.32	0.44	-0.52	-0.52	-0.52	-0.42	-0.36	-0.35	-0.35	-0.34	-0.34
	11.58	0.27	1.53	3.86	7.62	7.85	6.51	5.27	6.78	0.47	0.36	-0.54	-0.57	-0.56	-0.56	-0.43	-0.40	-0.39	-0.39	-0.39	-0.38
	12.63	0.30	1.67	4.21	7.98	7.41	7.03	6.41	7.38	0.54	0.40	-0.54	0.39	-0.60	-0.60	-0.46	-0.44	-0.43	-0.43	-0.43	-0.43
	13.68	0.32	1.81	4.55	8.08	7.40	7.60	7.53	3.34	0.70	0.44	-0.36	-0.34	-0.64	-0.65	-0.50	-0.48	-0.48	-0.47	-0.47	-0.47
	14.74	0.35	1.94	4.91	8.07	7.64	7.78	7.81	6.72	3.48	0.47	-0.37	-0.66	-0.69	-0.69	-0.55	-0.53	-0.52	-0.52	-0.51	-0.51
	15.79	0.37	2.09	5.25	7.96	7.73	7.78	7.80	7.75	6.84	0.52	-0.47	-0.71	0.39	-0.73	-0.59	-0.57	-0.56	-0.56	-0.56	-0.55
	16.84	0.40	2.22	5.60	7.82	7.71	7.71	7.75	7.75	4.91	0.57	-0.58	-0.73	-0.73	-0.77	-0.64	-0.61	-0.61	-0.60	-0.60	-0.60
	17.89	0.42	2.36	5.94	7.75	7.63	7.59	7.67	7.64	4.63	0.64	-0.66	-0.78	-0.79	-0.81	-0.70	-0.65	-0.65	-0.64	-0.64	-0.64
	18.95	0.45	2.50	6.28	7.72	7.52	7.43	7.55	7.59	7.67	0.75	-0.72	-0.83	-0.84	0.34	-0.81	-0.70	-0.69	-0.69	-0.68	-0.68
	20.00	0.47	2.63	6.59	7.66	7.41	7.26	7.33	7.58	7.49	1.44	-0.74	-0.88	-0.88	-0.85	-0.89	-0.74	-0.73	-0.73	-0.72	-0.72

Ay US		Vx																		
		2.00	4.68	7.37	10.05	12.74	15.42	18.11	20.79	23.47	26.16	28.84	31.53	34.21	36.89	39.58	42.26	44.95	47.63	50.32	53.00
Delta	-20.00	-0.39	-2.22	-4.99	-7.09	-7.22	-7.07	-7.06	-7.09	-7.20	-7.08	-5.53	-6.99	-6.68	-7.34	-1.06	-0.34	0.93	1.07	0.78	1.14
	-18.95	-0.35	-2.16	-4.77	-6.98	-7.30	-7.14	-7.13	-7.16	-7.19	-6.73	-6.40	-6.90	-6.93	-6.49	-0.92	-0.72	0.68	0.81	-4.33	0.99
	-17.89	-0.47	-2.10	-4.56	-6.81	-7.39	-7.23	-7.19	-7.18	-7.12	-6.20	-7.33	-6.87	-7.29	-5.23	-0.84	-0.79	0.04	-0.68	1.04	0.92
	-16.84	-0.41	-1.93	-4.28	-6.66	-7.48	-7.32	-7.26	-7.19	-6.96	-6.38	-7.23	-7.00	-7.50	-1.96	-0.79	-0.75	-0.74	-6.67	0.99	0.86
	-15.79	-0.40	-1.86	-4.10	-6.47	-7.52	-7.40	-7.25	-7.14	-6.69	-7.00	-7.15	-7.39	-5.09	-1.03	-0.75	-0.72	-0.74	0.94	0.87	0.81
	-14.74	-0.29	-1.78	-3.90	-6.23	-7.38	-7.50	-7.32	-7.11	-6.85	-7.53	-7.23	-7.71	-6.97	-0.88	-0.73	-0.71	-2.67	0.88	0.77	0.75
	-13.68	-0.39	-1.64	-3.59	-5.85	-7.21	-7.56	-7.38	-7.15	-7.34	-7.47	-7.54	-6.21	-6.62	-0.85	-0.72	-0.74	0.83	0.83	0.71	0.69
	-12.63	-0.23	-1.47	-3.31	-5.46	-6.97	-7.56	-7.50	-7.37	-7.68	-7.53	-7.84	-6.10	-5.40	-0.86	-0.75	-3.06	0.78	0.77	0.66	0.64
	-11.58	-0.24	-1.35	-3.08	-4.99	-6.66	-7.53	-7.61	-7.62	-7.81	-7.79	-7.35	-7.65	-4.11	-0.95	-0.90	0.72	0.72	0.72	0.60	0.58
	-10.53	-0.24	-1.29	-2.77	-4.67	-6.43	-7.23	-7.61	-7.72	-7.89	-7.95	-6.29	-7.52	-4.57	-1.31	-1.47	0.66	0.67	0.67	0.56	0.53
	-9.47	-0.20	-1.13	-2.50	-4.30	-5.91	-7.00	-7.52	-7.67	-7.95	-7.98	-6.03	-7.61	-5.82	-2.21	-4.29	0.61	0.61	0.61	0.57	0.50
	-8.42	-0.18	-0.98	-2.19	-3.80	-5.40	-6.62	-7.31	-7.49	-7.82	-8.00	-6.96	-7.88	-6.93	-4.80	-5.36	0.55	0.55	0.55	0.55	0.55
	-7.37	-0.19	-0.82	-1.95	-3.29	-4.84	-6.04	-6.88	-7.26	-7.46	-7.94	-7.93	-5.72	-7.79	-6.96	-6.00	0.50	0.49	0.49	0.49	0.49
	-6.32	-0.15	-0.77	-1.71	-2.83	-4.15	-5.38	-6.30	-6.88	-7.17	-7.31	-7.89	-7.89	-5.99	-7.83	-7.49	-7.34	0.44	0.44	0.44	0.44
	-5.26	-0.12	-0.62	-1.37	-2.33	-3.44	-4.51	-5.56	-6.18	-6.69	-6.99	-6.99	-7.54	-7.92	-7.60	-5.32	-7.50	-7.92	-7.75	0.39	0.38
	-4.21	-0.10	-0.47	-1.06	-1.84	-2.76	-3.63	-4.55	-5.37	-5.92	-6.28	-6.53	-6.69	-6.67	-7.27	-7.78	-7.65	-6.09	-5.20	-6.51	-6.72
	-3.16	-0.07	-0.34	-0.84	-1.37	-2.04	-2.72	-3.37	-3.99	-4.75	-5.24	-5.59	-5.86	-6.05	-6.12	-6.04	-6.29	-6.97	-7.48	-7.54	-7.08
	-2.11	-0.04	-0.26	-0.51	-0.91	-1.29	-1.72	-2.13	-2.63	-3.06	-3.52	-4.02	-4.37	-4.68	-4.93	-5.12	-5.25	-5.33	-5.32	-5.33	-5.51
	-1.05	-0.03	-0.14	-0.25	-0.44	-0.63	-0.83	-1.02	-1.23	-1.41	-1.59	-1.81	-2.02	-2.18	-2.41	-2.61	-2.84	-3.04	-3.36	-3.52	-3.63
	0.00	0.00	0.00	0.00	0.00	0.00	0.00	0.00	0.00	0.00	0.00	0.00	0.00	0.00	0.00	0.00	0.00	0.00	0.00	0.00	0.00
	1.05	0.03	0.14	0.25	0.44	0.63	0.83	1.02	1.23	1.41	1.59	1.81	2.02	2.18	2.41	2.61	2.84	3.04	3.36	3.52	3.63
	2.11	0.04	0.26	0.51	0.91	1.29	1.72	2.13	2.63	3.06	3.52	4.02	4.37	4.68	4.93	5.12	5.25	5.33	5.32	5.33	5.51
	3.16	0.07	0.34	0.84	1.37	2.04	2.72	3.37	3.99	4.75	5.24	5.59	5.86	6.05	6.12	6.04	6.29	6.97	7.48	7.54	7.08
	4.21	0.10	0.47	1.06	1.84	2.76	3.63	4.55	5.37	5.92	6.28	6.53	6.69	6.67	7.27	7.78	7.65	6.09	5.20	6.51	6.72
	5.26	0.12	0.62	1.37	2.33	3.44	4.51	5.56	6.18	6.69	6.99	6.99	7.54	7.92	7.60	5.32	7.50	7.92	7.75	-0.39	-0.38
	6.32	0.15	0.77	1.71	2.83	4.15	5.38	6.30	6.88	7.17	7.31	7.89	7.89	5.99	7.83	7.49	7.34	-0.44	-0.44	-0.44	-0.44
	7.37	0.19	0.82	1.95	3.29	4.84	6.04	6.88	7.26	7.46	7.94	7.93	5.72	7.79	6.96	6.00	-0.50	-0.49	-0.49	-0.49	-0.49
	8.42	0.18	0.98	2.19	3.80	5.40	6.62	7.31	7.49	7.82	8.00	6.96	7.88	6.93	4.80	5.36	-0.55	-0.55	-0.55	-0.55	-0.55
	9.47	0.20	1.13	2.50	4.30	5.91	7.00	7.52	7.67	7.95	7.98	6.03	7.61	5.82	2.21	4.29	-0.61	-0.61	-0.61	-0.57	-0.50
	10.53	0.24	1.29	2.77	4.67	6.43	7.23	7.61	7.72	7.89	7.95	6.29	7.52	4.57	1.31	1.47	-0.66	-0.67	-0.67	-0.56	-0.53
	11.58	0.24	1.35	3.08	4.99	6.66	7.53	7.61	7.62	7.81	7.79	7.35	7.65	4.11	0.95	0.90	-0.72	-0.72	-0.72	-0.60	-0.58
	12.63	0.23	1.47	3.31	5.46	6.97	7.56	7.50	7.37	7.68	7.53	7.84	6.10	5.40	0.86	0.75	3.06	-0.78	-0.77	-0.66	-0.64
	13.68	0.39	1.64	3.59	5.85	7.21	7.56	7.38	7.15	7.34	7.47	7.54	6.21	6.62	0.85	0.72	0.74	-0.83	-0.83	-0.71	-0.69
	14.74	0.29	1.78	3.90	6.23	7.38	7.50	7.32	7.11	6.85	7.53	7.23	7.71	6.97	0.88	0.73	0.71	2.67	-0.88	-0.77	-0.75
	15.79	0.40	1.86	4.10	6.47	7.52	7.40	7.25	7.14	6.69	7.00	7.15	7.39	5.09	1.03	0.75	0.72	0.74	-0.94	-0.87	-0.81
	16.84	0.41	1.93	4.28	6.66	7.48	7.32	7.26	7.19	6.96	6.38	7.23	7.00	7.50	1.96	0.79	0.75	0.74	6.67	-0.99	-0.86
	17.89	0.47	2.10	4.56	6.81	7.39	7.23	7.19	7.18	7.12	6.20	7.33	6.87	7.29	5.23	0.84	0.79	-0.04	0.68	-1.04	-0.92
	18.95	0.35	2.16	4.77	6.98	7.30	7.14	7.13	7.16	7.19	6.73	6.40	6.90	6.93	6.49	0.92	0.72	-0.68	-0.81	4.33	-0.99
	20.00	0.39	2.22	4.99	7.09	7.22	7.07	7.06	7.09	7.20	7.08	5.53	6.99	6.68	7.34	1.06	0.34	-0.93	-1.07	-0.78	-1.14

Error (m/s^2)	Vx (m/s)														
	2.00	5.64	9.29	12.93	16.57	20.21	23.86	27.50	31.14	34.79	38.43	42.07	45.71	49.36	53.00
0.00	0.00	0.00	0.00	0.01	0.01	0.01	0.02	0.02	0.03	0.03	0.04	0.04	0.05	0.05	0.06
1.43	0.01	0.05	0.25	0.60	1.15	1.84	2.62	2.81	2.67	2.44	1.73	-1.87	1.99	2.61	2.18
2.86	0.01	0.12	0.45	1.08	2.01	2.48	1.36								
4.29	0.01	0.19	0.68	1.54	1.74	-5.53									
5.71	0.02	0.18	0.83	1.86	-5.48										
7.14	-0.01	0.27	1.03	-5.18											
8.57	0.05	0.32	1.21	-5.66											
10.00	0.04	0.31	1.40	-0.93											
11.43	0.06	0.36	1.77	-0.88											
12.86	0.07	0.42	-4.36	-1.23											
14.29	0.04	0.40	-5.12	-1.75											
15.71	0.02	0.47	-5.20	-2.18											
17.14	0.01	0.54	-5.49	-2.38											
18.57	0.10	0.55	-0.18	-2.54											
20.00	0.13	0.64	-0.61	-2.74											

Delta (deg)

Ay	Vx														
	2.00	5.64	9.29	12.93	16.57	20.21	23.86	27.50	31.14	34.79	38.43	42.07	45.71	49.36	53.00
0.00	0.00	0.00	0.00	0.01	0.01	0.01	0.02	0.02	0.03	0.03	0.04	0.04	0.05	0.05	0.06
1.43	0.03	0.28	0.76	1.47	2.38	3.47	4.60	5.28	5.48	5.56	5.17	1.76	3.79	4.73	4.46
2.86	0.07	0.56	1.51	2.92	4.64	5.54	5.63	-3.57	-3.54	-3.53	-3.51	-3.54	-3.60	-3.69	-3.75
4.29	0.10	0.83	2.26	4.32	5.64	-3.59									
5.71	0.13	1.10	3.00	5.48	-3.60										
7.14	0.16	1.38	3.72	-3.74											
8.57	0.19	1.64	4.42	-3.74											
10.00	0.23	1.90	5.08	4.83											
11.43	0.26	2.16	5.72	5.41											
12.86	0.29	2.40	-3.63	5.58											
14.29	0.31	2.64	-3.66	5.41											
15.71	0.34	2.87	-3.63	5.24											
17.14	0.37	3.09	-3.69	5.04											
18.57	0.39	3.31	5.66	4.80											
20.00	0.42	3.51	5.50	4.54											

Delta

Beta	Vx														
	2.00	5.64	9.29	12.93	16.57	20.21	23.86	27.50	31.14	34.79	38.43	42.07	45.71	49.36	53.00
0.00	-0.03	-0.03	-0.03	-0.03	-0.03	-0.03	-0.04	-0.04	-0.04	-0.04	-0.05	-0.05	-0.05	-0.05	-0.05
1.43	0.71	0.60	0.36	0.00	-0.53	-1.33	-2.67	-4.29	-5.23	-5.90	-12.29	-26.01	63.48	62.33	62.39
2.86	1.46	1.22	0.73	-0.12	-1.93	-4.57	-5.41	-62.73	-62.48	-63.31	-63.03	-63.08	-63.09	-63.80	-64.27
4.29	2.20	1.84	1.07	-0.67	-4.38	-62.54									
5.71	2.94	2.46	1.35	-2.49	-61.87										
7.14	3.69	3.08	1.52	-62.64											
8.57	4.43	3.69	1.51	-62.21											
10.00	5.17	4.30	1.12	-9.83											
11.43	5.92	4.89	-0.71	-6.84											
12.86	6.66	5.48	-62.04	-3.91											
14.29	7.39	6.05	-61.97	-1.66											
15.71	8.12	6.61	-62.10	-1.25											
17.14	8.85	7.16	-62.23	-0.89											
18.57	9.56	7.70	0.17	-0.59											
20.00	10.27	8.22	1.33	-0.35											

Delta

Error (m/s^2)		Vx (m/s)														
		2.00	5.64	9.29	12.93	16.57	20.21	23.86	27.50	31.14	34.79	38.43	42.07	45.71	49.36	53.00
Delta (deg)	0.00	0.00	0.00	0.00	0.01	0.01	0.01	0.02	0.02	0.03	0.03	0.04	0.04	0.05	0.05	0.06
	1.43	-0.56	0.84	-0.97	-1.90	2.35	-4.49	-4.19	-4.26	-4.39	3.36	2.76	3.06	-8.20	-7.99	-8.38
	2.86	0.37	-0.61	1.42	-0.07	-4.60	-4.45	1.97	-5.63	1.16	1.62	1.50	0.85	-10.01	-10.67	-10.87
	4.29	0.04	0.51	0.13	-4.64	-4.57	-5.28									
	5.71	0.53	0.27	0.66	-4.54	-5.04										
	7.14	-0.44	-0.74	0.46	-4.73											
	8.57	0.39	0.06	-1.21	-0.06											
	10.00	0.07	-0.17	-1.14	-0.58											
	11.43	-0.40	-0.82	-4.32	-1.30											
	12.86	0.46	-0.72	-4.57	-1.99											
	14.29	-0.05	-0.47	-4.89	-2.59											
	15.71	0.23	0.63	-4.70	-3.13											
	17.14	0.25	0.85	-5.40	-3.44											
	18.57	-0.33	0.79	-0.40	-3.69											
	20.00	0.51	0.08	-1.16	-3.96											

Ay		Vx														
		2.00	5.64	9.29	12.93	16.57	20.21	23.86	27.50	31.14	34.79	38.43	42.07	45.71	49.36	53.00
Delta	0.00	0.00	0.00	0.00	0.01	0.01	0.01	0.02	0.02	0.03	0.03	0.04	0.04	0.05	0.05	0.06
	1.43	-0.53	1.08	-0.43	-1.07	3.60	-3.92	-3.47	-3.38	-3.32	4.93	4.46	4.75	-6.45	-5.94	-6.11
	2.86	0.43	-0.19	2.49	1.73	-3.75	-3.33	3.75	-3.66	3.69	4.44	4.72	4.33	-6.17	-6.48	-6.24
	4.29	0.12	1.14	1.74	-3.84	-3.33	-3.43									
	5.71	0.64	1.19	2.81	-3.44	-3.24										
	7.14	-0.27	0.35	3.19	-3.34											
	8.57	0.54	1.41	2.07	5.08											
	10.00	0.25	1.41	2.62	5.32											
	11.43	-0.21	1.00	-3.23	5.06											
	12.86	0.68	1.28	-3.32	4.83											
	14.29	0.22	1.80	-3.40	4.58											
	15.71	0.56	3.03	-3.19	4.29											
	17.14	0.61	3.43	-3.55	3.98											
	18.57	-0.03	3.59	5.43	3.65											
	20.00	0.79	2.95	4.96	3.31											

Beta (deg)		Vx (m/s)														
		2.00	5.64	9.29	12.93	16.57	20.21	23.86	27.50	31.14	34.79	38.43	42.07	45.71	49.36	53.00
Delta (deg)	0.00	-0.03	-0.03	-0.03	-0.03	-0.03	-0.03	-0.04	-0.04	-0.04	-0.04	-0.05	-0.05	-0.05	-0.05	-0.05
	1.43	0.75	0.37	0.18	2.38	-1.25	-61.59	-62.56	-63.51	-63.75	62.71	62.18	64.17	-64.40	-63.22	-64.14
	2.86	1.24	2.69	1.45	2.68	-61.69	-63.18	60.44	-62.82	60.84	62.60	62.94	63.43	-63.80	-64.03	-63.77
	4.29	3.24	3.38	1.42	-60.98	-63.15	-62.32									
	5.71	3.66	4.21	3.78	-62.05	-62.93										
	7.14	3.56	5.16	2.48	-62.83											
	8.57	4.35	4.26	3.41	-8.17											
	10.00	6.29	6.69	3.83	-5.87											
	11.43	6.84	5.94	-61.51	-5.94											
	12.86	6.74	6.65	-61.71	-5.64											
	14.29	7.23	7.13	-62.04	-5.40											
	15.71	7.97	9.20	-62.14	-5.21											
	17.14	8.73	8.85	-62.65	-5.08											
	18.57	10.04	9.26	-2.98	-5.00											
	20.00	10.85	11.28	-2.58	-4.96											

Error (m/s^2)		Vx (m/s)														
		2.00	5.64	9.29	12.93	16.57	20.21	23.86	27.50	31.14	34.79	38.43	42.07	45.71	49.36	53.00
Delta (deg)	0.00	0.00	0.00	0.00	0.01	0.01	0.01	0.02	0.02	0.03	0.03	0.04	0.04	0.05	0.05	0.06
	1.43	-0.07	0.20	0.64	1.71	3.50	3.64	-2.37	-0.59	2.11	-2.45	-5.50	-9.34	-10.24	-9.18	-8.19
	2.86	-0.15	0.22	0.96	2.29	3.02	-5.03	-5.41	-5.80	-6.18	-6.56	-6.93	3.23	-7.71	-7.98	-8.22
	4.29	-0.41	0.31	1.25	2.67	-5.20	-5.71									
	5.71	-0.62	0.32	1.42	-5.01	-5.71										
	7.14	-0.45	0.42	1.62	-5.34											
	8.57	0.91	0.48	1.79	-5.61											
	10.00	0.31	0.47	-4.66	-5.94											
	11.43	-0.48	0.53	-4.75	-0.57											
	12.86	1.44	0.59	-4.87	-1.11											
	14.29	-1.04	0.56	-5.17	-1.75											
	15.71	1.25	0.63	-5.38	-2.20											
	17.14	0.30	0.70	-5.35	-2.47											
	18.57	-0.17	0.70	-5.62	-2.71											
	20.00	1.00	0.79	-0.28	-3.31											

Ay		Vx														
		2.00	5.64	9.29	12.93	16.57	20.21	23.86	27.50	31.14	34.79	38.43	42.07	45.71	49.36	53.00
Delta	0.00	0.00	0.00	0.00	0.01	0.01	0.01	0.02	0.02	0.03	0.03	0.04	0.04	0.05	0.05	0.06
	1.43	-0.04	0.42	1.15	2.56	4.67	5.13	-0.89	1.57	5.05	0.75	-1.94	-5.52	-6.29	-5.08	-3.91
	2.86	-0.10	0.65	2.01	4.06	5.52	-3.75	-3.77	-3.70	-3.67	-3.66	-3.69	5.86	-3.64	-3.92	-3.82
	4.29	-0.34	0.94	2.79	5.30	-3.87	-3.81									
	5.71	-0.52	1.22	3.52	-3.85	-3.83										
	7.14	-0.30	1.50	4.20	-3.90											
	8.57	1.04	1.76	4.83	-3.85											
	10.00	0.47	2.01	-3.66	-3.80											
	11.43	-0.31	2.26	-3.64	5.48											
	12.86	1.62	2.49	-3.59	5.50											
	14.29	-0.82	2.71	-3.69	5.25											
	15.71	1.52	2.92	-3.74	5.10											
	17.14	0.59	3.12	-3.63	4.88											
	18.57	0.06	3.30	-3.71	4.62											
	20.00	1.21	3.48	5.39	4.01											

Beta (deg)		Vx (m/s)														
		2.00	5.64	9.29	12.93	16.57	20.21	23.86	27.50	31.14	34.79	38.43	42.07	45.71	49.36	53.00
Delta (deg)	0.00	-0.03	-0.03	-0.03	-0.03	-0.03	-0.03	-0.04	-0.04	-0.04	-0.04	-0.05	-0.05	-0.05	-0.05	-0.05
	1.43	0.13	0.34	-0.19	-1.17	-1.54	-11.74	-39.61	-26.54	-8.81	2.46	3.61	6.62	10.86	17.81	19.64
	2.86	1.06	0.91	-0.01	-1.74	-5.84	-61.30	-61.84	-61.21	-61.29	-61.41	-62.13	-69.76	-62.03	-63.83	-64.00
	4.29	1.55	1.47	0.19	-3.30	-61.34	-61.63									
	5.71	2.04	2.03	0.36	-61.06	-61.21										
	7.14	4.15	2.61	0.42	-61.34											
	8.57	4.43	3.18	0.26	-61.20											
	10.00	6.20	3.76	-61.86	-61.56											
	11.43	3.65	4.33	-61.38	-4.17											
	12.86	6.74	4.90	-60.83	-3.29											
	14.29	9.34	5.46	-61.18	-2.36											
	15.71	6.22	6.02	-61.05	-2.06											
	17.14	11.53	6.57	-61.08	-1.78											
	18.57	7.05	7.11	-61.51	-1.51											
	20.00	12.55	7.65	1.48	-5.33											

Error (m/s^2)		Vx (m/s)														
		2.00	5.64	9.29	12.93	16.57	20.21	23.86	27.50	31.14	34.79	38.43	42.07	45.71	49.36	53.00
Delta (deg)	0.00	0.00	0.00	0.00	0.01	0.01	0.01	0.02	0.02	0.03	0.03	0.04	0.04	0.05	0.05	0.06
	1.43	0.01	0.05	0.25	0.63	1.23	2.01	2.82	3.19	1.66	2.43	1.74	-0.70	-2.21	2.49	3.41
	2.86	0.01	0.12	0.45	1.13	2.10	-5.02	-5.52	-6.02	2.09	2.36	1.80	2.07	1.92	-7.88	0.40
	4.29	0.02	0.19	0.69	1.58	-5.15	-5.67									
	5.71	0.02	0.18	0.84	1.91	-5.73										
	7.14	0.00	0.27	1.03	1.51											
	8.57	0.05	0.31	1.20	-0.41											
	10.00	0.05	0.30	1.37	-0.48											
	11.43	0.06	0.36	1.60	-0.64											
	12.86	0.08	0.41	-4.93	-1.22											
	14.29	0.05	0.39	-5.21	-1.55											
	15.71	0.03	0.45	0.77	-2.10											
	17.14	0.02	0.52	0.71	-2.25											
	18.57	0.11	0.52	0.30	-2.49											
	20.00	0.15	0.61	-0.15	-2.72											

Ay		Vx														
		2.00	5.64	9.29	12.93	16.57	20.21	23.86	27.50	31.14	34.79	38.43	42.07	45.71	49.36	53.00
Delta	0.00	0.00	0.00	0.00	0.01	0.01	0.01	0.02	0.02	0.03	0.03	0.04	0.04	0.05	0.05	0.06
	1.43	0.03	0.27	0.76	1.49	2.45	3.63	4.79	5.43	4.48	5.54	5.16	2.91	1.59	4.11	5.36
	2.86	0.06	0.55	1.51	2.94	4.69	-3.81	-3.69	-3.64	3.86	4.69	4.04	4.95	5.83	-3.58	4.67
	4.29	0.09	0.82	2.25	4.31	-3.80	-3.70									
	5.71	0.12	1.08	2.97	5.42	-3.75										
	7.14	0.15	1.35	3.66	5.60											
	8.57	0.18	1.60	4.32	5.27											
	10.00	0.21	1.86	4.93	5.26											
	11.43	0.24	2.10	5.48	5.39											
	12.86	0.26	2.33	-3.71	5.43											
	14.29	0.29	2.56	-3.72	5.46											
	15.71	0.31	2.77	5.29	5.21											
	17.14	0.33	2.97	5.75	5.11											
	18.57	0.35	3.17	5.73	4.84											
	20.00	0.37	3.35	5.56	4.59											

Beta (deg)		Vx (m/s)														
		2.00	5.64	9.29	12.93	16.57	20.21	23.86	27.50	31.14	34.79	38.43	42.07	45.71	49.36	53.00
Delta (deg)	0.00	-0.03	-0.03	-0.03	-0.03	-0.03	-0.03	-0.04	-0.04	-0.04	-0.04	-0.05	-0.05	-0.05	-0.05	-0.05
	1.43	0.71	0.59	0.35	-0.03	-0.60	-1.50	-3.03	-4.92	-2.55	-6.37	-12.89	-21.62	-27.02	67.89	66.19
	2.86	1.45	1.22	0.72	-0.17	-2.06	-63.95	-62.06	-61.90	68.35	66.56	69.39	67.29	66.45	-63.42	66.57
	4.29	2.20	1.84	1.06	-0.71	-62.32	-61.92									
	5.71	2.94	2.46	1.34	-2.30	-61.89										
	7.14	3.69	3.08	1.53	-6.75											
	8.57	4.43	3.70	1.59	-9.19											
	10.00	5.18	4.30	1.39	-0.27											
	11.43	5.92	4.91	0.66	-6.51											
	12.86	6.66	5.50	-61.47	-0.69											
	14.29	7.40	6.08	-61.49	-2.95											
	15.71	8.14	6.65	-5.27	-0.73											
	17.14	8.86	7.22	0.92	-1.03											
	18.57	9.58	7.77	-0.41	-0.51											
	20.00	10.29	8.31	1.76	-0.31											

Error (m/s^2)		V_R (m/s)														
		2.00	5.64	9.29	12.93	16.57	20.21	23.86	27.50	31.14	34.79	38.43	42.07	45.71	49.36	53.00
Delta (deg)	0.00	0.00	0.00	0.00	-0.01	-0.02	-0.02	-0.03	-0.04	-0.06	-0.07	-0.09	-0.11	-0.14	-0.18	-0.22
	1.43	0.01	0.05	0.26	0.68	1.40	2.45	3.03	2.85	2.45	2.21	1.84	1.55	1.49	1.27	0.73
	2.86	0.01	0.12	0.49	1.27	2.35	2.04	1.17	0.50	0.17	-0.69	-4.53	-1.86	-2.27	-2.29	-13.09
	4.29	0.01	0.20	0.74	1.84	1.56	0.36									
	5.71	0.02	0.19	0.93	1.80	0.88										
	7.14	-0.01	0.28	1.16	1.06											
	8.57	0.05	0.33	1.37	0.31											
	10.00	0.04	0.33	1.55	-0.48											
	11.43	0.06	0.38	1.57	-1.02											
	12.86	0.07	0.44	1.23	-1.64											
	14.29	0.04	0.42	0.74	-2.18											
	15.71	0.02	0.49	0.31	-2.68											
	17.14	0.01	0.57	-0.12	-2.97											
	18.57	0.09	0.58	-0.64	-3.22											
	20.00	0.13	0.68	-1.18	-3.53											

Ay		V_R														
		2.00	5.64	9.29	12.93	16.57	20.21	23.86	27.50	31.14	34.79	38.43	42.07	45.71	49.36	53.00
Delta	0.00	0.00	0.00	0.00	-0.01	-0.02	-0.02	-0.03	-0.04	-0.06	-0.07	-0.09	-0.11	-0.14	-0.18	-0.22
	1.43	0.03	0.28	0.78	1.55	2.63	4.07	5.01	5.23	5.30	5.34	5.35	5.35	5.46	5.43	5.06
	2.86	0.07	0.56	1.55	3.11	4.97	5.39	5.45	5.46	5.60	5.13	1.30	3.90	4.45	4.84	-6.23
	4.29	0.10	0.84	2.33	4.61	5.48	5.50									
	5.71	0.13	1.11	3.09	5.42	5.53										
	7.14	0.16	1.39	3.85	5.58											
	8.57	0.19	1.66	4.57	5.57											
	10.00	0.23	1.92	5.20	5.50											
	11.43	0.26	2.18	5.59	5.38											
	12.86	0.29	2.43	5.70	5.22											
	14.29	0.32	2.67	5.68	5.02											
	15.71	0.34	2.90	5.60	4.77											
	17.14	0.37	3.13	5.48	4.47											
	18.57	0.39	3.34	5.29	4.12											
	20.00	0.42	3.55	5.04	3.73											

Beta		V_R														
		2.00	5.64	9.29	12.93	16.57	20.21	23.86	27.50	31.14	34.79	38.43	42.07	45.71	49.36	53.00
Delta	0.00	-0.03	-0.02	-0.02	-0.02	-0.02	-0.01	-0.01	0.00	0.00	0.01	0.02	0.03	0.04	0.06	0.08
	1.43	0.60	0.49	0.24	-0.16	-0.81	-2.07	-3.65	-4.35	-4.70	-4.92	-5.08	-5.19	-6.06	-5.95	-12.64
	2.86	1.23	0.99	0.48	-0.50	-2.84	-4.29	-4.76	-4.99	-7.17	-9.13	-0.76	-17.91	-12.59	-3.78	10.26
	4.29	1.86	1.50	0.68	-1.47	-4.02	-4.58									
	5.71	2.49	2.00	0.80	-2.88	-4.14										
	7.14	3.12	2.50	0.79	-3.30											
	8.57	3.75	2.99	0.55	-3.20											
	10.00	4.38	3.47	-0.07	-2.90											
	11.43	5.01	3.95	-0.89	-2.52											
	12.86	5.63	4.42	-1.17	-2.12											
	14.29	6.25	4.87	-0.98	-1.72											
	15.71	6.87	5.31	-0.60	-1.35											
	17.14	7.48	5.74	-0.16	-1.02											
	18.57	8.08	6.16	0.27	-0.74											
	20.00	8.67	6.56	0.67	-0.52											

Error (m/s^2)		Vx (m/s)														
		2.00	5.64	9.29	12.93	16.57	20.21	23.86	27.50	31.14	34.79	38.43	42.07	45.71	49.36	53.00
Delta (deg)	0.00	0.00	0.00	0.00	-0.01	-0.02	-0.02	-0.03	-0.04	-0.06	-0.07	-0.09	-0.11	-0.14	-0.18	-0.22
	1.43	-0.27	0.21	-0.53	2.23	2.80	2.87	2.41	2.25	5.66	1.83	1.69	1.62	1.73	2.03	1.97
	2.86	0.29	-1.35	0.33	1.81	-4.35	-0.48	-0.12	2.10	1.66	1.00	0.84	0.25	-0.18	-0.33	-0.52
	4.29	-0.17	-1.21	1.28	-3.30	1.75	-3.47									
	5.71	0.66	-0.92	0.78	-1.43	1.94										
	7.14	0.40	-1.01	1.21	1.05											
	8.57	-0.49	1.06	0.51	0.39											
	10.00	-0.45	-1.39	1.42	-1.68											
	11.43	-0.45	0.43	-4.54	-1.93											
	12.86	-0.52	0.23	-0.22	-2.72											
	14.29	0.21	-1.33	0.31	-3.42											
	15.71	0.54	-0.49	0.33	-4.07											
	17.14	-0.03	-0.91	-1.78	-4.48											
	18.57	-0.45	-1.20	-2.24	-4.82											
	20.00	-0.36	-0.01	-3.20	-5.16											

Ay		Vx														
		2.00	5.64	9.29	12.93	16.57	20.21	23.86	27.50	31.14	34.79	38.43	42.07	45.71	49.36	53.00
Delta	0.00	0.00	0.00	0.00	-0.01	-0.02	-0.02	-0.03	-0.04	-0.06	-0.07	-0.09	-0.11	-0.14	-0.18	-0.22
	1.43	-0.24	0.46	0.02	3.10	3.21	3.49	3.17	3.17	-4.00	3.11	3.13	3.22	3.50	4.07	4.25
	2.86	0.34	-0.91	1.36	3.63	-1.68	2.73	3.84	4.25	4.28	4.04	4.49	4.39	3.94	4.15	4.26
	4.29	-0.08	-0.56	2.85	-0.49	5.66	1.96									
	5.71	0.77	0.03	2.93	2.31	2.67										
	7.14	0.57	0.11	3.92	5.44											
	8.57	-0.34	2.39	3.79	5.57											
	10.00	-0.27	0.20	5.14	4.33											
	11.43	-0.26	2.25	-3.45	4.50											
	12.86	-0.30	2.24	4.29	4.17											
	14.29	0.49	0.92	4.98	3.80											
	15.71	0.86	1.91	5.51	3.39											
	17.14	0.33	1.69	3.86	2.96											
	18.57	-0.15	1.58	3.76	2.52											
	20.00	-0.07	2.92	3.11	2.08											

Beta		Vx														
		2.00	5.64	9.29	12.93	16.57	20.21	23.86	27.50	31.14	34.79	38.43	42.07	45.71	49.36	53.00
Delta	0.00	-0.03	-0.02	-0.02	-0.02	-0.02	-0.01	-0.01	0.00	0.00	0.01	0.02	0.03	0.04	0.06	0.08
	1.43	0.22	-0.04	-0.16	-0.21	64.08	62.55	64.50	63.66	-63.92	64.31	64.29	64.34	63.92	62.79	62.61
	2.86	2.35	1.48	2.68	1.34	1.72	-23.21	-22.34	61.71	61.77	62.01	61.75	62.03	62.37	62.07	62.22
	4.29	1.51	2.01	2.71	2.69	-4.47	-5.16									
	5.71	2.68	2.37	3.68	0.70	-26.49										
	7.14	2.87	3.24	2.76	-6.87											
	8.57	3.79	4.46	2.07	-7.47											
	10.00	4.38	5.80	2.62	-5.13											
	11.43	6.16	5.02	-63.37	-6.06											
	12.86	5.94	5.63	4.16	-5.79											
	14.29	6.11	7.74	-7.99	-5.57											
	15.71	7.57	8.71	1.50	-5.41											
	17.14	7.31	7.51	-2.67	-5.30											
	18.57	8.79	8.78	-3.81	-5.22											
	20.00	9.79	7.94	-3.91	-5.18											

Error (m/s^2)		Vx (m/s)														
		2.00	5.64	9.29	12.93	16.57	20.21	23.86	27.50	31.14	34.79	38.43	42.07	45.71	49.36	53.00
Delta (deg)	0.00	0.00	0.00	0.00	-0.01	-0.02	-0.02	-0.03	-0.04	-0.06	-0.07	-0.09	-0.11	-0.14	-0.18	-0.22
	1.43	-0.01	0.01	0.62	1.78	4.33	4.06	3.58	3.08	2.68	2.38	1.99	1.66	1.47	1.24	1.01
	2.86	0.02	0.21	0.97	2.45	2.87	2.18	1.26	0.43	-0.07	-0.47	-8.92	-0.49	-3.32	-0.34	-0.96
	4.29	0.02	0.30	1.29	2.61	1.76	0.44									
	5.71	0.03	0.31	1.49	2.10	0.46										
	7.14	0.00	0.42	1.70	1.27											
	8.57	0.06	0.47	1.88	0.43											
	10.00	0.06	0.47	1.98	-0.28											
	11.43	1.34	0.54	1.94	-0.97											
	12.86	-1.61	0.59	1.69	-1.58											
	14.29	1.20	0.57	1.16	-2.21											
	15.71	1.47	0.64	0.68	-2.79											
	17.14	-0.35	0.71	0.28	-3.15											
	18.57	0.83	0.71	-0.24	-3.49											
	20.00	0.73	0.80	-0.82	-3.36											

Ay		Vx														
		2.00	5.64	9.29	12.93	16.57	20.21	23.86	27.50	31.14	34.79	38.43	42.07	45.71	49.36	53.00
Delta	0.00	0.00	0.00	0.00	-0.01	-0.02	-0.02	-0.03	-0.04	-0.06	-0.07	-0.09	-0.11	-0.14	-0.18	-0.22
	1.43	0.01	0.24	1.12	2.63	5.50	5.60	5.51	5.31	5.45	5.47	5.46	5.44	5.42	5.39	5.38
	2.86	0.07	0.64	2.02	4.22	5.39	5.45	5.44	5.33	5.32	5.32	-5.48	5.38	3.66	3.94	3.65
	4.29	0.10	0.93	2.83	5.24	5.53	5.46									
	5.71	0.13	1.22	3.58	5.53	5.45										
	7.14	0.16	1.49	4.27	5.55											
	8.57	0.19	1.76	4.90	5.48											
	10.00	0.22	2.02	5.39	5.46											
	11.43	1.51	2.26	5.66	5.21											
	12.86	-1.43	2.50	5.70	5.11											
	14.29	1.43	2.72	5.69	4.87											
	15.71	1.75	2.93	5.57	4.57											
	17.14	-0.05	3.14	5.47	4.24											
	18.57	1.05	3.32	5.31	3.85											
	20.00	0.96	3.51	5.03	3.94											

Beta (deg)		Vx (m/s)														
		2.00	5.64	9.29	12.93	16.57	20.21	23.86	27.50	31.14	34.79	38.43	42.07	45.71	49.36	53.00
Delta (deg)	0.00	-0.03	-0.02	-0.02	-0.02	-0.02	-0.01	-0.01	0.00	0.00	0.01	0.02	0.03	0.04	0.06	0.08
	1.43	0.20	0.17	-0.31	-1.38	-4.51	-9.98	-3.79	-11.03	-6.66	-7.00	-7.16	-7.16	-7.20	-7.15	-7.31
	2.86	1.06	0.69	-0.29	-2.23	-4.97	-5.66	-5.94	-5.45	-5.65	-5.81	-62.34	-6.45	-4.06	63.19	63.40
	4.29	1.69	1.13	-0.23	-3.58	-5.61	-5.68									
	5.71	2.31	1.56	-0.23	-4.38	-4.89										
	7.14	2.95	2.01	-0.33	-4.35											
	8.57	3.58	2.46	-0.66	-3.69											
	10.00	4.21	2.91	-1.36	-4.36											
	11.43	3.99	3.36	-2.22	-2.95											
	12.86	5.45	3.81	-2.10	-2.94											
	14.29	4.16	4.25	-2.34	-2.54											
	15.71	7.16	4.68	-1.12	-2.16											
	17.14	4.58	5.11	-0.72	-1.89											
	18.57	10.77	5.54	-0.49	-1.64											
	20.00	6.01	5.96	-0.02	-7.66											

Error (m/s^2)	Vx (m/s)														
	2.00	5.64	9.29	12.93	16.57	20.21	23.86	27.50	31.14	34.79	38.43	42.07	45.71	49.36	53.00
0.00	0.00	0.00	0.00	-0.01	-0.02	-0.02	-0.03	-0.04	-0.06	-0.07	-0.09	-0.11	-0.14	-0.18	-0.22
1.43	0.01	0.05	0.27	0.71	1.49	2.61	3.10	2.88	2.39	2.15	2.00	1.79	1.45	0.97	0.60
2.86	0.01	0.12	0.49	1.32	2.40	2.63	1.39	-0.22	-0.33	-0.24	-0.28	-1.24	-6.75	-3.38	-8.65
4.29	0.02	0.19	0.75	1.86	1.66	0.00									
5.71	0.02	0.18	0.93	1.87	0.39										
7.14	0.00	0.28	1.15	1.22											
8.57	0.05	0.32	1.35	0.51											
10.00	0.05	0.32	1.51	-0.29											
11.43	0.06	0.37	1.61	-0.77											
12.86	0.08	0.43	1.46	-1.52											
14.29	0.05	0.41	1.08	-1.98											
15.71	0.03	0.47	0.72	-2.59											
17.14	0.02	0.54	0.32	-2.88											
18.57	0.11	0.55	-0.15	-3.18											
20.00	0.14	0.64	-0.67	-3.52											

Delta (deg)

Ay	Vx														
	2.00	5.64	9.29	12.93	16.57	20.21	23.86	27.50	31.14	34.79	38.43	42.07	45.71	49.36	53.00
0.00	0.00	0.00	0.00	-0.01	-0.02	-0.02	-0.03	-0.04	-0.06	-0.07	-0.09	-0.11	-0.14	-0.18	-0.22
1.43	0.03	0.27	0.78	1.57	2.71	4.22	5.06	5.23	5.18	5.25	5.49	5.56	5.38	5.10	4.93
2.86	0.06	0.55	1.55	3.12	4.98	5.39	5.59	4.70	5.10	5.55	5.51	4.71	-4.48	3.72	-5.69
4.29	0.09	0.82	2.31	4.57	5.48	5.06									
5.71	0.12	1.09	3.06	5.39	5.41										
7.14	0.15	1.36	3.78	5.57											
8.57	0.18	1.62	4.46	5.59											
10.00	0.21	1.87	5.05	5.51											
11.43	0.24	2.12	5.48	5.43											
12.86	0.27	2.35	5.68	5.20											
14.29	0.29	2.58	5.71	5.11											
15.71	0.32	2.80	5.68	4.78											
17.14	0.34	3.01	5.57	4.52											
18.57	0.36	3.20	5.45	4.16											
20.00	0.38	3.39	5.22	3.77											

Delta

Beta (deg)	Vx (m/s)														
	2.00	5.64	9.29	12.93	16.57	20.21	23.86	27.50	31.14	34.79	38.43	42.07	45.71	49.36	53.00
0.00	-0.03	-0.02	-0.02	-0.02	-0.02	-0.01	-0.01	0.00	0.00	0.01	0.02	0.03	0.04	0.06	0.08
1.43	0.60	0.48	0.23	-0.19	-0.89	-2.29	-3.83	-4.39	-4.34	-4.80	-6.32	-8.47	-10.61	-12.02	-12.44
2.86	1.23	0.99	0.46	-0.55	-2.91	-4.35	-5.97	-2.45	-4.60	-9.17	-8.73	-4.86	4.48	-16.99	6.18
4.29	1.86	1.50	0.66	-1.47	-4.11										
5.71	2.49	2.00	0.79	-2.79											
7.14	3.12	2.50	0.82	-3.25											
8.57	3.75	2.99	0.67	-3.29											
10.00	4.38	3.48	0.26	-2.75											
11.43	5.01	3.96	-0.39	-2.92											
12.86	5.64	4.43	-0.88	-1.74											
14.29	6.26	4.90	-0.87	-2.02											
15.71	6.88	5.35	-0.61	-1.26											
17.14	7.49	5.79	0.04	-1.06											
18.57	8.10	6.23	0.26	-0.74											
20.00	8.70	6.66	0.77	-0.52											

Delta (deg)

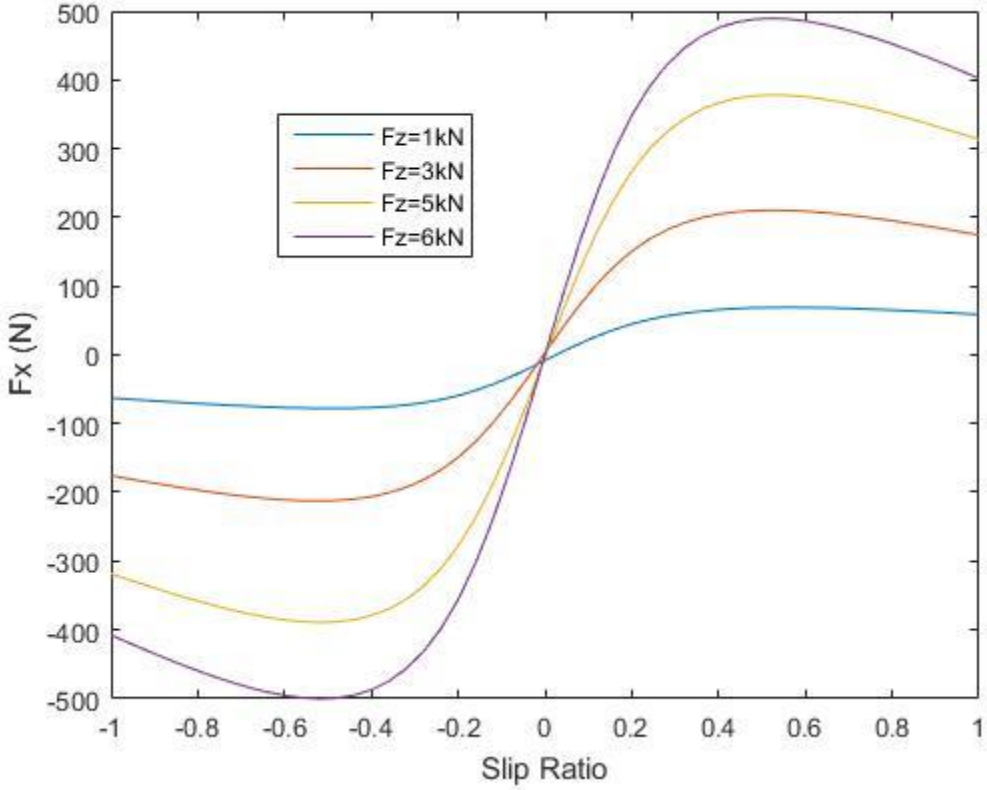
Fz=1kN
Fz=3kN
Fz=5kN
Fz=6kN
Fx (N)
Slip Ratio
500
400
300
200
100
0
-100
-200
-300
-400
-500
-1
-0.8
-0.6
-0.4
-0.2
0
0.2
0.4
0.6
0.8
1

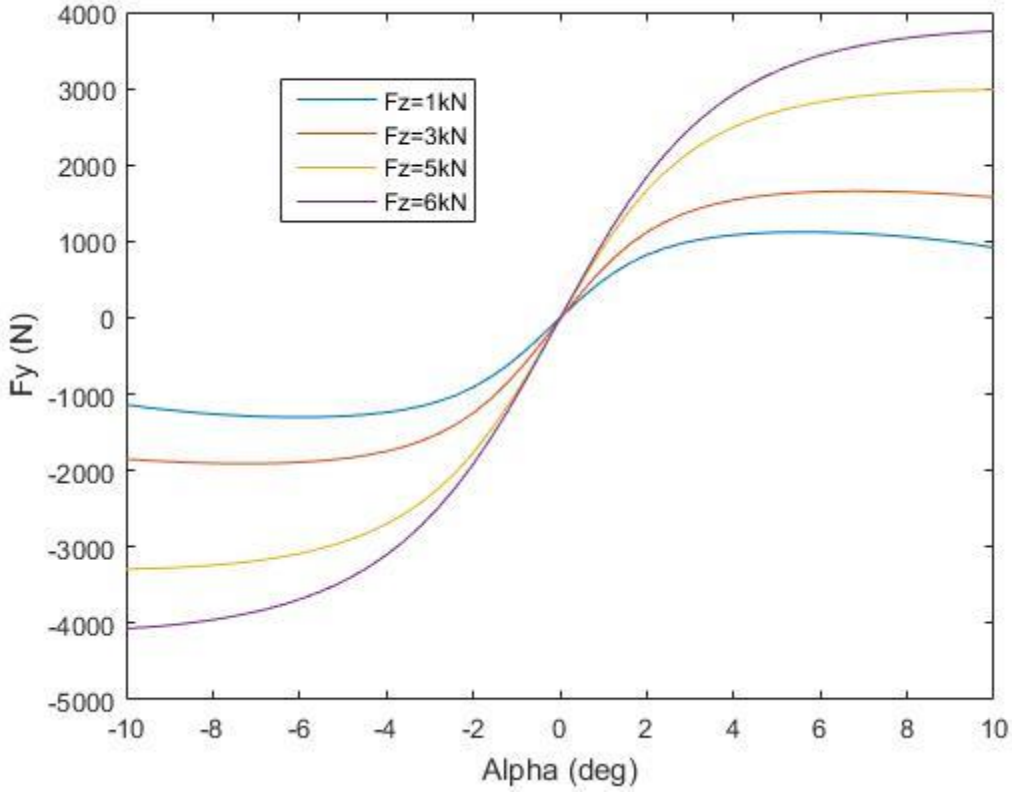
Fz=1kN
Fz=3kN
Fz=5kN
Fz=6kN
Fy (N)
Alpha (deg)
4000
3000
2000
1000
0
-1000
-2000
-3000
-4000
-5000
-10
-8
-6
-4
-2
0
2
4
6
8
10

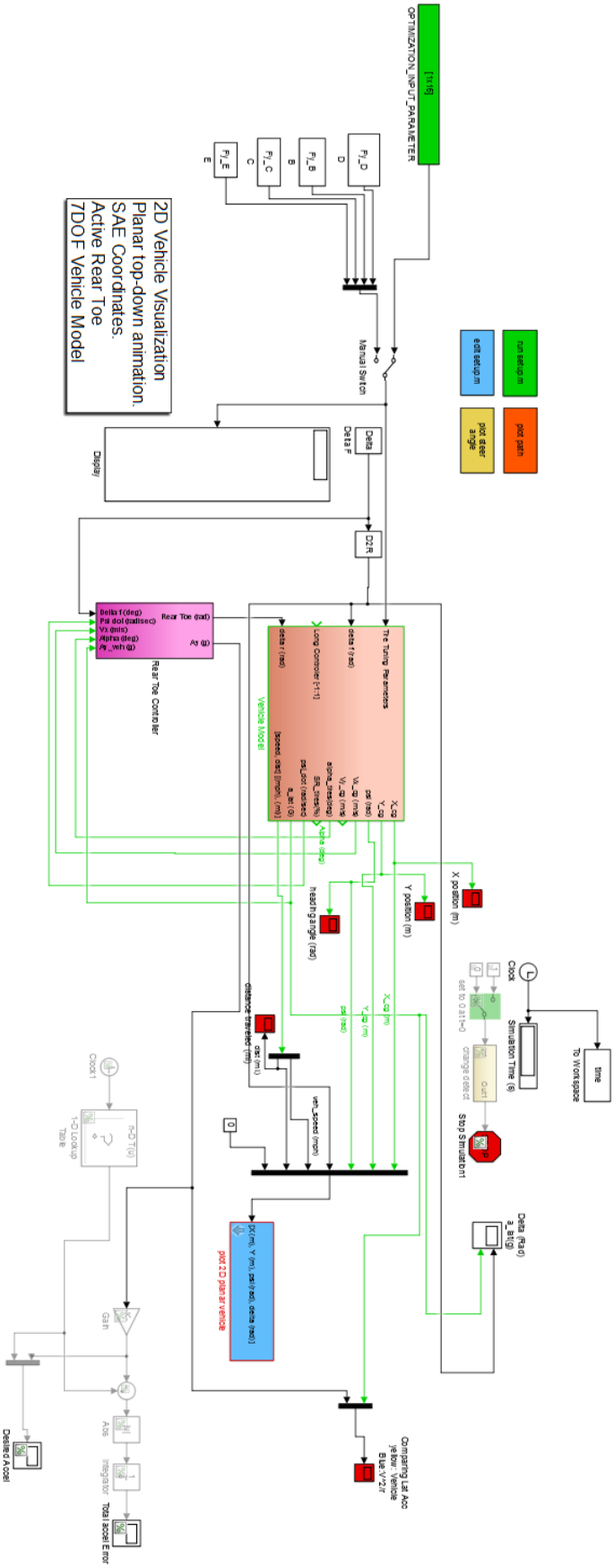
2D Vehicle Visualization
Planar top-down animation.
SAE Coordinates.
Active Rear Toe
7DOF Vehicle Model
[1:16]
OPTIMIZATION_INPUT_PARAMETER
Fy_E
E
Fy_C
C
Fy_B
B
Fy_D
D
Manual Switch
edit setup.m
run setup.m
plot steer angle
plot path
Display
Delta
Delta F
D2R
Rear Toe Controller
Vehicle Model
Tire Tramp Parameters
Long Commander [-1:1]
X position (m)
Y position (m)
Heading angle (rad)
Clock
Simulation Time (s)
time
To Workspace
Stop Simulation
Delta (Rad)
a_lat(g)
plot 2D planar vehicle
Comparing Lat Acc
Blue:Y2.lr
Desired Accel
Gain
Abs
Integrator
Total accel Error

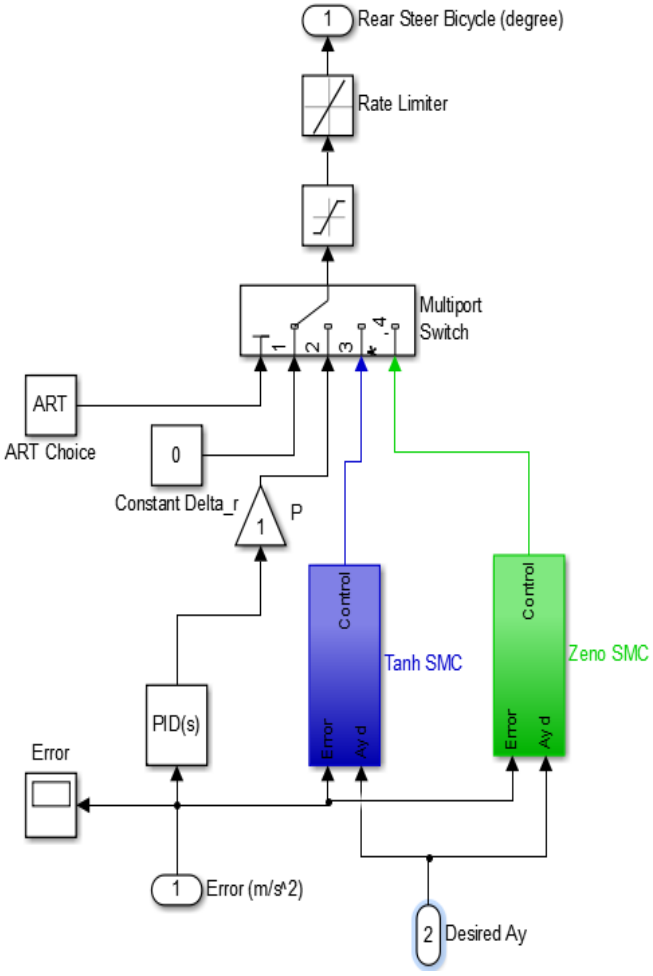

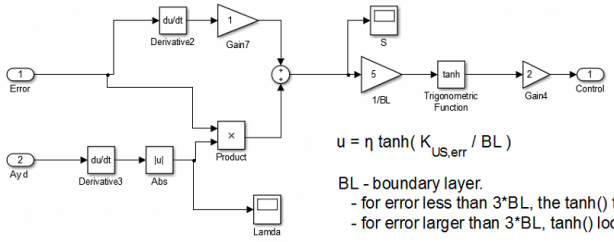

$u = \eta \tanh(K_{US,err} / BL)$

BL - boundary layer.
- for error less than 3*BL, the tanh() function is approximately linear
- for error larger than 3*BL, tanh() looks like signum, which is -1, 0, or +1

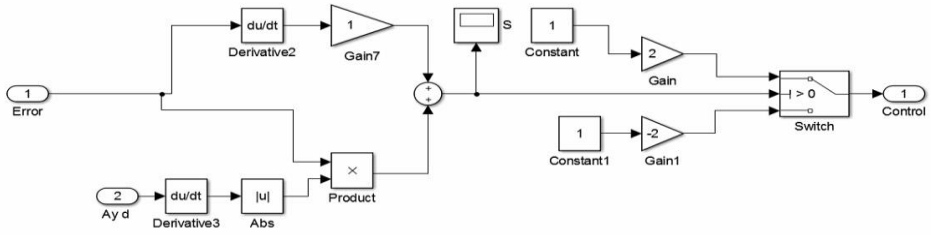

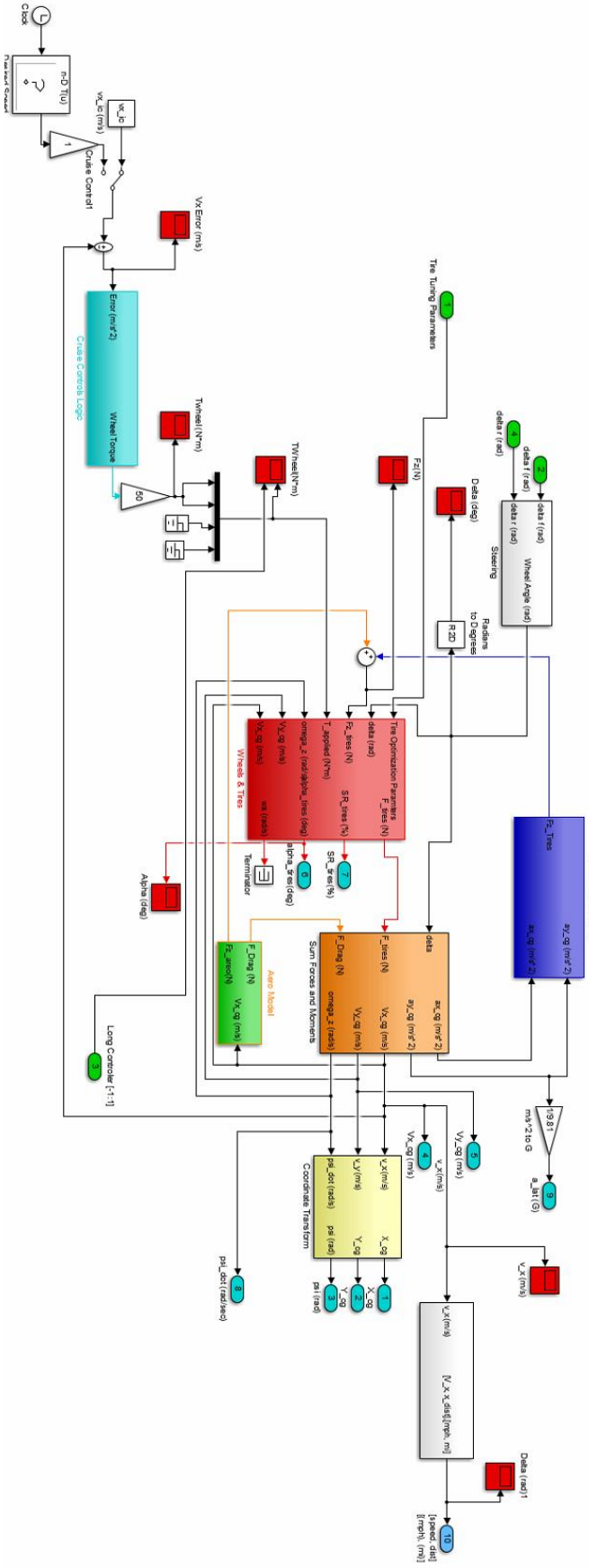
Clock
n-D Tu(u)
vx_ie (m/s)
Cruise Control1
Vx Error (m/s)
Error (m/s^2)
Wheel Torque
Cruise Controller Logic
Twheel (N*m)
50
TWheel (N*m)
Fz(N)
Tire Tuning Parameters
Data (deg)
delta f (rad)
delta r (rad)
Steering
Wheel Angle (rad)
R2D
Radians to Degrees
Tire Optimization Parameters
delta (rad)
Fz_tires (N)
F_tires (N)
SR_tires (%)
omega_z (rad/s)
alpha_tires (deg)
Vx_cg (m/s)
Vy_cg (m/s)
ax_cg (m/s^2)
ay_cg (m/s^2)
Wheels & Tires
Terminator
Alpha (deg)
SR_tires(%)
Fz_Tires
Normal Force Estimate
Aero Model
F_Drag (N)
Fz_tires(N)
Vx_cg (m/s)
Sum Forces and Moments
Long Controller [-1:1]
1/9.81
m/s^2 to G
a_lat (G)
psi_dot (rad/s)
psi (rad)
X_cg
Y_cg
Coordinate Transform
v_x (m/s)
[V_x, s_dot] (mph, mi)
Delta (rad)1
[speed, dist] ([mph], [mi])

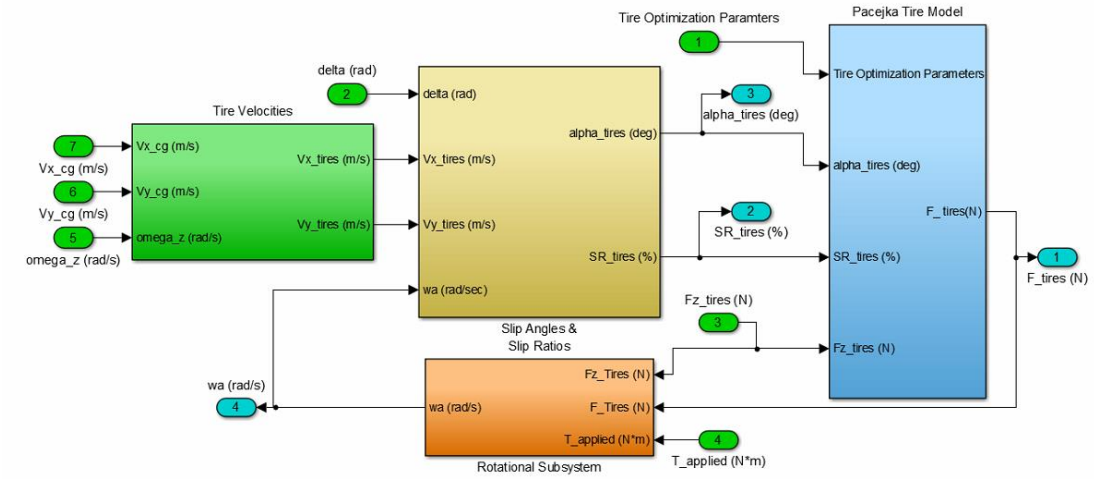

Pacejka Combined Slip Model